DEVELOPMENT OF CONTROL ORIENTED VEHICLE MODELS AND THEIR APPLICATION TO ADAPTIVE CONTROL ALLOCATION PROBLEMS

A THESIS SUBMITTED TO

THE GRADUATE SCHOOL OF ENGINEERING AND SCIENCE

OF BILKENT UNIVERSITY

IN PARTIAL FULFILLMENT OF THE REQUIREMENTS FOR

THE DEGREE OF

MASTER OF SCIENCE

IN

MECHANICAL ENGINEERING

By

Ozan Temiz

September 2018

DEVELOPMENT OF CONTROL ORIENTED VEHICLE MODELS AND THEIR APPLICATION TO ADAPTIVE CONTROL ALLOCATION PROBLEMS

By Ozan Temiz

September 2018

We certify that we have read this thesis and that in our opinion it is fully adequate, in scope and in quality, as a thesis for the degree of Master of Science.

Melih Çakmakcı(Advisor)

Yıldıray Yıldız

Kerem Bayar

Approved for the Graduate School of Engineering and Science:

Ezhan Karaşan
Director of the Graduate School

ABSTRACT

DEVELOPMENT OF CONTROL ORIENTED VEHICLE MODELS AND THEIR APPLICATION TO ADAPTIVE CONTROL ALLOCATION PROBLEMS

Ozan Temiz
M.S. in Mechanical Engineering
Advisor: Melih Çakmakcı
September 2018

Emerging vehicle control systems have increased the need for valid vehicle models. In this study, two controller oriented vehicle models are developed and linearized for easier controller design. These models are validated by using an advanced vehicle simulation commercial suite. Then by using these models, an adaptive, fault-tolerant control allocation method which simultaneously commands all traction and steering related actuators is developed. The proposed control scheme consists of a high level controller that creates a virtual control input vector and a low level control allocator that distributes the virtual control effort among redundant actuators. Virtual control input consists of desired forces and moments to ensure stability while following a given reference. Based on this virtual control input vector, the allocation module determines actuator inputs. Performance of the proposed system is evaluated via an object avoidance maneuver in various scenarios such as different velocities and effectiveness loss at actuators. Results show that the proposed approach can follow the references despite the loss of actuator effectiveness in the driving cycle.

Keywords: Vehicle modeling, Control-oriented, Adaptive control allocation.

ÖZET

KONTROLE YÖNELİK ARAÇ MODELLEME VE ADAPTİF KONTROL UYGULAMASI

Ozan Temiz
Makine Mühendisliği, Yüksek Lisans
Tez Danışmanı: Melih Çakmakcı
Eylül 2018

Araçlardaki, kontrol ve sürücü yardım sistemlerinin gelişmesi endustride araç sistemini doğru temsil eden matematik model ihtiyacını arttırmıştır. Bu çalışmada, bahsi geçen probleme değinmek adına iki adet kontrolcü geliştirmeye yönelik araç modeli geliştirilmiş ve sonrasında da lineerize edilmiştir. Geliştirilen lineer ve lineer olmayan modeller endustriyel bir program ile doğrulanmıştır. Daha sonrasında ise geliştirilen modeller özgün bir adaptif kontrol dağıtımı sistemi kurulmasında kullanılmıştır. Geliştirilen adaptif kontrol dağılım sistemi aracın tüm aktüatörlerini eşzamanlı olarak kontrol etmekte ve sistemde gerçekleşebilecek olası arızaları tolore edebilmektedir. Bu sistem iki kademeden oluşmaktadır. İlk aşamada adaptif kontrol dağıtımı için gerekli olan sanal kontrol girdisi vektörü oluşturulmakta, daha sonrasında ise bu vektör aktüatörlerin girdilerine karar verilmesinde kullanılmaktadır. Geliştirilen sistemin performansı çeşitli hızlarda ve arıza koşullarında bir kaçış manevrası ile değerlendirilmiştir. Sonuçlar göstermektedir ki önerilen sistem verilen referansları sistemdeki etkinlik kaybı durumlarında bile takip edebilmektedir.

Anahtar sözcükler: Kontrole yönelik, Araç modelleme, Adaptif, Kontrol.

Acknowledgement

First of all, I would like to express my sincere gratitude to my valuable advisor Melih Çakmakcı for his unflagging professional and personal support throughout my graduate study. Thanks to his guidance I not only improved my knowledge about control engineering, but also I learned beyond the academics which will help me in my entire life.

I want to thank Yıldıray Yıldız for the constant guidance and advices that thought me learning the theory underneath the applications. I thank to Kerem Bayar for being in my thesis committee, his time and his valuable suggestions. I also thank to Shahab Tohidi for his time and great advices that help me go through this research.

This study had its ups and downs and It would be very hard to earn this degree without the support of my friends. I thank Muge Özcan for her unmatched accompany and her teachings about life's instability and uncertainty. I have special thanks to Mert Yüksel and Cem Kurt for one being great roommate, one being great mentor and both being great friends and cyclists. I praise Murat Yücel Arslan for his miles long stories and friendship. I appreciate Orhun Ayar for being good listener and Dilara Uslu for her unique support. I want to acknowledge Cem Aygül, Levent Dilaveroğlu, Mehmet Kelleci, Hande Aydoğmus and Selçuk Erbil for their comfort and friendship.

I wish to thank to family, Ayşe Temiz, Turhan Temiz, Bilge Temiz and Zehra Afacan for all the opportunities they provided me by hard work and sacrifice. Nothing would be possible without them on my back. I thank all of them for being the greatest and their unlimited patience. I also want to thank to Peri for her unconditional love.

Lastly I want to praise Matlab, for the Simulink, matrix operations, integrals and the most important of all 'help' command.

Contents

List of Figures

List of Tables

Chapter 1

Introduction

1.1 Vehicle Modeling

Increasing competition in the automobile industry motivates companies to develop better cars. Due to this competition, slight differences in handling, comfort and safety systems may cause consumers to prefer one vehicle over another. In modern engineering projects such as vehicle development, model based system development methods can be used to handle complexity and performance. Therefore, development of accurate mathematical models of vehicle is critical for the later stages of the design process.

Dynamic motion of the vehicle body and its components is studied by many researchers. In [1], a two track reduced vehicle model is developed by using vehicle's side slip angle as a model state to focus on lateral stability. Moreover, in books such as [2, 3, 4] bicycle model (shown in Fig. 1.1) is used to evaluate vehicle dynamics. Parameters for bicycle model can be found in Table 1.1. In these sources quarter or half car models are also presented to investigate driver comfort. Neglecting one dynamic behavior of the vehicle such as vertical motion results in simplifications for mathematical model. However, this may affect the fidelity of the mathematical model reducing the validity of the simulation results.

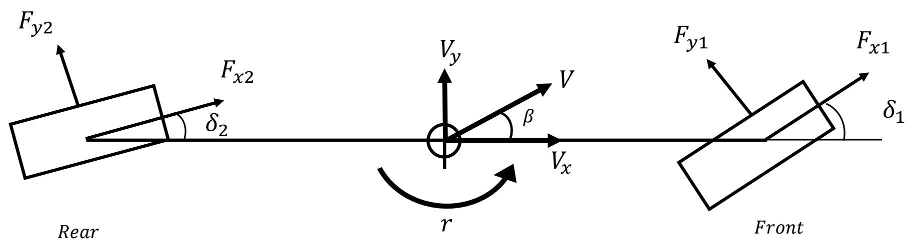

Figure 1.1: Bicycle Vehicle Model

For example in case of bicycle model, roll and pitch dynamics of the vehicle is neglected and normal forces at each wheel are approximated. As a result, friction forces used in longitudinal and lateral motions are also approximated. Because emergency maneuvers usually include extreme steering and brake/throttle input, those approximations are not accurate. Thus, more detailed vehicle model is needed.

Table 1.1: List of Bicycle Model Variables

δ_i	Steering angle at i^{th} wheel where $i \in \{1,2\}$
F_{xi}	Longitudinal force at i^{th} wheel where $i \in \{1,2\}$
F_{yi}	Lateral force at i^{th} wheel where $i \in \{1,2\}$
V_x	Longitudinal Velocity
V_y	Lateral Velocity
r	Yaw Rate

There are frequently used commercial software packages that offer vehicle models with various complexities. In Adams Car [5] a non-linear mathematical dynamic model of a vehicle can be obtained with great complexity that includes the details of the subsystems of a car including steering and suspension parts. This kind of vehicle models can represent the real vehicle behavior very well, however their mathematical complexity increases the solution time. Therefore they are usually better for component design. On the other hand, Carsim [6] and Amesim [7] in Fig. 1.2 use a simpler approach for vehicle modeling. In these programs,

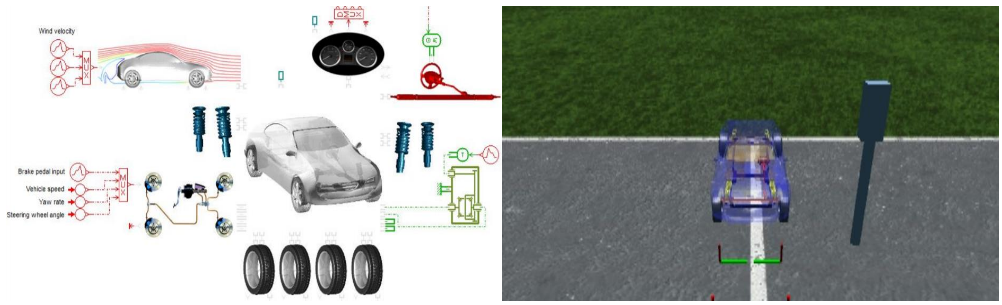

(a) Amesim iCar

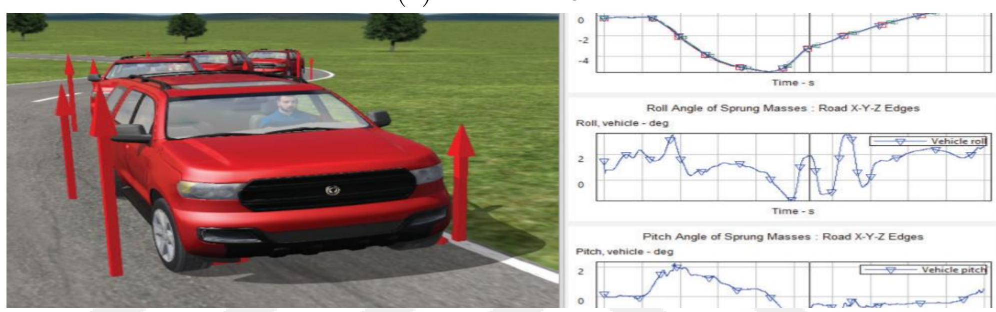

(b) Carsim

Figure 1.2: Commercial Vehicle Simulation Software

vehicles are modeled with lesser degrees of freedom which still allows representing the coupling between vertical, lateral and longitudinal dynamics of a vehicle but still they can provide fast solution. These models are usually used for evaluation of the whole system. In particular, Amesim iCar includes 15 degree of freedom; all three rotations and translations of the vehicle body and one rotational and one translational degree of freedom for each tire and rotation of the steering system. However, since these mathematical models are not open for the user, equations of motion for detailed vehicle model is still required. For this purpose some vehicle models are presented in various sources such as [8, 9, 10] and [11]. Knowledge of equations from such models allows better understanding of vehicle dynamics therefore better design of vehicle parameters and components. Moreover a control oriented vehicle model that integrates the different sub-systems of the vehicle is also important for developing stability and driver assistance controllers.

Typically, for fuel economy simulations, only longitudinal vehicle dynamics are considered. However, to correctly estimate load forces acting on the motor and traction forces more detailed models are required. For example, type of

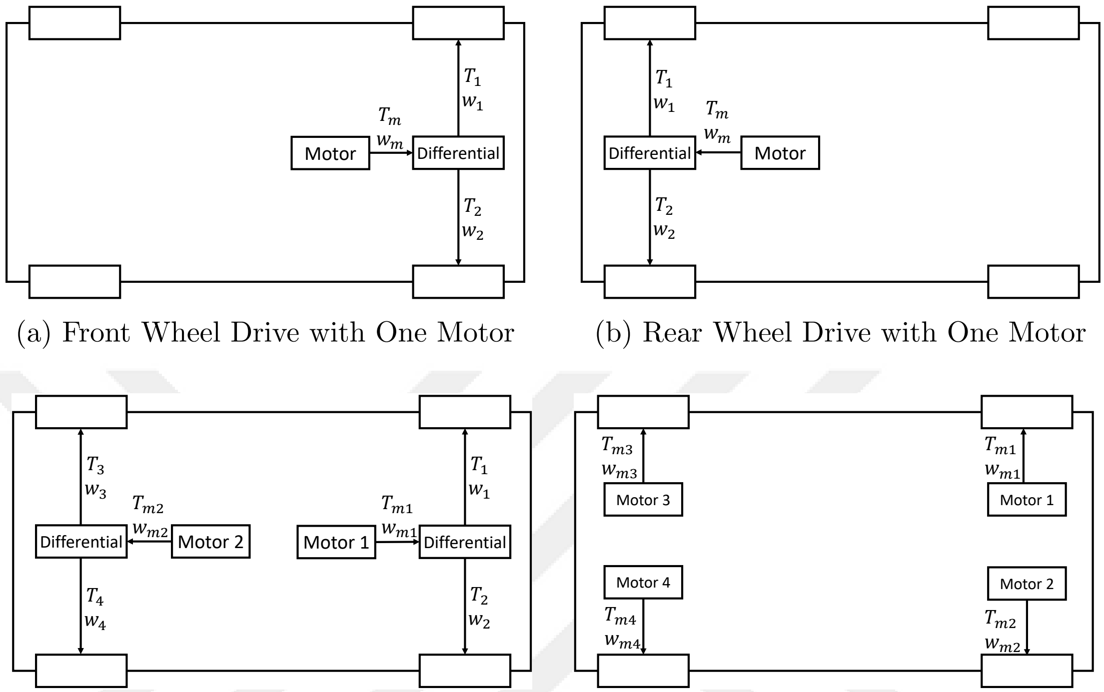

(a) Front Wheel Drive with One Motor

(b) Rear Wheel Drive with One Motor

(c) Four Wheel Drive with Two Motors

(d) Four Wheel Drive with Four Motors

Figure 1.3: Some of the Possible Power Delivery Options

power delivery to the wheels in Fig 1.3 affects the fuel economy and without the wheel dynamics it is not possible to correctly model the power delivery and the resistance coming from the wheels. Also, normal forces acting on each tire is critical because it effects the load transferred to the motor which affects the efficiency. It is not possible to model the normal forces accurately without the vertical model. Therefore, it is possible to evaluate the fuel economy better with a more detailed model that includes vertical and longitudinal portions of the vehicle motion.

Choosing suspension parts and designing a suspension system is a challenging part of the vehicle design process. In [12, 13] vertical vehicle models and active suspension controllers are developed. However comfort is not the only criteria for the design of suspension systems due to the their effect on the vehicle handling. Therefore, vertical dynamics of a vehicle should be studied in a model which also includes handling model. This enables controlling normal forces at each wheel for handling purposes and creating better traction.

In recent years, cheaper and better performing sensors are developed and computation capability of vehicles are increased. These developments allowed advanced vehicle stability controllers such as assisted braking system (ABS), electronic stabilization program (ESP) and advanced driver assistance (ADAS) and autonomous vehicle systems to develop [9]. Stability of a vehicle can be investigated in three forms. First, vehicle should be able to stop in different road conditions longitudinally. Second, vehicle should be stable during cornering and emergency maneuvers. Cornering stability of the vehicle is closely related to side-slip angle of the vehicle [14]. Side-slip angle is the angle between total velocity, which is composed of longitudinal and lateral velocity, and longitudinal velocity of the vehicle. Stability systems usually regulates the side-slip angle. Lastly, for vertical stability, vehicle should be able to maintain the contact between road and tires. Roll over prevention systems in commercial, agricultural and off-road vehicles plays important role for their stability. Some of the strategies for the roll over prevention systems can be found in [15] and [16]. Primary stability control systems used in automobiles can be listed as:

- **Assisted Braking System (ABS):** By measuring the rotational velocities and controlling the brakes at each wheel, ABS tries to maximize the friction coefficient at each wheel such that stopping distance of the vehicle is reduced. Some of the strategies for the ABS can be found in [17, 18, 19]. Valid tire models and load transfer models are required to develop ABS systems.

- **Electronic Stability Program (ESP):** By using the inertial sensors, wheel velocity sensors and individual brakes, this system stabilizes the vehicle when the side-slip angle of the vehicle is in critical state. In the literature there are various strategies for electronic stability control such as the ones given in [20] and [21]. For ESP system development lateral dynamics of the vehicle should be modeled.

Moreover, with more advanced sensors such as LIDAR and Radar, ADAS systems are developed. These systems can be used for increasing the comfort or safety.

Increasing competition in the industry forced companies to develop these kind of systems to maintain their market share. To develop functioning ADAS, Accurate vehicle models. Some of the ADAS can be listed as:

- **Adaptive Cruise Control:** This system measures the distance and the rate of change of distance between two vehicles and adjusts vehicle velocity accordingly. Proper operation requires good representation of longitudinal dynamics.
- **Lane Keep Assist:** By detecting lanes on the road, this system assists the driver by warning them or helps steer the vehicle into the lane. Quality monitoring of the lateral vehicle dynamics is required.
- **Collision Prevention Assist:** Similar to the adaptive cruise control, this system measures the distance between vehicles. When the relative velocity of the vehicle is high, system warns the driver and applies the emergency brake if necessary. Good representation of longitudinal and tire dynamics are required to calculate for the safe stopping distance.

With advanced vehicle systems new controllers are introduced to the vehicles and need for detailed vehicle models has increased. Since vehicle states affects each other, valid vehicle model should be considered as whole instead of separate longitudinal, lateral and vertical dynamic models.

1.2 Vehicle Controllers and Control Allocation

Over the past two decades, there have been many advancements in the automotive field with the increased interaction of vehicle subsystems that are traditionally designed separately. Vehicle communication networks, low-cost sensors and dependable mechatronic actuators play an important role in this new trend, which leads to designing the vehicle as a single mechatronic system, generating redundancies in control problems [2, 22]. Because there are various actuators in the vehicle and different dynamics of the vehicle is closely related with each other integrated vehicle control algorithms such as [23, 24, 25, 26] are proposed. In the literature the way to control over-actuated systems is called control allocation.

One example of this redundancy can be seen when yaw rate control (i.e. regulation of rotation of the vehicle about the z-axis) in vehicle stability control is considered. Recently, electric in-wheel motors are getting popular which leads to an increased ability of traction control at each wheel. Using torque vectoring, traction controllers can regulate the yaw rate of the vehicle by changing the torque at each wheel. Four-wheel steering is another way of affecting the yaw rate in passenger vehicles. This technology is starting to become feasible due to dependable actuators at lower costs and control strategies for the four wheel steering. In the literature strategies for four wheel steered vehicles are proposed such as [27, 28].

There are a few examples of control development in automotive literature that exploits the redundancy provided by alternative actuation methods. In [29], wheel cost minimization based integrated traction and four wheel steering control is proposed. More recently, in [30], Tavasoli proposed an optimization algorithm including rear wheel steering and brakes to achieve vehicle control objectives. In [31], a robust approach for fault tolerance in integrated control of traction forces and active steering is presented. Moreover in [32], presented system can switch between to different optimal control allocation schemes in order to compensate the fault. In [22], a concurrent controller structure that regulates both the energy management and traction control for parallel hybrids was proposed. An important challenge to exploit these redundancies is to find common approaches that will work in most vehicle problems and to overcome the computational complexity due to the increased number of objectives and constraints originating from the subsystem design problems.

Existence of two additional actuation methods besides the conventional front wheel steering to create yaw moment around vehicle presents an interesting but more complicated control allocation problem for automotive systems.

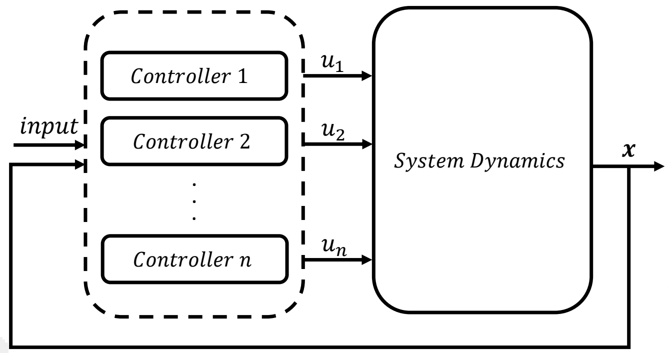

(a) System Controlled with Conventional Controller

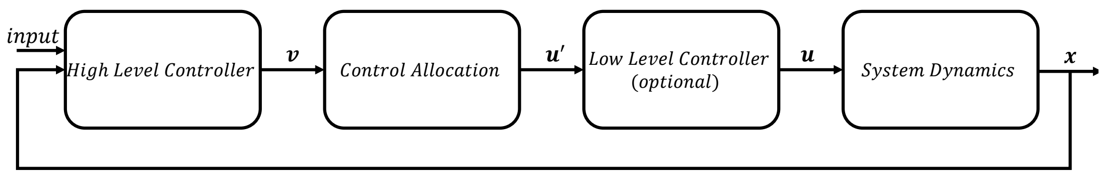

(b) System Controlled with Control Allocation Algorithm

Figure 1.4: Conventional Control and Control Allocation

Control allocation is widely used in flight control to distrubite control inputs among the redundant actuators[33]. Main advantage of use of control allocation over the other control schemes is its capacity to compensate the faults by using other available actuators [34]. The control scheme for over-actuated systems are usually composed of three levels. In the first level virtual control input is determined by high level controllers (i.e. forces and moments) in order to meet the overall motion control objectives [35]. In the middle level control allocation takes place which is a systematic approach where a virtual control effort is distributed among redundant actuators [36]. Finally, if necessary low level controllers determines the actuator inputs depending on the allocation output. General block diagram of control allocation and traditional control can be seen in Fig. 1.4 One example of such methods is given for vehicle control in [37], where the approach presented in [38] is used. Typically, controllers feature allocation contain two sequential calculation steps. In the first step, the overall control effort is calculated using conventional control methods. This effort is then distributed to available actuators as the second step. A detailed survey of recent work about control allocation explaining various methodologies can be found in [35].

1.3 Motivation and Contribution

As tradionally mechanical vehicles transitioned to complex mechatronic systems over the recent years, the role of controllers in vehicle performance have increased. In this work, our objective is to develop tools (models and controller synthesis) in order to fully utilize the control action that are available in these new generation of modern vehicles. When using analytical methods, the performance of the control system highly depends on the vehicle model that is used during the development phase. Developing an accurate mathematical representation of a dynamical system is a challenge and may often result in computationally bloated with unnecessary features. An accurate and detailed model of a system increases the overall performance of the designed system if it also considers interactions between different sub-system dynamics. Main motivation of this thesis is to develop valid modular vehicle models and a novel vehicle stability controller that simultaneously controls the different subsystems of the vehicle.

The primary contributions of this thesis can be given as development of a modular control oriented non-linear and linear mathematical vehicle models and a new adaptive control allocation method for vehicle stability control. First, a two track handling model with three degrees of freedom is developed. Including of two track allows normal force calculation in each tire but this model still neglects the wheel and vertical dynamics. To develop a more accurate mathematical model these dynamics are included the model and 14 degrees of freedom vehicle model is developed. The proposed non-linear mathematical models here also linearized for ease of controller development. Then an adaptive control allocation system is developed by solving a yaw rate and vehicle acceleration feedback control problem first and then allocating the calculated controller effort to wheel, steering and suspension actuators by solving an adaptive control allocation problem. The crucial and perhaps life saving benefits of this new controller for the cases where vehicle dynamics parameters vary during operation and/or device failures is also demonstrated using complex model simulations.

In the next section of this thesis, control oriented mathematical models will be developed and validated. Then, later in the thesis an adaptive allocation algorithm will be developed to control the steering angles and traction forces. In the Chapter 4, the proposed adaptive control allocation algorithm will be applied on 14 degrees of freedom vehicle model to add active suspension control action. Furthermore, formulation of the controller will be modified to include some of the non-linearities in the vehicle. Lastly conclusion and future work will be presented.

Chapter 2

Vehicle Modeling

Vehicles can be modeled as rigid bodies connected to each other with basic mechanical elements such as springs and dampers [11]. In this chapter two vehicle models are presented. First, the coordinate system is selected for the problem. Then, 3 degrees of freedom vehicle model with two track is developed to be used in simple lateral stability control design problems. Finally, 14 degree of freedom vehicle model, which incorporates tire and vertical dynamics to previous model for more detailed analysis and active suspension design will be presented.

2.1 Coordinate System

Two coordinate systems will be used to derive the vehicle model as it can be seen at Fig. 2.1. Equations for the model will be developed for non-inertial vehicle frame by using the inertial frame. Position of the vehicle can be expressed as

$$\mathbf{R} = \eta_x \mathbf{x} + \eta_y \mathbf{y}, \tag{2.1}$$

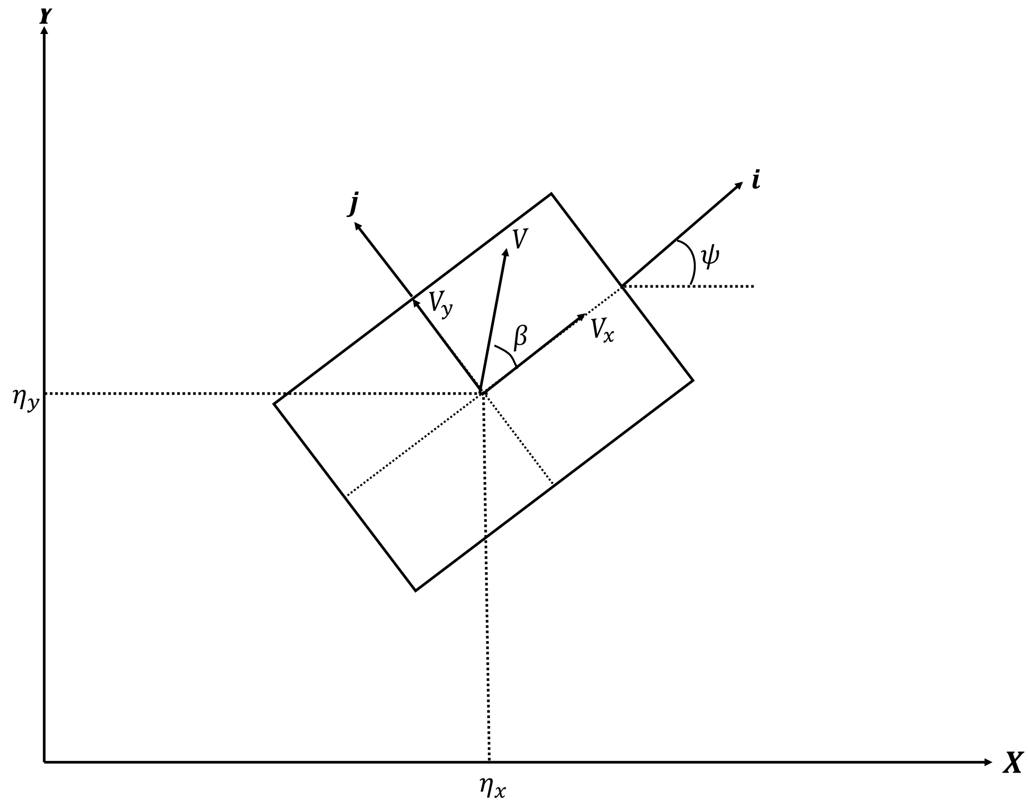

Figure 2.1: Coordinate System

where η_x, η_y are distances from the origin, **x** and **y** are unit vectors of the inertial frame. Inertial unit vectors can be expressed in non-inertial vehicle frame as

$$\begin{aligned}\mathbf{x} =& cos\psi\ \mathbf{i} - sin\psi\ \mathbf{j} \\ \mathbf{y} =& cos\psi\ \mathbf{j} + sin\psi\ \mathbf{i}\end{aligned} \tag{2.2}$$

where ψ is yaw degree, **i** and **j** are unit vectors of the non-inertial vehicle frame. Substituting (2.2) in (2.1), vehicle position can be expressed as

$$\mathbf{R} = (\eta_x cos\psi + \eta_y sin\psi)\mathbf{i} + (\eta_y cos\psi - \eta_x sin\psi)\mathbf{j} \tag{2.3}$$

Taking time derivative of (2.1) and expressing V_x and V_y in Fig. 2.1 as

$$\begin{aligned}V_x &= \dot{\eta}_x cos\psi - \dot{\eta}_y sin\psi \\ V_y &= \dot{\eta}_y cos\psi + \dot{\eta}_x sin\psi,\end{aligned} \tag{2.4}$$

velocity of the vehicle can be expressed as

$$\mathbf{V} = V_x \ \mathbf{i} + V_y \ \mathbf{j}. \tag{2.5}$$

Acceleration of the vehicle body with respect to non-inertial frame can be found by using the formula

$$\dot{\mathbf{V}} = \frac{d^2\mathbf{R}}{dt^2} = \frac{d\mathbf{V}}{dt} + \boldsymbol{\Omega} \times \mathbf{V}. \tag{2.6}$$

Where $\boldsymbol{\Omega}$ corresponds to yaw rate r which is equal to

$$\mathbf{r} = \boldsymbol{\Omega} = \dot{\psi}\mathbf{k}. \tag{2.7}$$

Substituting (2.5) and (2.7) in (2.6) acceleration of vehicle body can be found as.

$$\dot{\mathbf{V}} = (\dot{V}_x - \dot{\psi}V_y)\mathbf{i} + (\dot{V}_y + \dot{\psi}V_x)\mathbf{j} \tag{2.8}$$

2.2 3 Degrees of Freedom Vehicle Model

In this section computationally simpler 3 degree of freedom vehicle model will be developed. The schematic representation for the two-track vehicle model can be seen in Fig. 2.2 explaining the forces acting on the vehicle and the related geometrical relationships. The variables that describe the states of the vehicle model are assumed as the longitudinal velocity V_x, the lateral velocity V_y , and the yaw rate r. The dynamic equations describing the motion of the vehicle can be developed by using the physical relationships shown in Fig. 2.2.

Based on the diagram given in Fig. 2.2 the net forces on the vehicle in x- and y- directions can be calculated as shown in (2.9) and (2.10).

$$f_x = \sum_{i=\{f,r\}} \sum_{j=\{l,r\}} F_{xij} \tag{2.9}$$

$$f_y = \sum_{i=\{f,r\}} \sum_{j=\{l,r\}} F_{yij} \tag{2.10}$$

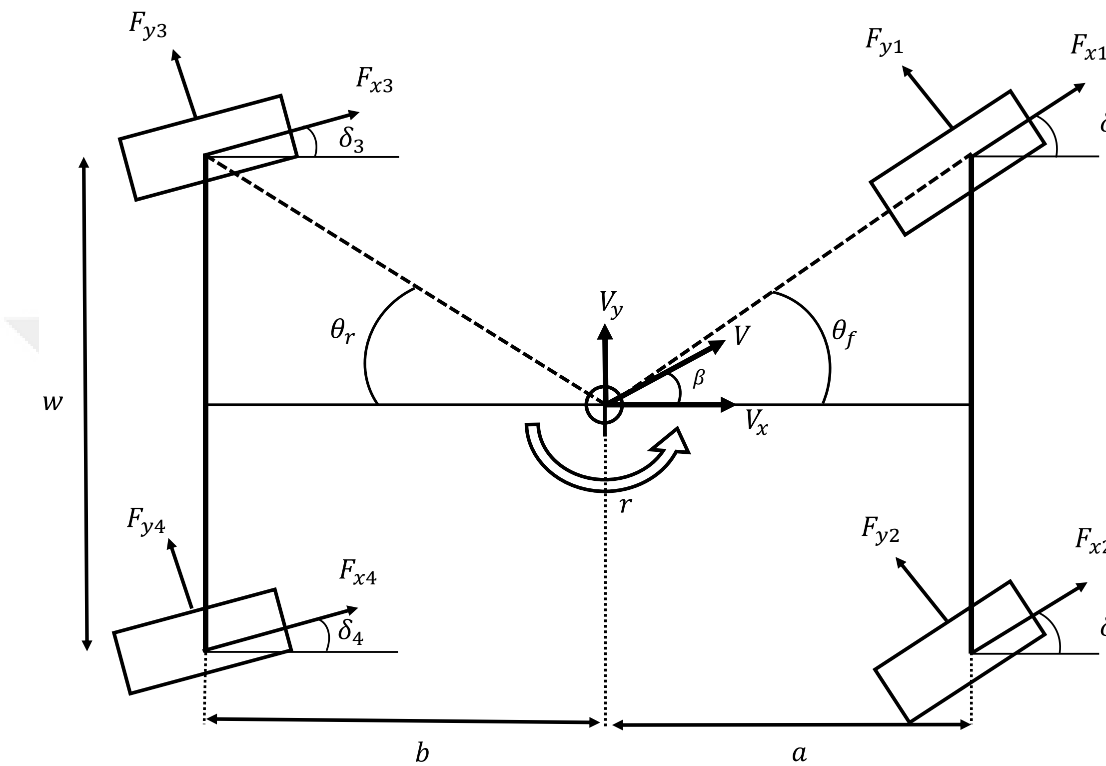

Figure 2.2: Longitudinal and Lateral Vehicle Dynamics

The contribution to (2.9) and (2.10) from each wheel can be calculated using the force acting on each wheel and the steering angles, δ_1 and δ_2 for front and rear wheels respectively as shown in (2.11).

$$
\begin{aligned}
F_{xfl} &= F_{x1}cos\delta_1 - F_{y1}sin\delta_1 \\
F_{yfl} &= F_{y1}cos\delta_1 + F_{x1}sin\delta_1 \\
F_{xfr} &= F_{x2}cos\delta_2 - F_{y2}sin\delta_2 \\
F_{yfr} &= F_{y2}cos\delta_2 + F_{x2}sin\delta_2 \\
F_{xrl} &= F_{x3}cos\delta_3 - F_{y3}sin\delta_3 \\
F_{yrl} &= F_{y3}cos\delta_3 + F_{x3}sin\delta_3 \\
F_{xrr} &= F_{x4}cos\delta_4 - F_{y4}sin\delta_4 \\
F_{yrr} &= F_{y4}cos\delta_4 + F_{x4}sin\delta_4,
\end{aligned}
\tag{2.11}
$$

where F_{xi} and F_{yi} are longitudinal and lateral force (i.e in the direction of the non-inertial frame) at i^{th} tire where $i \in \{1, 2, 3, 4\}$. The acceleration of the vehicle in vehicle coordinate frame can be calculated using the total force acting on the system.

$$a_x = \frac{1}{m}[f_x - \frac{1}{2}C_d \rho A_f V^2 - mgsinQ], \tag{2.12}$$

where C_d is drag coefficient, ρ is air density, A is frontal area of the vehicle, Q is road slope and m is mass of the vehicle. To find non-inertial car frame rate of longitudinal velocity change $\dot{V}_x$ use the equation (2.8):

$$\dot{V}_x = a_x + V_y r, \tag{2.13}$$

where V_y is non-inertial car frame lateral velocity and $r = \dot{\psi}$ is yaw rate of the vehicle. Similarly, lateral acceleration a_y of the vehicle can be calculated as

$$a_y = \frac{1}{m}[f_y] \tag{2.14}$$

By using the equation (2.8), non-inertial lateral velocity change $\dot{V}_y$ can be calculated as

$$\dot{V}_y = a_y - V_x r, \tag{2.15}$$

Side-slip angle β which is result of longutidunal and lateral velocity can then be calculated as

$$\beta = atan\left(\frac{V_x}{V_y}\right) \tag{2.16}$$

Furthermore the derivative of yaw rate, $\dot{r}$, can be calculated as

$$\dot{r} = \frac{1}{J_z}[\frac{w}{2}(F_{x2} + F_{x4} - F_{x1} - F_{x3}) + (F_{y1} + F_{y2})a - (F_{y3} + F_{y4})b], \tag{2.17}$$

where I_z is moment inertia about z axis, w is width of the wheelbase and a, b are distance between center of gravity and front and rear wheels respectively.

Lateral tire forces are calculated based on the slip ratios α_i, depending on the front tires and rear tires

$$\alpha_{1,2} = \delta_1 + \frac{V_y - ar}{V} \tag{2.18}$$

$$\alpha_{3,4} = \delta_2 + \frac{V_y + br}{V}. \tag{2.19}$$

When the slip angles are small, lateral forces can be calculated using the linear relationship as in Fig. 2.4 [2]. Linear lateral friction can be given as (2.20).

$$F_{Yi} = C_\alpha \alpha_i N_i \tag{2.20}$$

where C_α is the linearized lateral friction coefficient and N_i is the normal force acting on the i^{th} tire which is calculated by using vehicle geometry and moment balance around the vehicle assuming that center of gravity of the vehicle lies at $w/2$, 2D load transfer can be given as shown in (2.21).

$$\begin{aligned}
N_1 &= \frac{m(gb - a_x - a_y)}{2L} \\
N_2 &= \frac{m(gb - a_x + a_y)}{2L} \\
N_3 &= \frac{m(ga + a_x - a_y)}{2L} \\
N_4 &= \frac{m(ga + a_x + a_y)}{2L}
\end{aligned} \tag{2.21}$$

For $C_\alpha N_i$ multiplication to be linear effect of the accelerations on mass transfer can be neglected and equations for normal force can be simplified as

$$\begin{aligned}
N_f &= \frac{mgb}{2L} \\
N_r &= \frac{mga}{2L}.
\end{aligned} \tag{2.22}$$

For the longitudinal tire forces, F_{Xi} the effect of longitudinal slip dynamics is neglected. Using equations (2.18) - (2.20) and incorporating small angle assumptions, expressions in (2.11) can be linearized as shown in (2.23).

$$\begin{aligned}
F_{xfl} &= F_{x1} \\
F_{yfl} &= C_{\alpha f} \alpha_1 N_f \\
F_{xfr} &= F_{x2} \\
F_{yfr} &= C_{\alpha f} \alpha_2 N_f \\
F_{xrl} &= F_{x3} \\
F_{yrl} &= C_{\alpha r} \alpha_3 N_r \\
F_{xrr} &= F_{x4} \\
F_{yrr} &= C_{\alpha r} \alpha_4 N_r
\end{aligned} \tag{2.23}$$

3 degree of freedom nonlinear model given in (2.5)-(2.23) can be linearized around a constant velocity V_0 by assuming small side slip and steering angles. With these assumptions slip functions are linearized as well as equations of motions of the vehicle. Combining (2.5) - (2.17) a linear state space representation of the reduced two track model can be obtained as

$$\dot{\mathbf{x}} = \mathbf{A}\mathbf{x} + \mathbf{B_u}\mathbf{u_s} \tag{2.24}$$

where, $\mathbf{A}$, $\mathbf{B_u}$, $\mathbf{x}$ and $\mathbf{u_s}$ are given as

$$\mathbf{A} = \begin{bmatrix} 0 & 0 & 0 \\ 0 & \frac{C_{\alpha f}}{mV_0}(2N_f + 2N_r) & \frac{C_{\alpha r}}{mV_0}(2bN_r - 2aN_f) \\ 0 & \frac{C_{\alpha f}}{J_zV_0}(2aN_f - 2bN_r) & -\frac{C_{\alpha r}}{J_zV_0}(2a^2N_f + 2b^2N_r) \end{bmatrix} \tag{2.25}$$

$$\mathbf{B_u} = \begin{bmatrix} 0 & 0 & 0 & 0 & \frac{1}{m} & \frac{1}{m} & \frac{1}{m} & \frac{1}{m} \\ \frac{C_{\alpha f}N_f}{m} & \frac{C_{\alpha f}N_f}{m} & \frac{C_{\alpha r}N_r}{m} & \frac{C_{\alpha r}N_r}{m} & 0 & 0 & 0 & 0 \\ \frac{C_{\alpha f}N_f a}{J_z} & \frac{C_{\alpha f}N_f a}{J_z} & -\frac{C_{\alpha r}N_r b}{J_z} & -\frac{C_{\alpha r}N_r b}{J_z} & -\frac{w}{2J_z} & \frac{w}{2J_z} & -\frac{w}{2J_z} & \frac{w}{2J_z} \end{bmatrix} \tag{2.26}$$

$$\mathbf{x}^T = \begin{bmatrix} V_x & V_y & r \end{bmatrix} \tag{2.27}$$

$$\mathbf{u_s}^T = \begin{bmatrix} \delta_1 & \delta_2 & \delta_3 & \delta_4 & F_{x1} & F_{x2} & F_{x3} & F_{x4} \end{bmatrix} \tag{2.28}$$

2.3 14 Degrees of Freedom Vehicle Model

In this section a more detailed vehicle model is developed. Additional to the previously developed model this model includes wheel dynamics, non-linear friction dynamics and vertical dynamics of the vehicle. Equations for longitudinal, lateral and yaw accelerations can be found in (2.12) - (2.17). In this model lateral and longitudinal dynamics are non-linear. Therefore F_{xi} and F_{yi} are non-linear functions of slip.

2.3.1 Tire Friction Model

Modeling of tire friction is both challenging and critical part of vehicle modeling. In the literature there are two main types of tire models which are theoretical

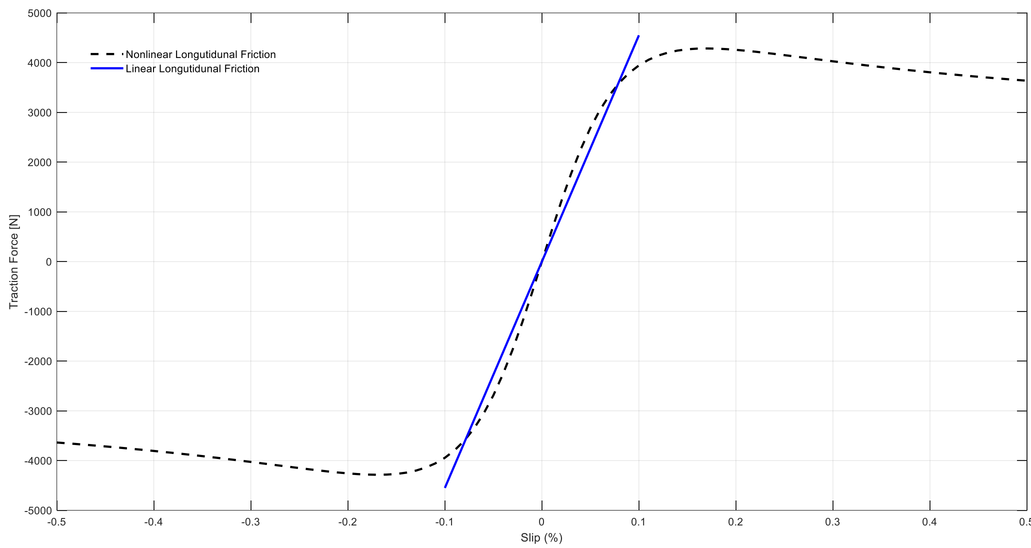

Figure 2.3: Longitudinal Friction versus Slip Ratio

and empirical tire models.

- **Theoretical Models:** These models explains the relationship between tire and road surface via physical equations. These models usually uses strain-stress relationships or friction models such as Lu/Gre and Dahl [39, 40, 41]. Resulting equations usually includes coupled non-linear equations and they can require advanced numerical solution techniques [42].

- **Empirical Models:** These uses experiment results to determine the characteristics of tire such as magic formula [43]. They do not require numerical solver and they are computationally less expensive. Therefore they are preferred for vehicle stability control and handling simulation applications.

In this work Pacejka's Magic formula will be used for friction coefficients. Longitudinal and lateral forces are function of slip ratios. The longitudinal slip

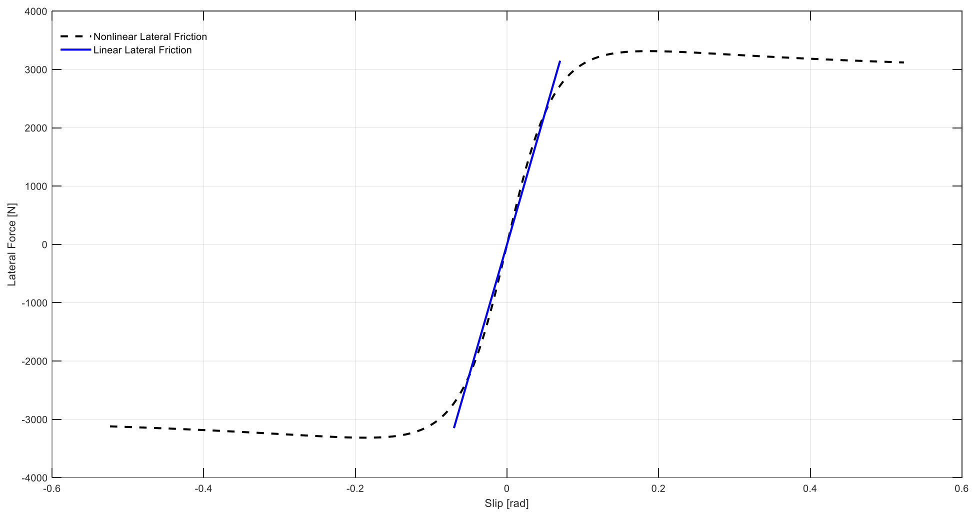

Figure 2.4: Lateral Friction versus Slip Ratio

is defined for driving and braking scenarios separately.

$$\begin{aligned} For\ driving; \quad \lambda_i(V_x, w_i) &= \frac{w_i R - V_x}{w_i r} \\ For\ braking; \quad \lambda_i(V_x, w_i) &= \frac{w_i R - V_x}{V_x}, \end{aligned} \tag{2.29}$$

where, w_i is rotational velocity of i^{th} wheel $i \in [1\ 4]$ and R is radius of wheel. Longitudinal traction force $F_x i$ can then be calculated with magic formula:

$$F_{xi} = D_1 sin[C_1 arctan(B_1\lambda_i - E_1(B_1\lambda_i - arctan B_1\lambda_i))], \tag{2.30}$$

where, resulting longutiunal friction is as in Fig. 2.3. The details of the parameters and tire model the can be found in the [44] and Appendix 1.

Similarly, lateral tire forces are functions of the slip ratios $\alpha_i(V_x, V_y, r)$, which can be calculated as

$$\begin{aligned}
\alpha_1(V_x, V_y, r) &= \delta_f - atan\left(\frac{V_y + r\ a\ cos(\theta_f)}{V_x - r\ a\ sin(\theta_f)}\right) \\
\alpha_2(V_x, V_y, r) &= \delta_f - atan\left(\frac{V_y + r\ a\ cos(\theta_f)}{V_x + r\ a\ sin(\theta_f)}\right) \\
\alpha_3(V_x, V_y, r) &= \delta_r - atan\left(\frac{V_y - r\ b\ cos(\theta_r)}{V_x - r\ b\ sin(\theta_r)}\right) \\
\alpha_4(V_x, V_y, r) &= \delta_r - atan\left(\frac{V_y - r\ b\ cos(\theta_r)}{V_x + r\ b\ sin(\theta_r)}\right)
\end{aligned} \tag{2.31}$$

where δ_f, δ_r are front and rear steering angles respectively and θ_f, θ_r can be seen in Fig. 2.2. The lateral force can then be calculated via the magic formula:

$$F_{yi} = D_2 sin[C_2 arctan(B_2\alpha_i - E_2(B_2\alpha_i - arctan B_2\alpha_i))], \tag{2.32}$$

Where, resulting longitidunal friction is as in Fig. 2.4. The details of the parameters and tire model the can be found in the [44] and Appendix 1. Resulting f_x and f_y can be found by using equation (2.11).

2.3.2 Differential Model

Differential is widely used component of vehicles which divides torque of the motor into certain number of wheels. In this section, traditional open differential is modeled. In Fig. 2.5 function of the differential can be seen. This kind of differential preferred in most of the vehicles due to its low cost. Open differential functions with following properties [45].

- There must be only one relationship between the three speeds; in this way the speed difference between the output shafts is undetermined
- The input torque is split into two output torques, in a constant ratio independent of speed [46].
- The two output torques must have the same direction.

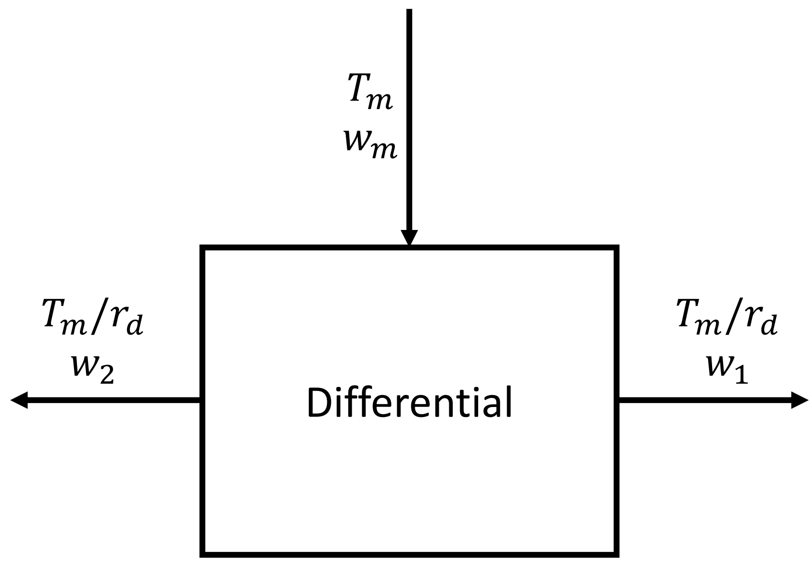

Figure 2.5: Schematic of the Differential

With these properties equations for differential can be written as

$$T_m = T_1 + T_2, \tag{2.33}$$

where T_m is motor torque, T_1 and T_2 are divided torques. Assuming there is no friction in the differential rotational velocity relationship between motor and wheels can be expressed by using the conversation of the energy.

$$T_m w_m = T_1 w_1 + T_2 w_2, \tag{2.34}$$

where w_m is rotational velocity of motor, w_1 and w_2 are divided wheel velocities. In this model, constant split ratio r_d for the motor torque T_m is 2. Therefore, gear ratio is

$$T_1 = T_2 = \frac{T_m}{2} \tag{2.35}$$

2.3.3 Wheel Dynamics

Wheels are responsible for creating the traction forces for vehicle acceleration. As wheel spins with the input torque, rotation starts and resulting slip causes the

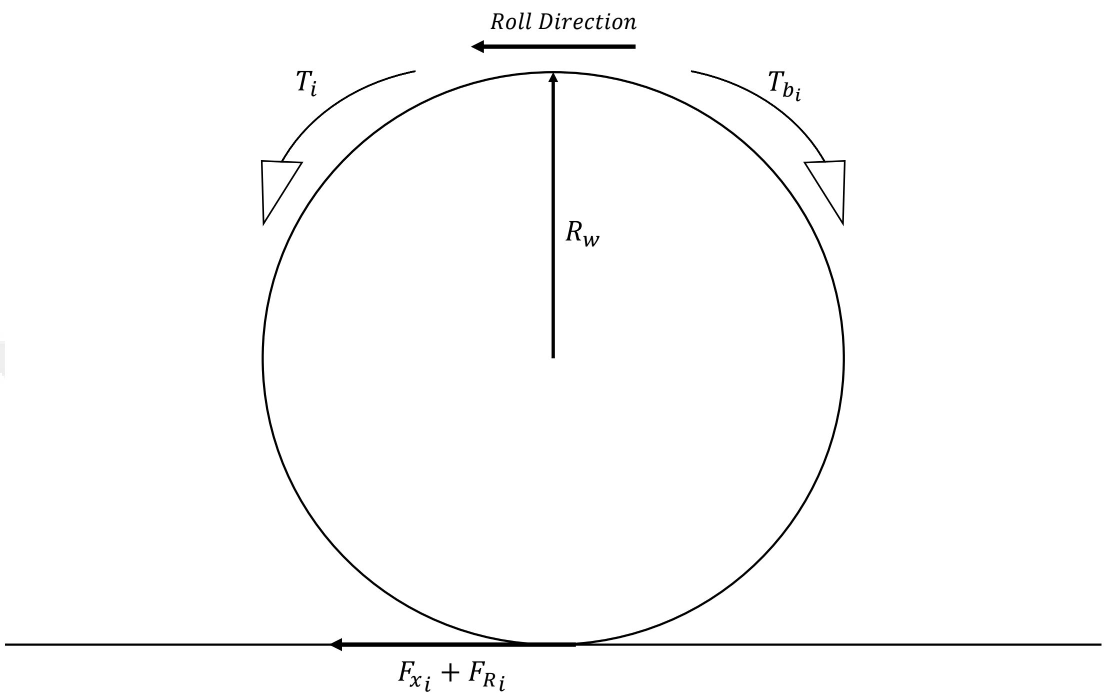

Figure 2.6: Wheel Dynamics

traction force. Degree of freedom of wheels are characterized with their rotational velocity w and equation of motion for wheels can be created by using 2.6 as,

$$I_w \dot{w}_i = T_i - T_{bi} - F_{xi}R - F_{ri}R \tag{2.36}$$

where T_i, T_{bi} are motor and brake torque applied on the i^{th} wheel respectively and F_{ri} is rolling resistance which is a resistance force born from deformable nature of the tire [47]. Rolling resistance can be calculated as

$$F_{ri} = f_0 F_{zi} + f_1 F_{zi}\frac{V_x}{30} + f_2 F_{zi}\frac{V_x^4}{30^4}, \tag{2.37}$$

where, F_{zi} is normal force acting on the i^{th} tire and f_0, f_1, f_2 are coefficients of formula which can be found at [1].

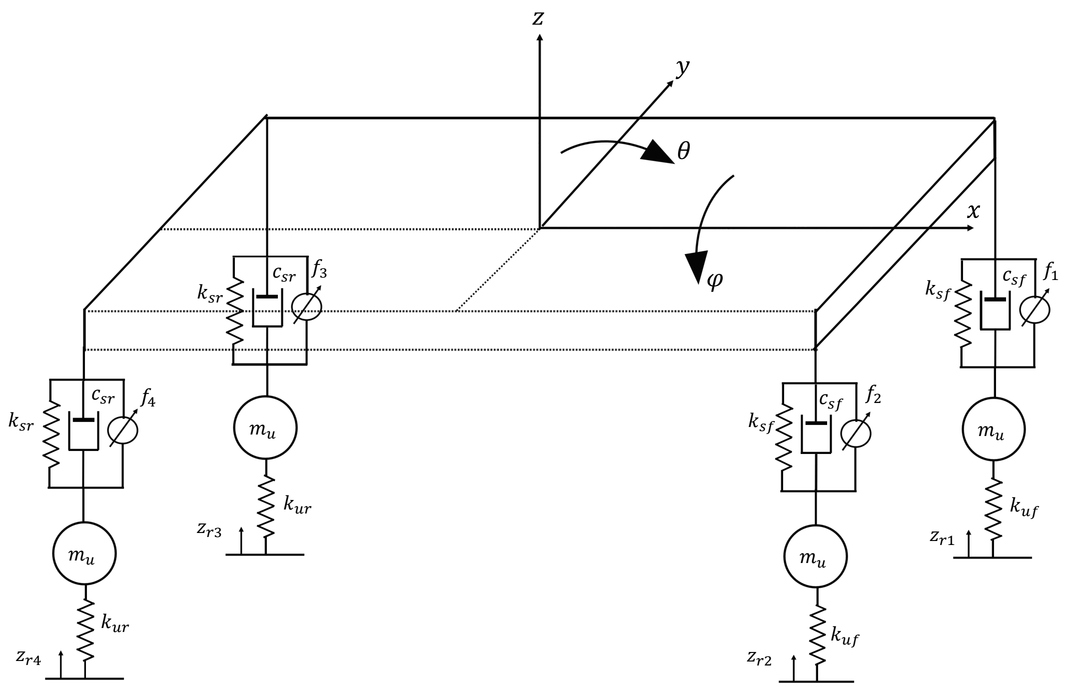

Figure 2.7: Vertical Dynamics

2.3.4 Vertical Dynamics

Vertical model is critical part of vehicle model due to its effect on driver comfort and handling. One of the main challenges of designing a comfortable car is setting suspension parameters for balance between comfort and handling. To achieve this a vertical model which is integrated with handling model is required. In this vertical model suspension system of a car is modeled as linear spring and damper while tire is modeled as spring. Using the (2.14) and Fig. 2.7, heave acceleration ($\ddot{z}$) can be calculated as [13],

$$\begin{aligned} m\ddot{z} &= (2k_{sf} + 2k_{sr})z - (2c_{sf} + 2c_{sr})\dot{z} + (2ak_{sf} - 2bk_{sr})sin\theta \\ &+ (2ac_{sf} - 2bc_{sr})\dot{\theta} + k_{sf}z_{ufl} + c_{sf}\dot{z}_{ufl} + k_{sf}z_{ufr} + c_{sf}\dot{z}_{ufr} \\ &+ k_{sr}z_{url} + c_{sr}\dot{z}_{url} + k_{sr}z_{urr} + c_{sr}\dot{z}_{urr} + f_1 + f_2 + f_3 + f_4 \end{aligned} \tag{2.38}$$

where k_{sf}, c_{sf} are front sprung mass spring and damping coefficients, k_{sr}, c_{sr} are rear sprung mass spring and damping coefficients, z_u is unsprung mass displacement and f_i is active suspension forces at i^{th} wheel of the vehicle where

$i \in [1, 4]$.

Using the Fig. 2.7 and equation (2.12) pitch ($\ddot{\theta}$) rotational acceleration can be calculated as

$$\begin{aligned} I_y\ddot{\theta} = & (2ak_{sf} - 2bk_{sr})z + (2ac_{sf} - 2bc_{sr})\dot{z} - (2a^2k_{sf} + 2b^2k_{sr})sin\theta \\ & - (2a^2c_{sf} + 2b^2c_{sr})\dot{\theta} - ak_{sf}z_{ufl} - ac_{sf}\dot{z}_{ufl} - ak_{sf}z_{ufr} - ac_s\dot{z}_{ufr} \\ & + bk_{sr}z_{url} + bc_{sr}\dot{z}_{url} + bk_{sr}z_{urr} + bc_{sr}\dot{z}_{urr} - ma_xh - af_1 - af_2 \\ & + bf_3 + bf_4 \end{aligned} \tag{2.39}$$

By using Fig. 2.7 and equation (2.14) roll ($\ddot{\phi}$) rotational acceleration can be calculated as

$$\begin{aligned} I_x\ddot{\phi} = & -0.25w^2(2k_{sf} + 2k_{sr})sin\phi + 0.5wk_{sf}z_{ufl} - 0.25w^2(2c_{sf} + 2c_{sr})\dot{\phi} \\ & + 0.5wc_{sf}\dot{z}_{ufl} - 0.5wk_{sf}z_{ufr} - 0.5wc_{sf}\dot{z}_{ufr} + 0.5wk_{sr}z_{url} \\ & + 0.5wc_{sr}\dot{z}_{url} - 0.5wk_{sr}z_{urr} - 0.5wc_{sr}\dot{z}_{urr} - ma_yh \\ & + \frac{w}{2}f_1 - \frac{w}{2}f_2 + \frac{w}{2}f_3 - \frac{w}{2}f_4. \end{aligned} \tag{2.40}$$

Finally, elevation of unsprung mass z_{uij} where $i \in \{f, r\}$ and $j \in \{l, r\}$ can be calculated as

$$\begin{aligned} m_u\ddot{z}_{ufl} = & k_{sf}z + c_{sf}\dot{z} - ak_{sf}sin\theta - ac_{sf}\dot{\theta} + 0.5wk_{sf}sin\phi + 0.5wc_{sf}\dot{\phi} \\ & - (k_{sf} + k_{uf})z_{ufl} - c_{sf}\dot{z}_{ufl} + k_{uf}z_{rfl} - f_1 \end{aligned} \tag{2.41}$$

$$\begin{aligned} m_u\ddot{z}_{ufr} = & k_{sf}z + c_{sf}\dot{z} - ak_{sf}sin\theta - ac_{sf}\dot{\theta} - 0.5wk_{sf}sin\phi - 0.5wc_{sf}\dot{\phi} \\ & - (k_{sf} + k_{uf})z_{ufr} - c_{sf}\dot{z}_{ufr} + k_{uf}z_{rfr} - f_2 \end{aligned} \tag{2.42}$$

$$\begin{aligned} m_u\ddot{z}_{url} = & k_{sr}z + c_{sr}\dot{z} + bk_{sr}sin\theta + bc_{sr}\dot{\theta} + 0.5wk_{sr}sin\phi + 0.5wc_{sr}\dot{\phi} \\ & - (k_{sr} + k_{ur})z_{url} - c_{sr}\dot{z}_{url} + k_{ur}z_{rrl} - f_3 \end{aligned} \tag{2.43}$$

$$\begin{aligned} m_u\ddot{z}_{url} = & k_{sr}z + c_{sr}\dot{z} + bk_{sr}\theta + bc_{sr}\dot{\theta} - 0.5wk_{sr}sin\phi - 0.5wc_{sr}\dot{\phi} \\ & - (k_{sr} + k_{ur})z_{urr} - c_{sr}\dot{z}_{urr} + k_{ur}z_{rrr} - f_4 \end{aligned} \tag{2.44}$$

where, z_r is the road disturbance, m_u is unsprung mass and k_{uf}, k_{ur} are unsprung spring coefficients at front and rear tires.

2.3.5 Linearized 14 Degrees of Freedom Vehicle Model

In this part detailed vehicle model will be linearized and equations of motions for linear model will be developed. The main advantage of the linear model is most of the controller designs methods rely on the linear models. Therefore with the provided equations, easier controller development for vehicles may be possible.

First, friction forces will be linearized then equations of motion will be linearized.

2.3.5.1 Linearization of Friction Forces

Longitudinal slip ratio can be linearized by applying Taylor expansion around V_{x0} and w_0 where $V_{x0} \approx w_0 R$ to equation (2.29).

$$\lambda_{li}(V_x, w) = \frac{w_i R}{V_{x0}} - \frac{V_x}{V_{x0}} \tag{2.45}$$

When the slip ratios are small, longitudinal traction force is linear function of the slip as in Fig 2.3. Longitudinal forces can be calculated using the linear relationship given in (2.46).

$$F_{Xi} = C_\lambda \lambda_i N_i \tag{2.46}$$

where C_λ is the linearized longitudinal friction coefficient and N_i is the normal force acting on the i^{th} tire which is given as shown in (2.21).

Moreover, lateral slip ratio α can be linearized by incorporating with small angle assumption where $atan(\theta) \approx \theta$, assuming small yaw rate r and vehicle longitudinal velocity $V_x \approx V_{x0}$. Applying Taylor expansion with these assumptions linear slip ratios can be written as,

$$\begin{aligned} \alpha_{l1,2}(\delta_f, V_y, r) &= \delta_f - \frac{V_y + r l_f cos(\theta_f)}{V_{x0}} \\ \alpha_{l3,4}(\delta_r, V_y, r) &= \delta_r - \frac{V_y - r l_r cos(\theta_r)}{V_{x0}} \end{aligned} \tag{2.47}$$

where lateral forces F_{yi} can be calculated as given is (2.20).

Drag force F_d can be linearized around V_{x0} by applying Taylor expansion as

$$F_{dl} = \frac{1}{2}\rho C_d A_f V_{x0}^2 - \rho C_d A_f V V_{x0}, \tag{2.48}$$

where ρ is air density, C_d is friction coefficient and A is frontal area of the vehicle.

Lastly, rolling resistance F_{ri} can be linearized by defining a rolling resistance coefficient C_r as

$$F_{ri} = C_r N_i. \tag{2.49}$$

2.3.5.2 Linear Equations of Motion

Longitudinal acceleration (2.12) can be linearized with taylor series around small lateral velocity V_y, yaw rate r and steering angles δ_f, δ_r and incorporating with small angle assumption where $sin(\theta) \approx \theta$ and $cos(\theta) \approx 1$.

$$ma_x = \lambda_1 N_f C_\lambda + \lambda_2 N_f C_\lambda + \lambda_3 N_r C_\lambda + \lambda_4 N_r C_\lambda - F_{dl} - mgQ \tag{2.50}$$

Similarly lateral acceleration (2.14) can be linearized around V_{x0}.

$$ma_y = \alpha_{l1} N_f C_\alpha + \alpha_{l2} N_f C_\alpha + \alpha_{l3} N_r C_\alpha + \alpha_{l4} N_r C_\alpha - V_{x0} r \tag{2.51}$$

Yaw rate (2.17) can be linearized with same assumptions as

$$\begin{aligned} I_z \dot{r} = &-\frac{w}{2}\lambda_1 N_f C_\lambda + \frac{w}{2}\lambda_2 N_f C_\lambda - \frac{w}{2}\lambda_3 N_r C_\lambda + \frac{w}{2}\lambda_4 N_r C_\lambda + a\alpha_l 1 N_f C_\alpha \\ &+ a\alpha_l 2 N_f C_\alpha - b\alpha_l 3 N_r C_\alpha - b\alpha_l 4 N_r C_\alpha \end{aligned} \tag{2.52}$$

Vertical model can be linearized by assuming roll and pitch angles θ and ϕ are small such that $sin\theta \approx \theta$. Resulting equation of motion for heave can be written as

$$\begin{aligned} m\ddot{z} = &(2k_{sf} + 2k_{sr})z - (2c_{sf} + 2c_{sr})\dot{z} + (2ak_{sf} - 2bk_{sr})\theta \\ &+ (2ac_{sf} - 2bc_{sr})\dot{\theta} + k_{sf} z_{ufl} + c_{sf}\dot{z}_{ufl} + k_{sf} z_{ufr} + c_{sf}\dot{z}_{ufr} \\ &+ k_{sr} z_{url} + c_{sr}\dot{z}_{url} + k_{sr} z_{urr} + c_{sr}\dot{z}_{urr} + f_{fl} + f_{fr} + f_{rl} + f_{rr}. \end{aligned} \tag{2.53}$$

Linear pitch rotational acceleration $\ddot{\theta}$ can be calculated as

$$\begin{aligned}I_y\ddot{\theta} &= (2ak_{sf} - 2bk_{sr})z + (2ac_{sf} - 2bc_{sr})\dot{z} - (2a^2k_{sf} + 2b^2k_{sr})\theta \\ &- (2a^2c_{sf} + 2b^2c_{sr})\dot{\theta} - ak_{sf}z_{ufl} - ac_{sf}\dot{z}_{ufl} - ak_{sf}z_{ufr} - ac_s\dot{z}_{ufr} \\ &+ bk_{sr}z_{url} + bc_{sr}\dot{z}_{url} + bk_{sr}z_{urr} + bc_{sr}\dot{z}_{urr} - ma_xh - af_{fl} - af_{fr} \\ &+ bf_{rl} + bf_{rr}.\end{aligned} \tag{2.54}$$

Linear roll rotational acceleration $\ddot{\phi}$ can be calculated as

$$\begin{aligned}I_x\ddot{\phi} &= -0.25w^2(2k_{sf} + 2k_{sr})\phi + 0.5wk_{sf}z_{ufl} - 0.25w^2(2c_{sf} + 2c_{sr})\dot{\phi} \\ &+ 0.5wc_{sf}\dot{z}_{ufl} - 0.5wk_{sf}z_{ufr} - 0.5wc_{sf}\dot{z}_{ufr} + 0.5wk_{sr}z_{url} \\ &+ 0.5wc_{sr}\dot{z}_{url} - 0.5wk_{sr}z_{urr} - 0.5wc_{sr}\dot{z}_{urr} - ma_yh \\ &+ \frac{w}{2}f_{fl} - \frac{w}{2}f_{fr} + \frac{w}{2}f_{rl} - \frac{w}{2}f_{rr}.\end{aligned} \tag{2.55}$$

Finally, linear elevation of unsprung mass z_{uij} where $i \in \{f, r\}$ and $j \in \{l, r\}$ can be calculated as

$$\begin{aligned}m_u\ddot{z}_{ufl} &= k_{sf}z + c_{sf}\dot{z} - ak_{sf}\theta - ac_{sf}\dot{\theta} + 0.5wk_{sf}\phi + 0.5wc_{sf}\dot{\phi} \\ &- (k_{sf} + k_{uf})z_{ufl} - c_{sf}\dot{z}_{ufl} + k_{uf}z_{rfl} - f_{fl}\end{aligned} \tag{2.56}$$

$$\begin{aligned}m_u\ddot{z}_{ufr} &= k_{sf}z + c_{sf}\dot{z} - ak_{sf}\theta - ac_{sf}\dot{\theta} - 0.5wk_{sf}\phi - 0.5wc_{sf}\dot{\phi} \\ &- (k_{sf} + k_{uf})z_{ufr} - c_{sf}\dot{z}_{ufr} + k_{uf}z_{rfr} - f_{fr}\end{aligned} \tag{2.57}$$

$$\begin{aligned}m_u\ddot{z}_{url} &= k_{sr}z + c_{sr}\dot{z} + bk_{sr}\theta + bc_{sr}\dot{\theta} + 0.5wk_{sr}\phi + 0.5wc_{sr}\dot{\phi} \\ &- (k_{sr} + k_{ur})z_{url} - c_{sr}\dot{z}_{url} + k_{ur}z_{rrl} - f_{rl}\end{aligned} \tag{2.58}$$

$$\begin{aligned}m_u\ddot{z}_{url} &= k_{sr}z + c_{sr}\dot{z} + bk_{sr}theta + bc_{sr}\dot{\theta} - 0.5wk_{sr}\phi - 0.5wc_{sr}\dot{\phi} \\ &- (k_{sr} + k_{ur})z_{urr} - c_{sr}\dot{z}_{urr} + k_{ur}z_{rrr} - f_{rr}\end{aligned} \tag{2.59}$$

Finally, equations for wheels (2.36) can be linearized by using linear rolling resistance and linear friction.

$$I_w\dot{w}_i = T_{fl} - R\lambda_iN_iC_\lambda - C_rN_i, \tag{2.60}$$

where w_i is lateral velocity of i^{th} wheel where $i \in [1, 4]$. Required matrices for state space form of the linearized model can be found in the Appendix A and B.

2.4 Validation of Mathematical Models

In this section developed vehicle models are validated by using Amesim iCar package. This vehicle dynamics oriented gui includes 15 degrees of freedom vehicle model which adds steering wheel dynamics additional to the proposed 14 degrees of freedom mathematical model. Vehicle parameters used in the simulations can be found in the Table 2.1. Used parameters are generic values from Amesim iCar model. Proposed vehicle models are tested in an emergency escape maneuver with initial longitudinal velocity $V_0 = 15\ m/s$ and $V_0 = 22\ m/s$. After the escape maneuver an brake input is applied to test braking dynamics.

2.4.1 Validation of 3 Degrees of Freedom Model

Initially in Fig. 2.8a, emergency escape maneuver with initial longitudinal velocity $V_0 = 15\ m/s$ is used to validate 3 degrees of freedom vehicle model. Results show that proposed 3 degrees of freedom vehicle model behaves very close to the Amesim iCar package with negligible differences. Secondly same maneuver is applied when $V_0 = 22\ m/s$. Results in Fig. 2.8b shows that model can represent the real behavior of a vehicle. Since saturation is added to linear slip dynamics and lateral friction coefficients $C_{\alpha f}$ and $C_{\alpha r}$ are calculated according to the tire model at Amesim, when there is a large amount of slip due to higher velocity proposed mathematical model can still perform well.

Table 2.1: List of Used Vehicle Parameters

Mass, m	1300 $[kg]$
Unsprung mass, m_u	30 $[kg]$
Gravitational acceleration, g	9.81 $[m/s^2]$
Air Density, ρ	1.292 $[kg/m^3]$
Air Friction Coefficient, C_d	0.3 [ ]
Moment of Inertia About x, I_x	250 $[kg.m^2]$
Moment of Inertia About y, I_y	1000 $[kg.m^2]$
Moment of Inertia About z, I_z	1300 $[kg.m^2]$
Moment of Inertia of Wheel, I_w	2.7 $[kg.m^2]$
Length between Front axle and Center of Gravity, a	1.05 $[m]$
Length between Rear axle and Center of Gravity, b	1.45 $[m]$
Wheelbase, w	1.6 $[m]$
Front Lateral Friction Coefficient, $C_{\alpha f}$	11.3 $[1/rad]$
Rear Lateral Friction Coefficient, $C_{\alpha r}$	12.6 $[1/rad]$
Frontal Area, A_f	2.2 $[m^2]$
Wheel Radius, R	0.33 $[m]$
Length Between Center of Gravity and Front Wheel, l_f	1.3 $[m]$
Length Between Center of Gravity and Rear Wheel, l_r	1.6 $[m]$
Front Spring Constant, k_{sf}	21000 $[N/m]$
Rear Spring Constant, k_{sr}	21000 $[N/m]$
Front Damping Coefficient, c_{sf}	1500 $[N.s/m]$
Rear Damping Coefficient, c_{sr}	1500 $[N.s/m]$
Front Unsprung Spring Constant, k_{uf}	200000 $[N/m]$
Rear Unsprung Spring Constant, k_{ur}	200000 $[N/m]$

2.4.2 Validation of 14 Degrees of Freedom Model

Secondly, the proposed 14 degree of freedom vehicle model is tested in the same case. When the initial longitudinal velocity $V_0 = 15$ m/s simulation results in

Fig. 2.9a shows convincing similarity with the Amesim iCar module. The only noticeable difference occurs at the lateral dynamics of the vehicle. This offset at lateral displacement is due to the different lateral friction models. Since tire model parameters at Amesim were not completely available it was not possible to use the same tire models. Moreover, as second test initial longitudinal velocity V_0 is increased to 22 m/s. The results in Fig. 2.9b shows both model performs similarly in the high speed scenario. Because non-linear tire dynamics are used and couplings between different dynamics of the vehicle model are modeled, more consistent results are obtained in this model.

2.4.3 Validation of Linear 14 Degrees of Freedom Model

Lastly in state-space form of 14 degrees of freedom model is tested. In the low velocity scenario at Fig. 2.10a, apart from the difference due to the different lateral friction coefficients proposed model shows close performance to the Amesim. However in the high speed scenario at Fig. 2.10b due to the absence of a saturation at lateral friction, this model fails to represent the behavior of the vehicle. Since lateral force is modeled with $F_{yi} = C_\alpha \alpha_i$, as slip ratio α increases vehicle generates more lateral force. This situation causes vehicle to never fail due to proportionally increasing lateral force. Therefore, as linearized tire frictions go out of the linearization region validity of the vehicle model decreases.

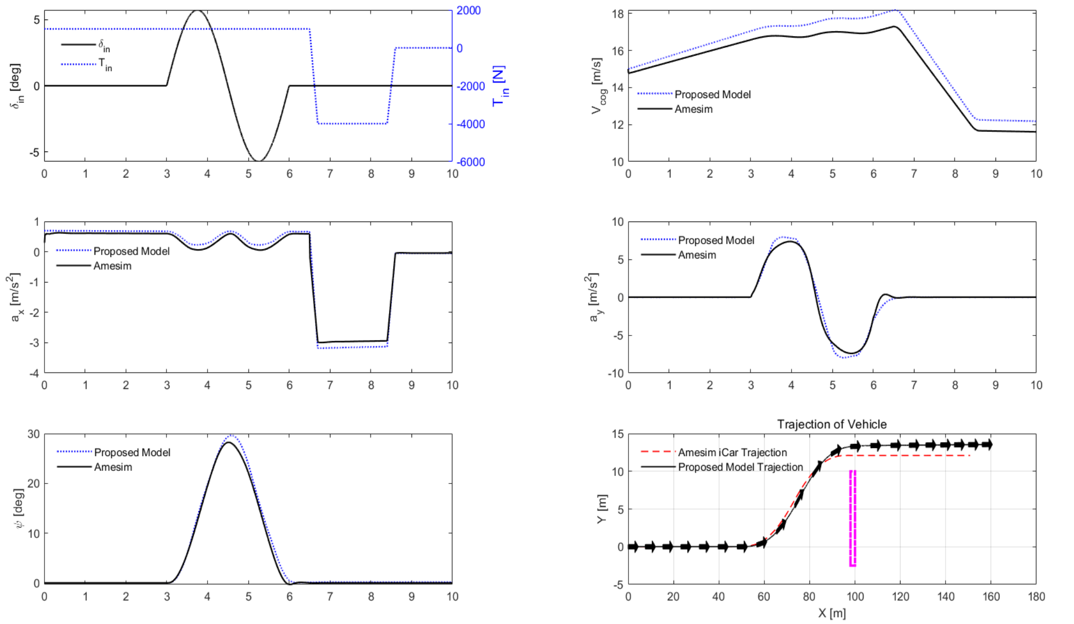

(a) Low Speed Scenario

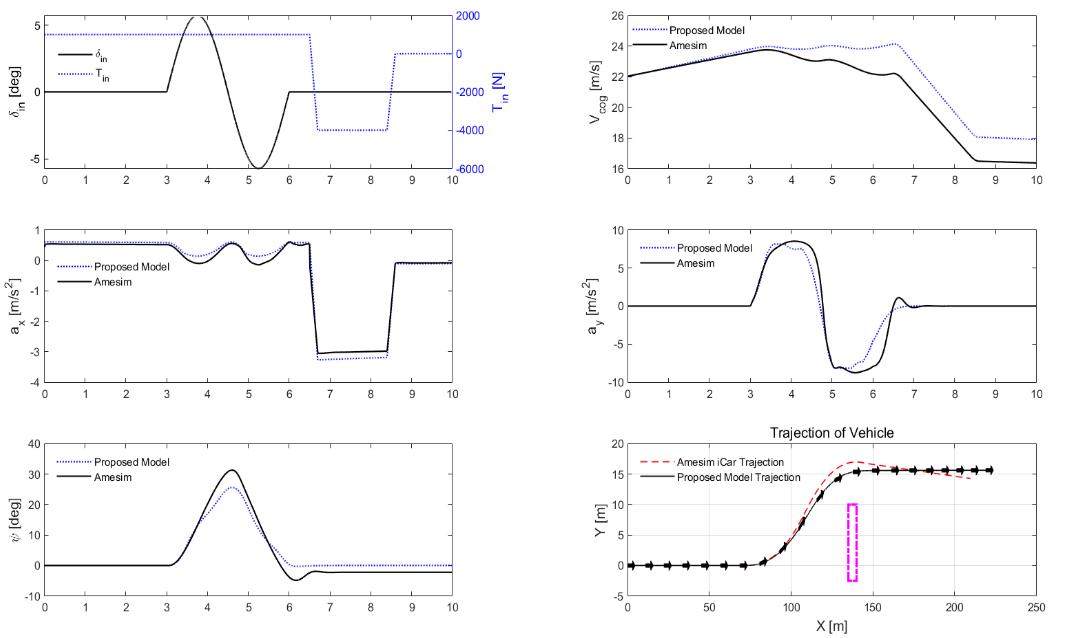

(b) High Speed Scenario

Figure 2.8: Validation of Proposed 3 Degrees of Freedom Mathematical Model in High and Low Speed Scenarios

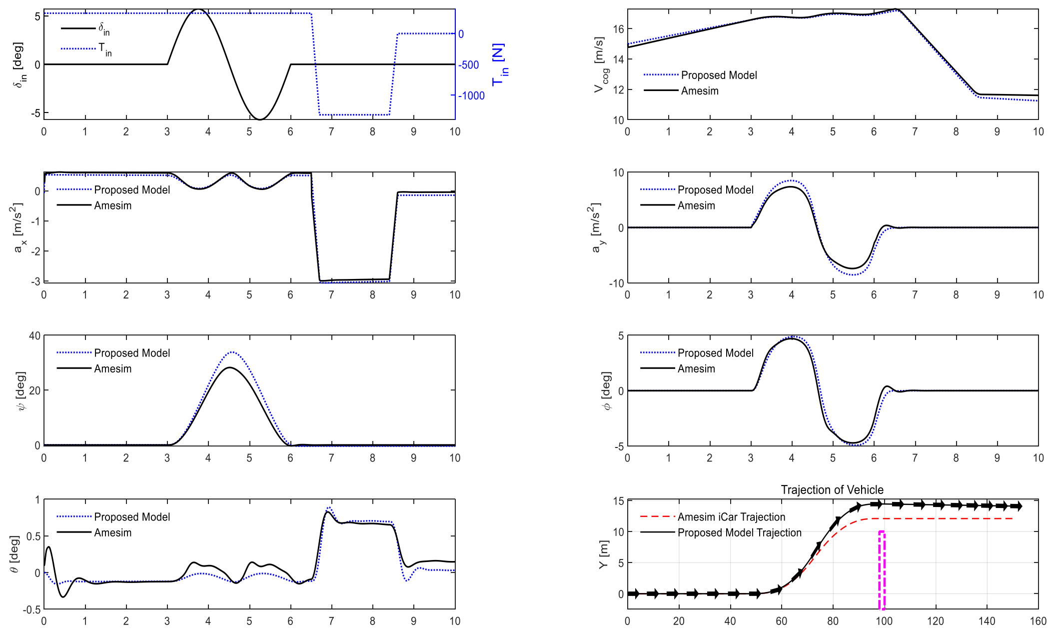

(a) Low Speed Scenario

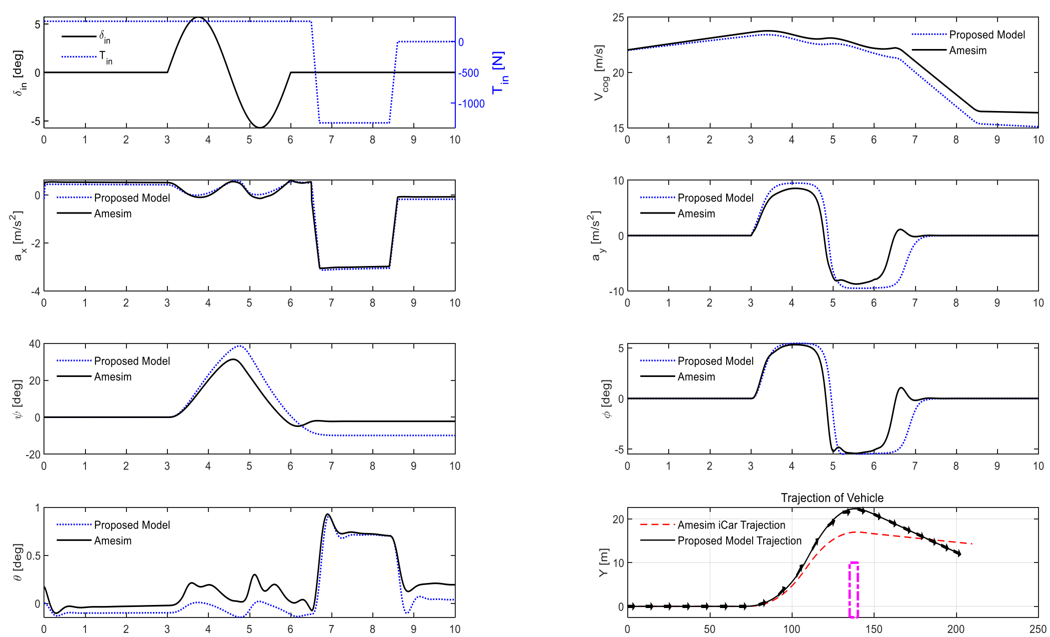

(b) High Speed Scenario

Figure 2.9: Validation of Proposed Non-linear 14 Degrees of Freedom Mathematical Model in High and Low Speed Scenarios

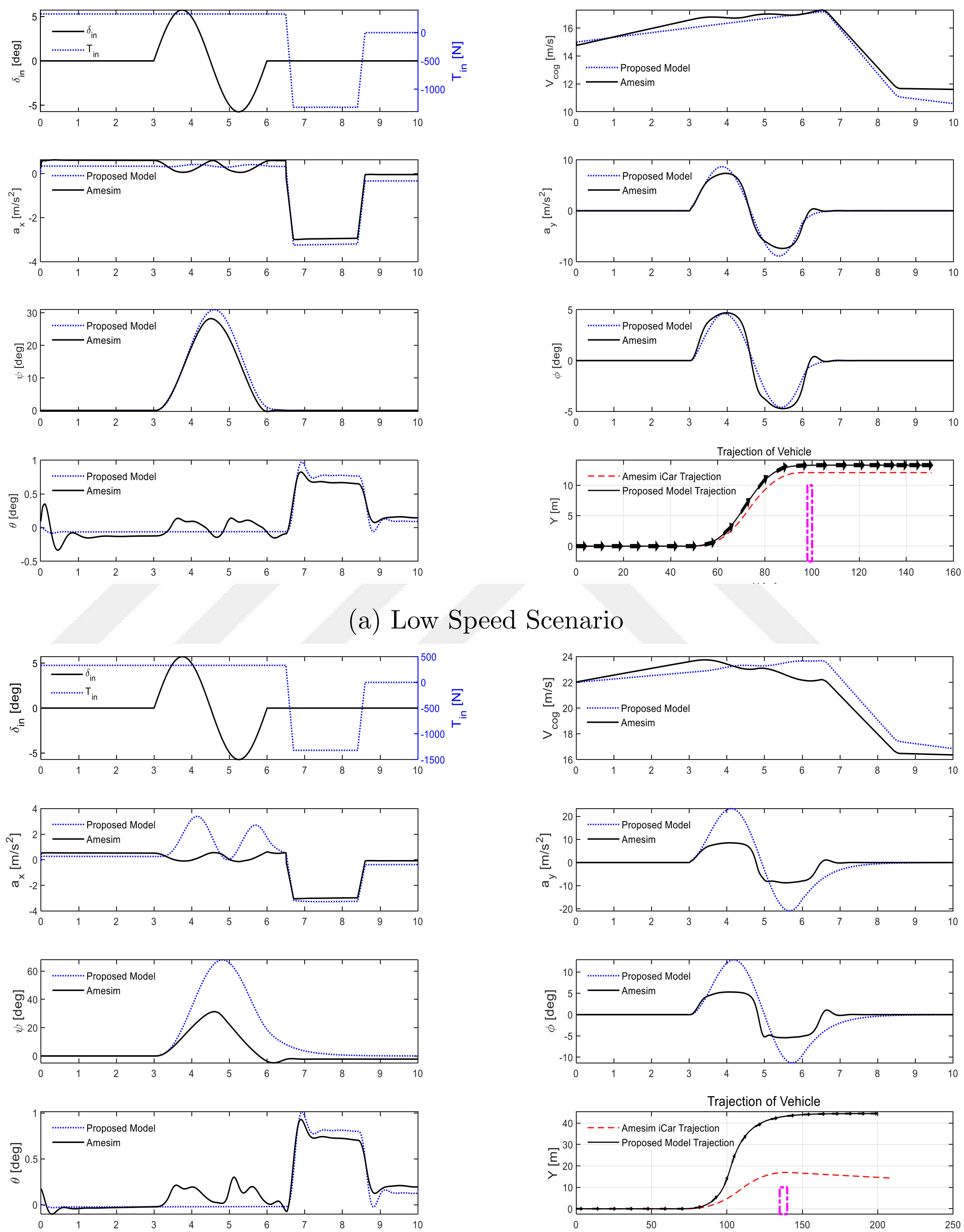

(a) Low Speed Scenario

(b) High Speed Scenario

Figure 2.10: Validation of Proposed Linear 14 Degrees of Freedom Mathematical Model in High and Low Speed Scenarios

Chapter 3

Adaptive Control Allocation with 3 Degree of Freedom Model

In this chapter adaptive control allocation scheme for three degree of freedom vehicle model is developed. The closed loop control structure described in this chapter can be seen in Fig. 3.1. Motion is initiated by a front steering input, δ_1, and a desired traction force, F_{in}, by driver's input to the steering wheel and the pedals respectively.

In the Virtual Control Input Generation stage, desired traction force, F_c, the desired correction moment M_c and the required lateral force correction F_{yc} is generated depending on the driver inputs and measured vehicle states. Then, based on the virtual control input, the adaptive control allocation algorithm determines the traction force F_{Xi} applied at each wheel, rear wheel steering angle δ_2 and front wheel steering angle correction $\Delta\delta_1$.

The control algorithm presented in this section is developed utilizing the linearized vehicle model given in (2.24) - (2.28), and the full non-linear model presented in (2.5) - (2.11) is used in the simulations shown in the next section.

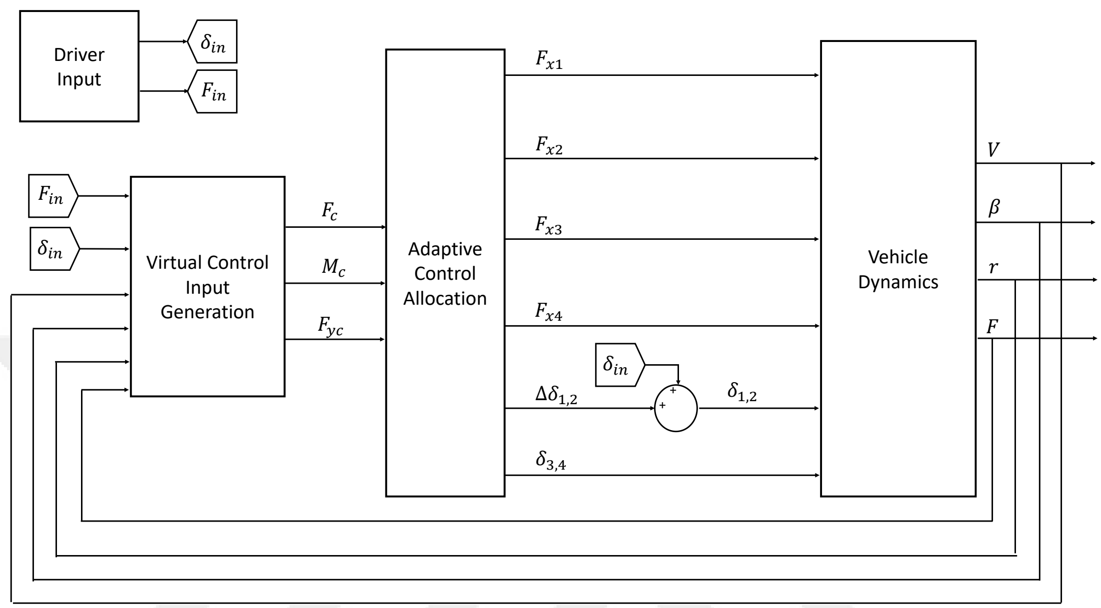

Figure 3.1: Control Structure

3.1 Virtual Control Input Generation

In order to determine the virtual control input elements, required traction force, F_c, yaw rate correction moment M_c and lateral force correction F_{yc} should be calculated.

For traction force, force input from driver F_{in} and the current total traction force F is used. In order to ensure that there is no steady-state error and vehicle is maintaining the driver's acceleration demand a PI scheme is used. Defining deviation from the desired value as $\tilde{F} = F_{in} - F$, the updated value of the desired traction force is as shown (3.1).

$$F_c = K_i \int \tilde{F} dt + K_p \tilde{F} \tag{3.1}$$

In order to calculate the desired yaw rate moment, M_c, first a desired yaw rate, r_{ref} should be defined for the vehicle based on steering input and its current forward velocity. Reference yaw rate, r_{ref}, is generated based on the approach presented in many vehicle dynamics literature such as [2], [48] as shown in (3.2).

$$
\begin{aligned}
r_{ref} &= \delta_{1in} \frac{V}{L + K_{us} V^2} \\
K_{us} &= \frac{mL_r}{LC_{\alpha f} N_f} - \frac{mL_f}{LC_{\alpha r} N_r}
\end{aligned}
\tag{3.2}
$$

Defining the deviation from the reference value as $\tilde{r} = r - r_{ref}$, a PI controller is designed for moment command calculation to ensure that there will be no steady state error as shown in (3.3).

$$
M_c = K_p \tilde{r} + K_i \int \tilde{r} dt \tag{3.3}
$$

Lastly, in order to ensure stability of the vehicle while following yaw reference signal, lateral force correction is provided to the adaptive allocation system. To assure stability of the vehicle, side-slip angle, β, should be in the stable region as discussed in [37]. Since side-slip is directly related to lateral velocity of the vehicle, growth of the side-slip prevented by applying lateral force in the negative direction. Assuming that the side-slip angle of the vehicle can be estimated or measured, following simple law can be used [2].

$$
\begin{aligned}
&If \quad |\beta| \geq \beta_{threshold} \quad and \quad \beta.\Delta\beta > 0 \\
&Then \quad F_{yc} = -K_p \beta - K_d \dot{\beta}
\end{aligned}
\tag{3.4}
$$

Resulting virtual control input vector for this application as follows

$$
\mathbf{v}^T = \begin{bmatrix} F_c & F_{yc} & M_c \end{bmatrix} \tag{3.5}
$$

3.2 Adaptive Control Allocation

The adaptive control allocation method used in this work is based on [49, 50] and the block diagram for this algorithm is presented in Fig. 3.2. The method is briefly explained below and the details can be found in [49].

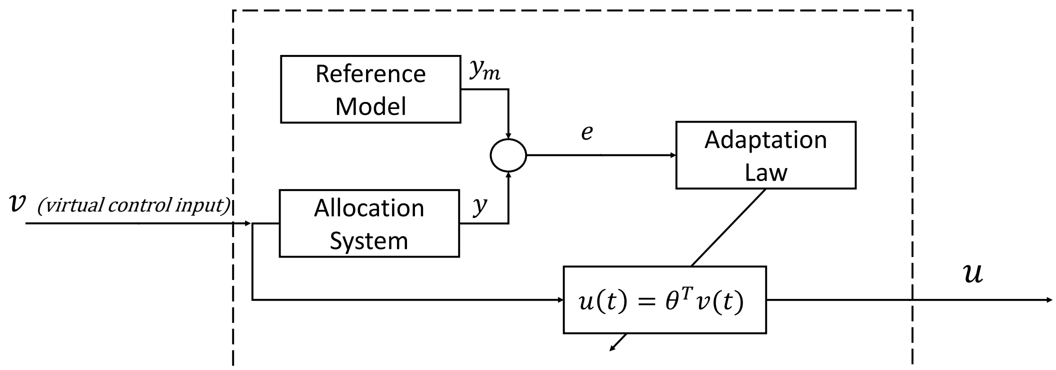

Figure 3.2: Block Diagram of Exploited Adaptive Control Allocation

In this adaptive control allocation design is is assumed that $\delta_1 = \delta_2$ and $\delta_3 = \delta_4$ Writing the actuator input vector with this approximation as $\mathbf{u_s} = \mathbf{u} + \mathbf{\Delta u}$, where

$$\begin{aligned} \mathbf{\Delta u} &= \begin{bmatrix} \delta_{in} & 0 & 0 & 0 & 0 & 0 \end{bmatrix} \\ \mathbf{u} &= \begin{bmatrix} \Delta\delta_{1,2} & \delta_{3,4} & F_{x1} & F_{x2} & F_{x3} & F_{x4} \end{bmatrix} \end{aligned} \tag{3.6}$$

and decomposing the input matrix $\mathbf{B_u} \in R^{3x6}$ as $\mathbf{B_u} = \mathbf{B_v}\mathbf{B}$, where $\mathbf{B_v}$ is a $3x3$ matrix and $\mathbf{B}$ is a $3x6$ matrix, (2.24) – (2.28) can be written as

$$\begin{aligned} \dot{\mathbf{x}} &= \mathbf{Ax} + \mathbf{B_u u} + \mathbf{B_u \Delta u} \\ &= \mathbf{Ax} + \mathbf{B_v B u} + \mathbf{B_u \Delta u} \end{aligned} \tag{3.7}$$

To introduce actuator effectiveness uncertainty, a diagonal positive definite matrix $\mathbf{\Lambda} \in R^{6x6}$ is added to (4.7), which leads to the following plant equations

$$\begin{aligned} \dot{\mathbf{x}} &= \mathbf{Ax} + \mathbf{B_v B \Lambda u} + \mathbf{B_u \Delta u} \\ &= \mathbf{Ax} + \mathbf{B_v v} + \mathbf{B_u \Delta u} \end{aligned} \tag{3.8}$$

where $\mathbf{v} \in R^3$ is virtual control input. The objective of the control allocation is to determine the actuator input vector $\mathbf{u}$ such that

$$\mathbf{B \Lambda u} = \mathbf{v}. \tag{3.9}$$

Consider the following dynamics

$$\dot{\mathbf{y}} = \mathbf{A_m y} + \mathbf{B \Lambda u} - \mathbf{v}, \tag{3.10}$$

where $\mathbf{A_m} \in R^{3x3}$ is stable, and a reference model

$$\dot{\mathbf{y}}_m = \mathbf{A_m}\mathbf{y_m}. \tag{3.11}$$

The goal is to make the state vector y follow the reference model output $\mathbf{y_m}$. Determining the actuator input vector as

$$\mathbf{u} = \boldsymbol{\theta}_v^T \mathbf{v}, \tag{3.12}$$

where $\boldsymbol{\theta} \in R^{3x6}$ is an adaptive parameter matrix and substituting (3.12) into (3.10), it is obtained that

$$\dot{\mathbf{y}} = \mathbf{A_m}\mathbf{y} + (\mathbf{B}\boldsymbol{\Lambda}\boldsymbol{\theta}_v^T - \mathbf{I})\mathbf{v}. \tag{3.13}$$

An ideal solution for the adaptive parameter vector is assumed to exist and satisfy $\mathbf{B}\boldsymbol{\Lambda}\boldsymbol{\theta}_v^T = \mathbf{I}$. Defining $\boldsymbol{\theta}_v^T = \boldsymbol{\theta}_v^{*T} - \tilde{\boldsymbol{\theta}}_v^T$, where $\tilde{\boldsymbol{\theta}}_v^T$ is the deviation of the adaptive parameter vector $\boldsymbol{\theta}_v^T$ from its ideal value $\boldsymbol{\theta}_v^{*T}$, (3.13) can rewritten as

$$\dot{\mathbf{y}} = \mathbf{A_m}\mathbf{y} + \mathbf{B}\boldsymbol{\Lambda}\tilde{\boldsymbol{\theta}}_v^T \mathbf{v} \tag{3.14}$$

Defining the tracking error as $\mathbf{e} = \mathbf{y} - \mathbf{y_m}$ and using (3.11)-(3.14), it is obtained that

$$\dot{\mathbf{e}} = \mathbf{A_m}\mathbf{e} + \mathbf{B}\boldsymbol{\Lambda}\tilde{\boldsymbol{\theta}}_v^T \mathbf{v}. \tag{3.15}$$

Using an adaptation rate matrix $\boldsymbol{\Gamma} = \boldsymbol{\Gamma}^T = \gamma\mathbf{I_r} \in R^{rxr} > 0$, where γ is a positive scalar and $\mathbf{I_r}$ is an identity matrix, it can be shown [49] that the following adaptive law

$$\dot{\boldsymbol{\theta}} = \boldsymbol{\Gamma} Proj(\boldsymbol{\theta}_v, -\mathbf{v}\mathbf{e}^T\mathbf{P}\mathbf{B}), \tag{3.16}$$

where $Proj$ is the projection operator [51], leads to a stable adaptive control allocation. It is noted that $\mathbf{P}$ in (3.16) is the positive definite symmetric solution of ${\mathbf{A_m}}^T\mathbf{P} + \mathbf{P}\mathbf{A_m} = -\mathbf{Q}$ where $\mathbf{Q}$ is a positive definite symmetric matrix.

The adaptive control allocation algorithm proposed in [49], and described above, is used to realize the virtual control input vector $\mathbf{v}$ in (3.9), consisting of the total traction force, the lateral force correction, and the moment correction, by determining the actuator input vector $\mathbf{u}$, whose elements are the front steering angle correction, the rear steering angle and the individual traction forces.

By using the linear equations of motion given in (2.24) – (2.28), the **B** matrix can be calculated. Each column of the **B** matrix corresponds to one of the allocated actuators while each row addresses one component of the **v** vector. For the proposed adaptive control allocation algorithm decomposition of $\mathbf{B_u}$ should be done as in [52].

1. For the first row of the matrix **B**, the first two elements corresponds to steering inputs. Since in the linearized version of the vehicle model steering has no effect on traction forces these elements are selected as zero. Furthermore, because in typical driving conditions equal distribution of traction forces at each tire is desired, the last four elements of first row are selected as ones.

2. For the second row, the first two elements are determined by calculating the effect of steering on lateral forces. The last four elements on this row are selected as zeros since the effect of traction forces on the lateral force is neglected due to the linearization.

3. For the third row, the contribution of steering angles on the moment M is calculated by using the lateral forces created due to steering angles, and the first two elements are created. Additionally the effect of the traction forces on the moment M is shown by setting the therefore last four elements of the second row as $w/2$.

The resulting **B** is given as

$$\mathbf{B} = \begin{bmatrix} 0 & 0 & 1 & 1 & 1 & 1 \\ C_{\alpha f}(N_1 + N_2) & C_{\alpha r}(N_3 + N_4) & 0 & 0 & 0 & 0 \\ C_{\alpha f}a(N_1 + N_2) & -C_{\alpha r}b(N_3 + N_4) & -\frac{w}{2} & \frac{w}{2} & -\frac{w}{2} & \frac{w}{2} \end{bmatrix}. \tag{3.17}$$

Therefore the $\mathbf{B_v}$ matrix which satisfies the decomposition $\mathbf{B_u} = \mathbf{B_v}\mathbf{B}$ can be calculated as

$$\mathbf{B_v} = \begin{bmatrix} \frac{1}{m} & 0 & 0 \\ 0 & -\frac{1}{m} & 0 \\ 0 & 0 & \frac{1}{J_z} \end{bmatrix}. \tag{3.18}$$

3.3 Simulations

A MATLAB/Simulink model is developed based on the system given in Fig. 3.1 using the nonlinear dynamic model from Section II. In order to evaluate the functionality and performance of the proposed control method, an object avoidance maneuver is simulated with different faults. Results are compared with a baseline vehicle control system where rear wheels are adjusted proportional to driver's front steering wheel input. Traction forces at the baseline vehicle are distributed evenly based on driver's acceleration request. Additionally in the Appendix B.1 and B.2 sensitivity study is conducted by adding parameter estimation noise and changing the mass in friction loss scenario.

3.3.1 Baseline Performance

In order to understand the forthcoming results better the baseline performance of controller is first examined when there is no fault in the vehicle. Simulations are executed with a one period of sinusoidal steering input which simulates an object avoidance maneuver. Fig. 3.3, shows the simulation variables from the vehicle and the controller during the simulation. It can be seen that at this vehicle speed both systems performs satisfactorily following commands. the proposed controller causes more deceleration. On the other hand it follows yaw reference signal slightly better. The reason for that is introduction of more steering wheel in order to follow yaw rate reference.

When the forward velocity is higher, it is harder to safely rotate the vehicle. When the same steering maneuver is applied to both systems when the velocity is 20 m/s baseline system fails. When the trajectory is examined both cars can make the first turn however once vehicles have the lateral velocities without torque vectoring, and required RWS and FWS corrections baseline system cannot turn properly due to over steering and it fails. Fig. 3.4.

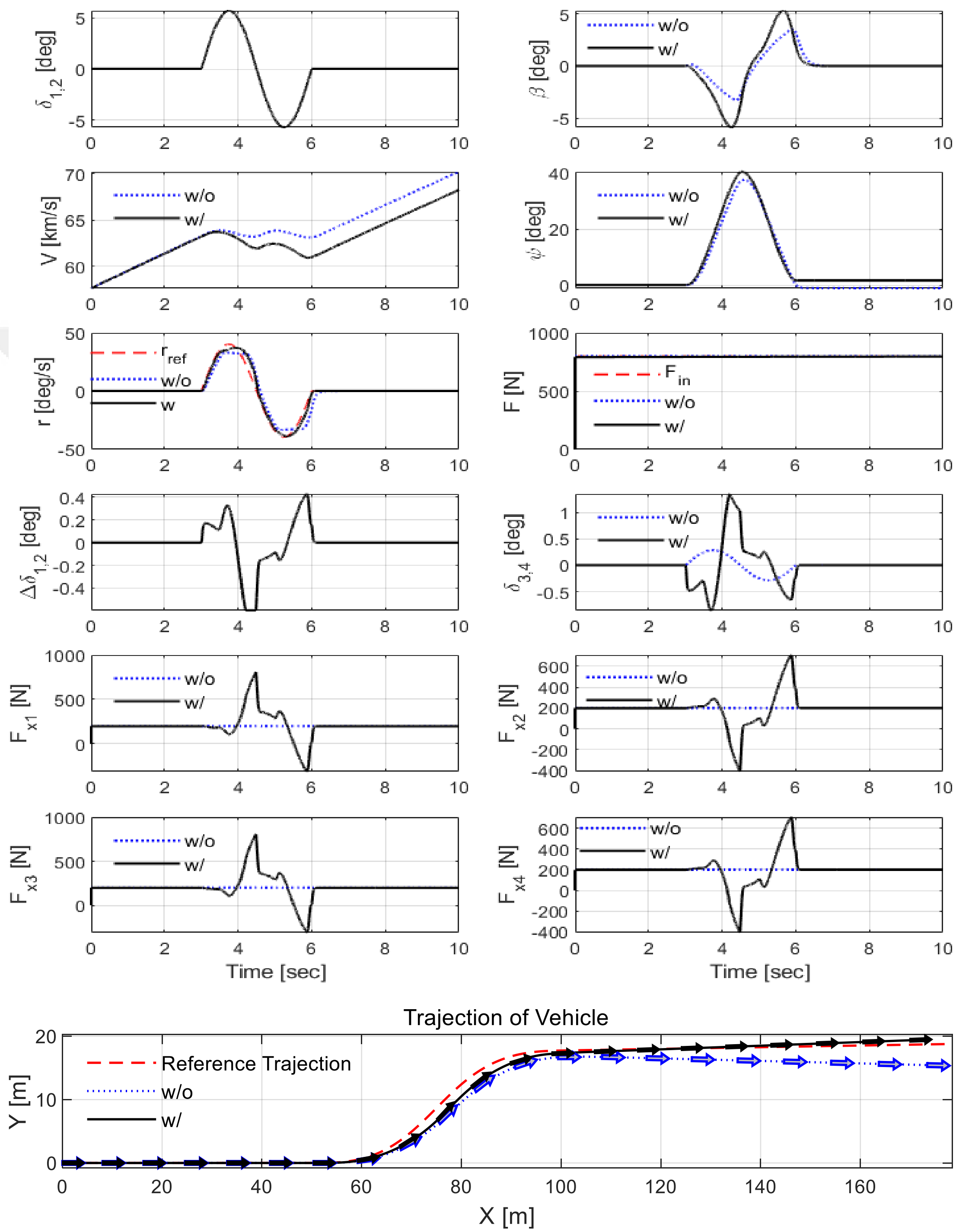

Figure 3.3: Object Avoidance Maneuver with V=16 m/s

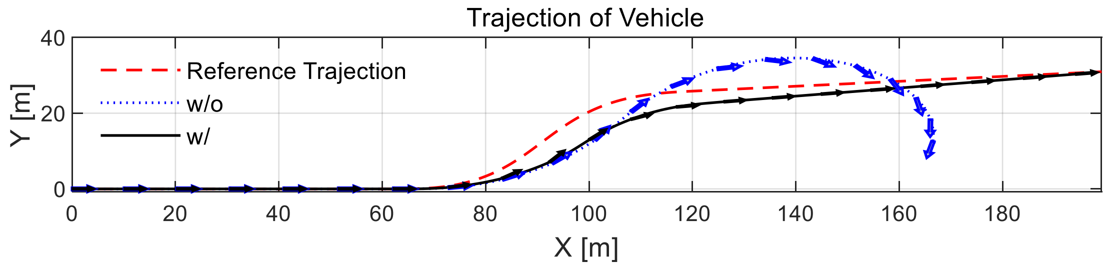

Figure 3.4: Object Avoidance Maneuver with V=20 m/s

3.3.2 Actuator Failure

To test the effectiveness of the proposed controller in emergency situations a scenario involving an actuator failure is considered. The rear right traction force reduced to 10% at $t = 3s$ which is also the start of the steering for the object avoidance maneuver. Results of the simulation can be seen at Fig. 3.5 When the results are examined, it can be seen that the yaw rate reference signal is successfully followed by the vehicle equipped with the new controller. Moreover, the traction forces at functioning wheels are increased to maintain desired acceleration while the front and the rear steering are used to compensate the moment due to uneven traction forces. Lastly since the rear right motor has failure vehicle tends turn right when the fault is not compensated. Therefore baseline system turn right much more than desired. As a result, it cannot follow the reference trajectory.

3.3.3 Varying Road Conditions

To emulate another type of an emergency condition and study the effectiveness of the proposed controller, the road surface conditions were used. In this simulation the road friction coefficient C_α for the right tires reduced to half of its value in order to simulate slippery road conditions starting at $t = 4.5s$ while the vehicle is commanded to perform the same object avoidance maneuver. The results in Fig.

3.6 show that the baseline vehicle had difficulty following the commands while the proposed controller performed as designed. In order to compensate varying road conditions, proposed system sends much more traction force to the right wheels. As a result it can follow the reference yaw signal. Moreover, trajectories, side slip angles and velocities show that vehicle equipped with the new controller remained stable while the baseline system failed, slipped and eventually stopped.

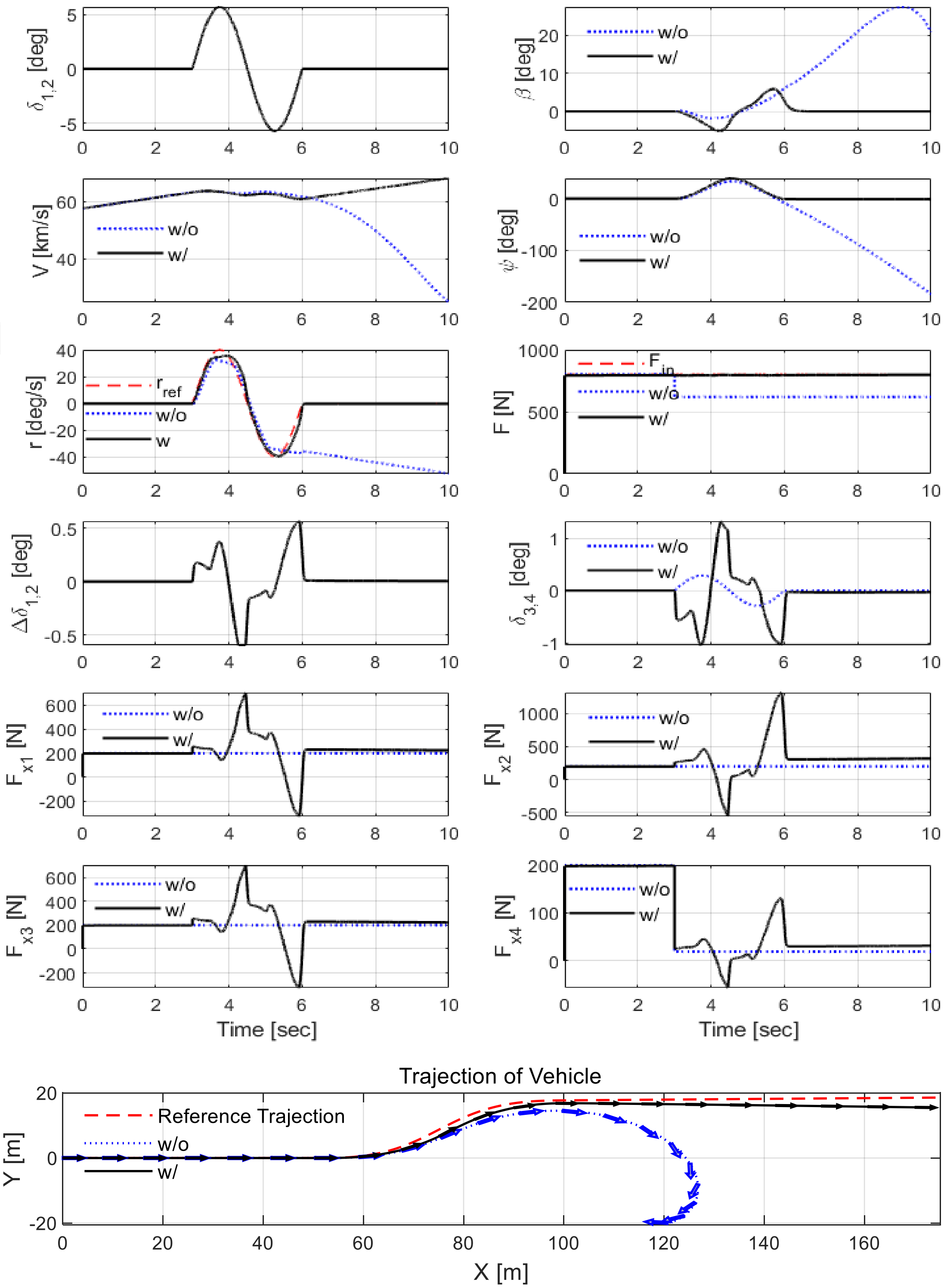

Figure 3.5: Object Avoidance Maneuver with Actuator Failure

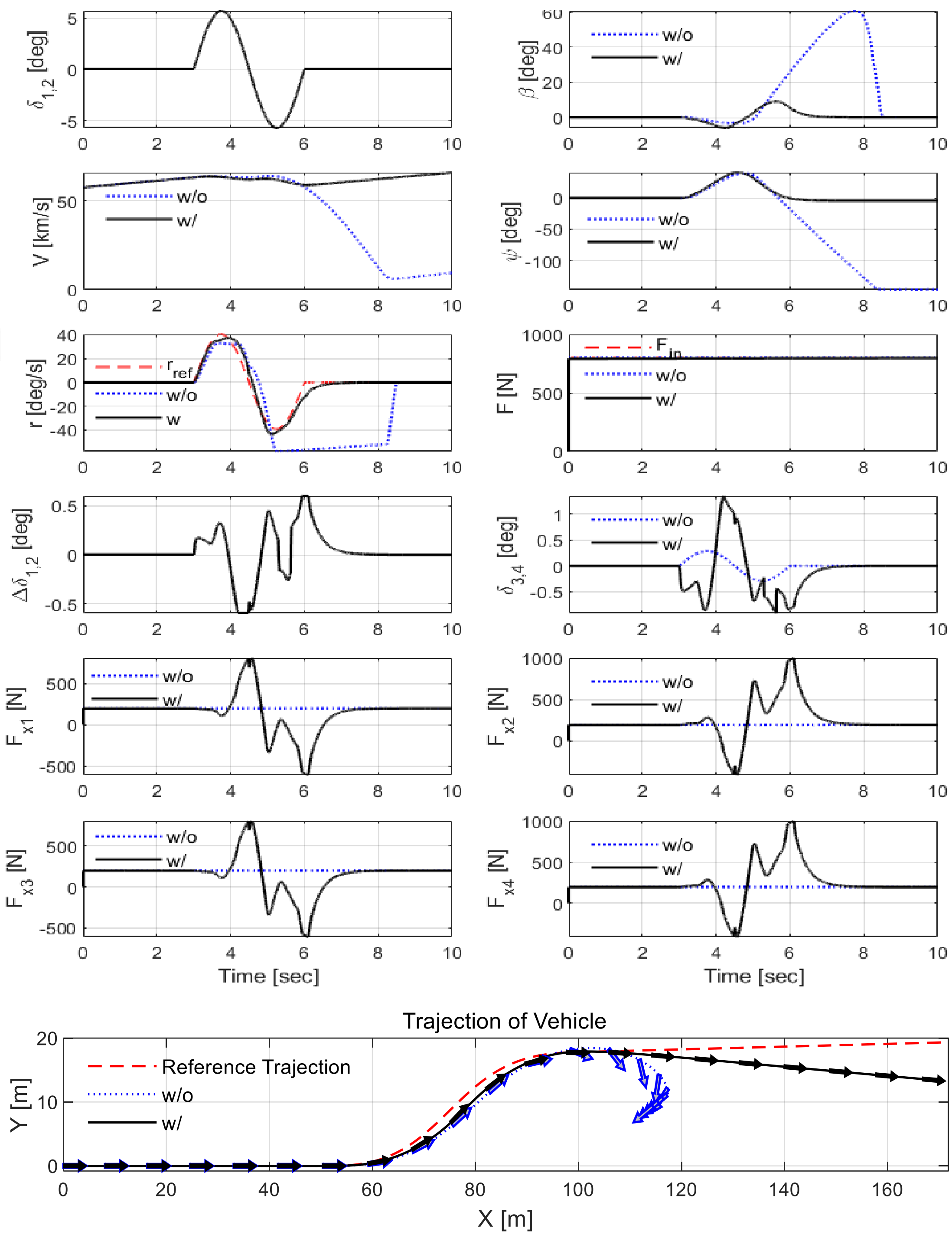

Figure 3.6: Object Avoidance Maneuver with Varying Road Conditions

Chapter 4

Adaptive Control Allocation with 14 Degree of Freedom Model

In this chapter previous adaptive control allocation system is modified to include time-varying coefficients of input matrix B_u and proposed controller is applied to previously developed 14 degree of freedom vehicle model.

Overall closed loop system structure including the proposed control framework is given in Fig. 4.1. In this structure, the driver gives the steering wheel and throttle inputs. These inputs, together with the vehicle states, are used by the controller to produce the virtual control input.

Virtual control input determines the objective of the adaptive control allocation system. In order to ensure that driver intentions are satisfied, the related desired traction force F_c, desired yaw , roll and pitch moment corrections M_z, M_x, M_y are calculated as the components of the virtual control input vector. Moreover, to ensure the yaw stability, the required lateral force correction F_{yc} is calculated as another component of the virtual control input. Then, the proposed adaptive control allocation algorithm determines the traction forces T_i to be applied at each wheel, rear wheel steering angles $\delta_3, \ \delta_4$, front wheel steering angle corrections $\Delta\delta_1, \ \Delta\delta_2$ and active suspension forces f_i, based on the created virtual control input vector where$i \in [1, 4]$.

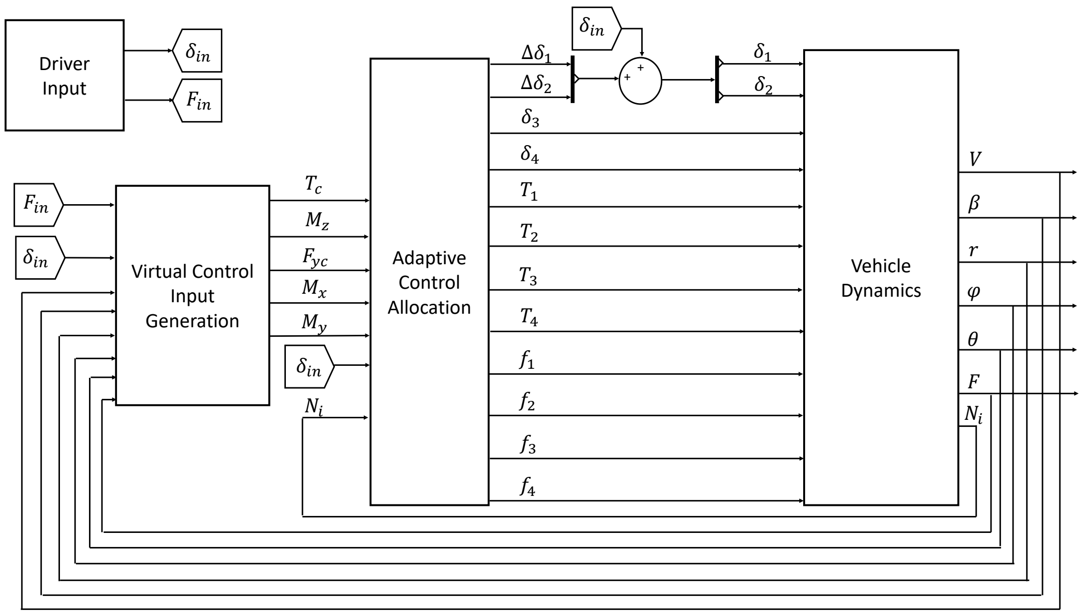

Figure 4.1: Overall Closed Loop System

4.1 Virtual Control Input Generation

In this section, elements of the virtual control input vector which are the desired traction force F_c, desired yaw , roll and pitch moment corrections M_z, M_x, M_y and the required lateral force correction F_{yc} are calculated. To ensure that the vehicle maintains the desired longitudinal acceleration, the traction force command F_c is calculated via a PI controller:

$$\begin{aligned} \tilde{F} &= F_{in} - F \\ F_c &= K_i \int \tilde{F} dt + K_p \tilde{F}, \end{aligned} \tag{4.1}$$

where F_{in} is the traction force requested by the driver, F is the current traction force and K_p and K_i are the PI controller gains.

To follow the steering input of the driver, first a reference yaw r_{ref} is calculated using the methods proposed in [48] and [2]. Then, by feeding the error between

r_{ref}, the measured yaw rate r and to a PI controller desired moment to follow the yaw reference is generated as in the equation (3.2). Additionally, to ensure stability while following the reference, side-slip angle β is feeded to a PI controller and generated moments are summed to create desired yaw moment correction M_z.

$$\begin{aligned} \tilde{r} &= r_{ref} - r \\ M_z &= K_{py}\tilde{r} + K_{iy}\int \tilde{r}dt + K_{ps}\beta + K_{is}\int \beta dt \end{aligned} \tag{4.2}$$

where L is length of the wheelbase, C_α is linearized lateral friction coefficient, N_f, N_r are normal forces at front and rear tires and K_{py}, K_{yi}, K_{ps}, K_{ys} are the PI controller gains.

Lateral and longitudinal accelerations may cause the vehicle to roll and pitch. These motions are not desirable since they shift the center of gravity and may brake the vehicle's stability. Therefore to reduce the roll and pitch motion, roll and pitch moment corrections, M_x and M_y are calculated by using a PI controller:

$$\begin{aligned} M_x &= -K_{pr}\phi - K_{ir}\int \phi dt \\ M_y &= -K_{pp}\theta - K_{ip}\int \theta dt, \end{aligned} \tag{4.3}$$

where ϕ and θ are roll and pitch angle of the vehicle and K_{pr}, K_{ir}, K_{pp} and K_{ip} are the PI controller gains.

The side-slip angle, β, should kept small since large side-slip angle causes vehicle to be unstable as discussed in [37]. β can be controlled by applying a lateral force to the vehicle. Assuming that the side-slip angle of the vehicle can be estimated or measured, The desired lateral force F_{yc} can be calculated using the following law [2] :

$$\begin{aligned} &If \quad |\beta| \geq \beta_{threshold} \quad and \quad \beta.\Delta\beta > 0 \\ &Then \quad F_{yc} = -K_p\beta - K_d\dot{\beta}, \end{aligned} \tag{4.4}$$

where β is side slip angle, K_p and K_d are the PD controller constants.

4.2 Adaptive Control Allocation

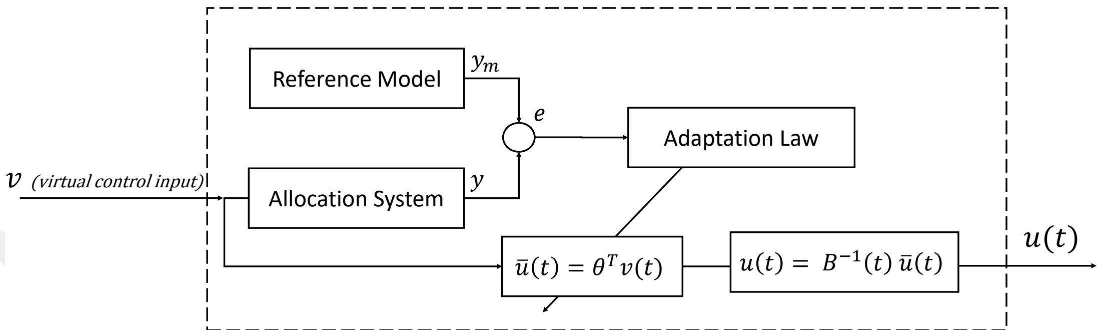

Figure 4.2: Block Diagram of Adaptive Control Allocation

The exploited adaptive control allocation method is based on [49] and the block diagram for this algorithm is given in Fig. 4.2. First, consider the actuator input vector u_i and plant dynamics as follows

$$\mathbf{u_i}^T = \begin{bmatrix} \delta_1 & \delta_2 & \delta_3 & \delta_4 & T_1 & T_2 & T_3 & T_4 & f_1 & f_2 & f_3 & f_4 \end{bmatrix} \tag{4.5}$$

$$\dot{\mathbf{x}} = \mathbf{Ax} + \mathbf{B_u}(t)\mathbf{u_i} + \mathbf{D}. \tag{4.6}$$

Where $\mathbf{A}$ is state matrix, $\mathbf{B_u}(t)$ is time varying input matrix, $\mathbf{u_i}$ is input vector and $\mathbf{D}$ is disturbance vector composed of road displacements. Decomposing the $\mathbf{u_i}$ vector as $\mathbf{u_i} = \mathbf{u} + \mathbf{\Delta u}$ and writing $\mathbf{B_u}(t)$ matrix as $\mathbf{B_u}(t) = \begin{bmatrix} \mathbf{B_{u1}}(t) \\ \mathbf{B_{u2}} \end{bmatrix}$, where $\mathbf{B_{u1}}(t)$ represents the vehicle dynamics that will be controlled by the adaptive control allocation and $\mathbf{B_{u2}}(t)$ represents the rest of the dynamics. Plant dynamics can be obtained as

$$\begin{aligned} \dot{\mathbf{x}} &= \mathbf{Ax} + \begin{bmatrix} \mathbf{B_{u1}}(t) \\ \mathbf{B_{u2}} \end{bmatrix} \mathbf{u} + \mathbf{B_u}(t)\mathbf{\Delta u} + \mathbf{D} \\ &= \mathbf{Ax} + \begin{bmatrix} \mathbf{B_v}\mathbf{B}(t) \\ \mathbf{B_{u2}} \end{bmatrix} \mathbf{u} + \mathbf{B_u}(t)\mathbf{\Delta u} + \mathbf{D} \end{aligned} \tag{4.7}$$

where

$$\begin{aligned}\mathbf{\Delta u}^T &= \begin{bmatrix}\delta_{in} & \delta_{in} & 0 & 0 & 0 & 0 & 0 & 0 & 0 & 0 & 0 & 0\end{bmatrix} \\ \mathbf{u}^T &= \begin{bmatrix}\Delta\delta_1 & \Delta\delta_2 & \delta_3 & \delta_4 & T_1 & T_2 & T_3 & T_4 & f_1 & f_2 & f_3 & f_4\end{bmatrix}\end{aligned} \tag{4.8}$$

$\mathbf{A} \in R^{28x28}$ is state matrix formed from linearized 14 degree of freedom vehicle model, $\mathbf{x} \in R^{28}$ is state vector and $\mathbf{B_u 1}(t) \in R^{10x12}$ is the known input matrix which is decomposed into two known matrices $\mathbf{B_v} \in R^{10x5}$ and $\mathbf{B}(t) \in R^{5x12}$.

$$\dot{\mathbf{x}} = \mathbf{Ax} + \begin{bmatrix}\mathbf{B_v B_l B_n}(t) \\ \mathbf{B_{u2}}\end{bmatrix}\mathbf{u} + \mathbf{B_u}(t)\mathbf{\Delta u} + \mathbf{D} \tag{4.9}$$

where $\mathbf{B}(t)$ is decomposed to two known matrices $\mathbf{B_l} \in R^{5x12}$ and $\mathbf{B_n}(t) \in R^{12x12}$ which is invertible.

Define $\bar{\mathbf{u}} = \mathbf{B_n}(t)\mathbf{u}$ and introduce actuator effectiveness uncertainty, a diagonal positive definite matrix $\mathbf{\Lambda} \in R^{12x12}$ which leads to the following plant dynamics

$$\begin{aligned}\dot{\mathbf{x}} &= \mathbf{Ax} + \begin{bmatrix}\mathbf{B_v B_l \Lambda \bar{u}} \\ \mathbf{B_{u2} u}\end{bmatrix} + \mathbf{B_u}(t)\mathbf{\Delta u} \\ &= \mathbf{Ax} + \begin{bmatrix}\mathbf{B_v v} \\ \mathbf{B_{u2} u}\end{bmatrix} + \mathbf{B_u}(t)\mathbf{\Delta u}.\end{aligned} \tag{4.10}$$

where $\mathbf{v} \in R^5$ is the virtual control input and note that uncertainty matrix $\mathbf{\Lambda}$ multiplies the $\mathbf{u}$ vector as $\mathbf{\Lambda B_n}(t)\mathbf{u}$. Which means uncertainty still manages to represent change of effectiveness at actuators. The objective of the control allocation is to determine the vector $\mathbf{u}$ to achieve

$$\mathbf{B_l \Lambda \bar{u}} = \mathbf{v}. \tag{4.11}$$

For the adaptive allocation system, consider the following dynamics

$$\dot{\mathbf{y}} = \mathbf{A_m y} + \mathbf{B_l \Lambda \bar{u}} - \mathbf{v} \tag{4.12}$$

where $\mathbf{A_m} \in R^{5x5}$ is stable and a reference model defined as

$$\dot{\mathbf{y}}_m = \mathbf{A_m y_m}. \tag{4.13}$$

To achieve (4.11), $\mathbf{y}$ is forced to follow $\mathbf{y_m}$ by setting the actuator input vector $\bar{\mathbf{u}}$ as

$$\bar{\mathbf{u}} = \boldsymbol{\theta}_v^T \mathbf{v} \tag{4.14}$$

where $\boldsymbol{\theta} \in R^{5x12}$ is an adaptive parameter vector to be estimated. Substituting (4.14) into (4.12), it is obtained that

$$\dot{\mathbf{y}} = \mathbf{A_m y} + (\mathbf{B_l} \boldsymbol{\Lambda} \boldsymbol{\theta}_v^T - \mathbf{I})\mathbf{v}. \tag{4.15}$$

An ideal adaptive parameter vector $\boldsymbol{\theta}^*$ is assumed to exist and satisfy $\mathbf{B_l} \boldsymbol{\Lambda} \boldsymbol{\theta}_v^{*T} = \mathbf{I}$. Defining $\tilde{\boldsymbol{\theta}}_v^T = \boldsymbol{\theta}_v^T - \boldsymbol{\theta}_v^{*T}$, where $\tilde{\boldsymbol{\theta}}_v^T$ is the deviation of the adaptive parameter vector $\boldsymbol{\theta}_v^T$ from its ideal value $\boldsymbol{\theta}_v^{*T}$, (4.15) can rewritten as

$$\dot{\mathbf{y}} = \mathbf{A_m y} + \mathbf{B_l} \boldsymbol{\Lambda} \tilde{\boldsymbol{\theta}}_v^T \mathbf{v} \tag{4.16}$$

Defining an error as $\mathbf{e} = \mathbf{y} - \mathbf{y_m}$ and using (4.13)-(4.16) it is obtained that

$$\dot{\mathbf{e}} = \mathbf{A_m e} + \mathbf{B_l} \boldsymbol{\Lambda} \tilde{\boldsymbol{\theta}}_v^T \mathbf{v}. \tag{4.17}$$

Using an adaptation rate matrix $\boldsymbol{\Gamma} = \boldsymbol{\Gamma}^T = \gamma \mathbf{I_r} \in R^{rxr} > 0$, where γ is a positive scalar and $\mathbf{I_r}$ is an identity matrix, it can be shown [49] that the following adaptive law

$$\dot{\boldsymbol{\theta}} = \boldsymbol{\Gamma} Proj(\boldsymbol{\theta}_v, -\mathbf{v}\mathbf{e}^T \mathbf{P} \mathbf{B_l}) \tag{4.18}$$

where $Proj$ refers to the projection [51] and $\mathbf{P}$ is the positive definite symmetric solution of the Lyapunov equation $\mathbf{A_m}^T \mathbf{P} + \mathbf{P} \mathbf{A_m} = -\mathbf{Q}$, where $\mathbf{Q}$ is a positive definite symmetric matrix.

4.3 Matrix Decomposition

In this section required decomposition for adaptive control allocation will be completed. Initially, in the proposed controller longitudinal, lateral, yaw, roll and pitch dynamics are controlled. Therefore, $\mathbf{B_{u1}}(t)$ in (A.2) is composed of the rows related to this dynamics. Moreover, for this case the non-linear longitudinal tire dynamics for longitudinal force and yaw moment is neglected and the traction force in yaw moment equation is assumed to be $F_i = T_i/R$. As a result time varying input matrix $\mathbf{B_u}(t)$, $\mathbf{B_{u1}}(t)$ and $\mathbf{B_{u2}}(t)$ can be written as in (A.1), (A.2) and (A.3).

Now, since $\mathbf{B_{u1}}(t)$ is known $\mathbf{B}(t)$ matrix should be calculated. Each column of the $\mathbf{B}(t)$ matrix corresponds to one of the allocated actuators. First four columns coincides with steering angles $\Delta\delta_1$, $\Delta\delta_2$, δ_3 and δ_4. Next four columns corresponds to torques T_i and last four columns addresses to active suspension forces f_i. Moreover, each row addresses one component of the v vector:

1. The first row corresponds to the desired traction force F_c. Since steering angles have no effect on linearized vehicle model [2] first two elements of the first row are zeros. Furthermore, because distributing equal traction force to each wheel is aimed in this paper next four elements are decomposed from the $\mathbf{B_u}$ matrix as ones. Finally, similar to the steering inputs since active suspension has no effect on traction forces, last four elements of the matrix are zeros.

2. The second row is related to yaw moment correction. First two elements are are the coefficients multiplying the steering angles in the linearized yaw moment equation [2]. Next four elements are used to determine the moment created by traction forces. Finally, last four elements are zeros since active suspension has no effect on the yaw moment M_z.

3. The third row is related to the required lateral force. The first two elements are drawn from the linearized lateral acceleration equations [2]. Due to linearization, the effect of traction forces on lateral forces are neglected resulting in zero entries for the next four elements. Lastly, the last four elements are zeros since active suspension has no effect on the lateral force.

4. The last two rows are related to required pitch and roll moment. first six elements are zeros since steering angles and traction forces have no effect on active suspension. Last four elements are constructed by using the coefficients of active suspension forces at equations (2.40), (2.39).

The resulting $\mathbf{B}(t)$ matrix can be found in (A.4). Furthermore for adaptive allocation to incorporate the time varying functions in $\mathbf{B}(t)$, $\mathbf{B_l}$ and $\mathbf{B_n}(t)$ matrices should be decomposed. Since in the $\mathbf{B}(t)$ matrix same time-varying functions appear in each column, a diagonal $\mathbf{B_n}(t)$ matrix with non-zero diagonal elements can be created as in the (A.6). Lastly, $\mathbf{B_l}$ can be calculated as,

$$\mathbf{B_l} = \mathbf{B}(t) \times \mathbf{B_n}^{-1}(t). \tag{4.19}$$

Resulting $\mathbf{B_l}$ matrix can be found in (A.5). Lastly, by using the $\mathbf{B_u}(\mathbf{t})$ matrix created by neglecting longitudinal slip dynamics in (A.1) and known $\mathbf{B}(t)$ matrix $\mathbf{B_v}$ can be calculated as in (A.7).

4.4 Simulations

In order to validate the proposed control scheme, a MatLab/Simulink model of the overall closed loop system is constructed. Different failure scenarios are simulated and the results are compared with a baseline controller. Additionally in the Appendix B.3 and B.4 sensitivity study is conducted by adding parameter estimation noise and changing the mass in friction loss scenario.

4.4.1 Baseline Controller

The baseline controller has three separate subsystems consisting of rear wheel steering control, traction force control and active suspension control.

4.4.1.1 Rear Wheel Steering Control

In the baseline system rear wheel's angle of rotation is determined to be proportional to the front wheels' rotation angle. This proportion can be found in [53, 2]. This varying gain between front and rear steering angle is designed to satisfy zero side slip angle for maximum stability. In low speeds rear steering gain K_s is negative to increase maneuverability. In high speeds however, gain is positive and increases the stability.

$$K_s = \frac{\delta_r}{\delta_f} = \frac{mV_x^2 a - bLC_{\alpha r}}{mV_x^2 b + aLC_{\alpha f}} \cdot \frac{C_{\alpha f}}{C_{\alpha r}} \tag{4.20}$$

where K_1, K_2 are positive real numbers, V_x is longitudinal velocity and δ_f, δ_r are front and rear steering angles respectively.

4.4.1.2 Traction Control

The total traction force F_c is generated via a PI controller similar to the one used in the proposed virtual control input (see (4.1)). Then, this total traction force is distributed among the wheels proportional to the normal force at the tire. Resulting law is as follows.

$$F_{xi} = \frac{F_c \, mg}{4N_i}, \tag{4.21}$$

where F_{xi} is the longitudinal force and N_i is the normal force at i^{th} tire where $i \in [1, 4]$.

4.4.1.3 Active Suspension Control

Active suspension forces in the baseline system are determined by two PI controllers to stabilize the roll and pitch motion. The PI controllers use the deviations of the roll θ and pitch ϕ angles to determine the required active suspension forces to stabilize the roll and pitch rotations. These forces are then distributed to the individual wheels according to their moment creation effects provided in (2.40) and (2.39).

$$\begin{aligned} f_{pitch} &= -K_{pp}\theta - K_{ip}\int \theta dt \\ f_{roll} &= -K_{pp}\phi - K_{ip}\int \phi dt \end{aligned} \tag{4.22}$$

$$
\begin{aligned}
f_{fl} &= -f_{pitch} + f_{roll} \\
f_{fr} &= -f_{pitch} - f_{roll} \\
f_{rl} &= f_{pitch} + f_{roll} \\
f_{fl} &= f_{pitch} - f_{roll}
\end{aligned} \tag{4.23}
$$

where f_{ij} is active suspension force at ij wheel where $i \in \{f, r\}$ and $j \in \{l, r\}$.

4.4.2 Low Speed Performance

Initially, the proposed controller is compared to the baseline system for the case of no failure and when the velocity of the vehicle $V_x = 13\ m/s$, in an object avoidance maneuver followed by an emergency breaking. The simulation results are given in Fig. 4.3, where the bottom right sub-figure shows the trajectories of the vehicles with the baseline and proposed controllers, together with the obstacle which is represented as a red dashed line at x=80m. In this scenario, steering maneuver starts at $t = 3s$ and ends at $t = 6s$. Later, at $t = 6.3s$ driver brakes for $1s$ and then driver gives no throttle or break input. Fig. 4.3 also shows the allocated signals, which are front steering angle correction, rear steering angle, traction forces, active suspension forces and vehicle states. Baseline system is noted as w/o while proposed system is labeled as $w/$. It can be seen that the proposed system performs similarly to the nominal system.

4.4.3 High Speed Performance

Moreover, the proposed controller is compared to the baseline system when the longitudinal velocity V_x is 20 m/s. Same steering and throttle/break input is applied as the previous case and there are no failures in the system. The simulation results can be found in Fig. 4.4. When the side-slip of the two vehicles are compared, it can be seen that baseline vehicle has much less side-slip. This is due to the used rear wheel steering gain. As velocity of the vehicle increases the rear steering gain K_s increases to maintain yaw stability of the vehicle which results with lower side-slip angle. However, because there is more rear steering in the baseline system than the proposed controller baseline vehicle's yaw rotation is not as much as the proposed system. As result baseline system cannot follow the reference trajectory.

4.4.4 Varying Road Conditions

To emulate another type of an emergency condition and study the effectiveness of the proposed controller, the road surface conditions were used. In this simulation the road friction coefficient C_α for the right tires reduced to half of its value in order to simulate slippery road conditions starting at $t = 4s$ while the vehicle is commanded to perform the same object avoidance maneuver. The results in Fig. 4.5 show that the baseline vehicle had difficulty following the commands while the proposed controller performed as designed. In order to compensate varying road conditions, proposed system sends much more traction force to the right wheels. As a result it can follow the reference yaw signal. Moreover, trajectories, side slip angles and velocities show that vehicle equipped with the new controller remained stable while the baseline system failed and spun.

4.4.5 Actuator Failure with Varying Road Conditions

In order to test the performance of the proposed controller in challenging situations, an "effectiveness loss at wheel" scenario is created. In this scenario, rear right wheel traction force and steering angle are reduced to 10% at $t = 1$ $[s]$ of their original values, respectively. Additionally at $t = 4$ $[s]$ effectiveness of lateral friction is reduced to 90%. Results of the simulation can be seen at Fig. 4.6. After traction failures, the proposed controller modifies the steering angles to compensate for the undesired moments created by the actuator effectiveness losses. When the object avoidance maneuver is performed since the effectiveness loss at steering and traction force is not compensated, the baseline system cannot make a stable turn and spins. The proposed controller, on the other hand, can provide a stable turn around the obstacle and follows the reference trajectory.

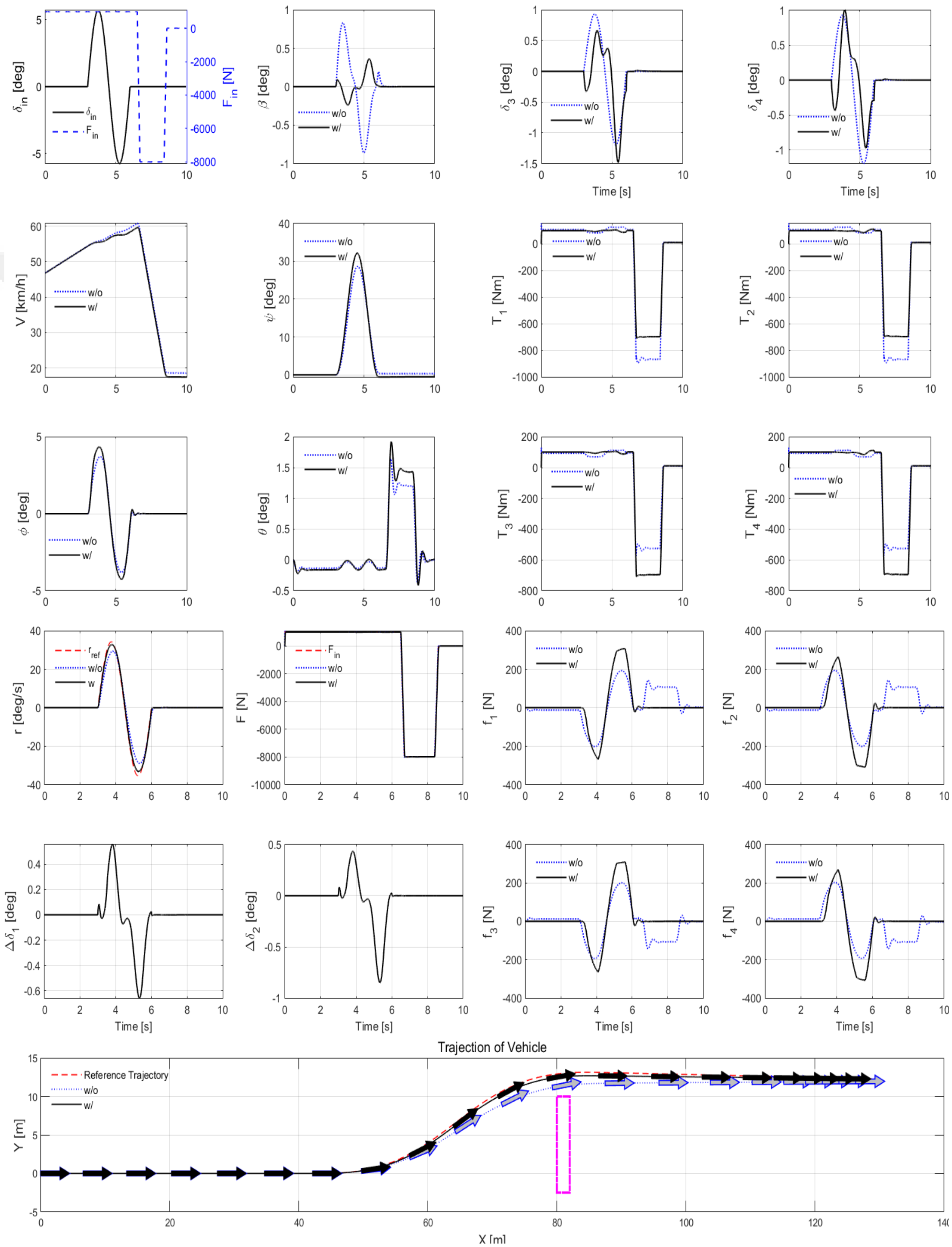

Figure 4.3: Low Speed Performance

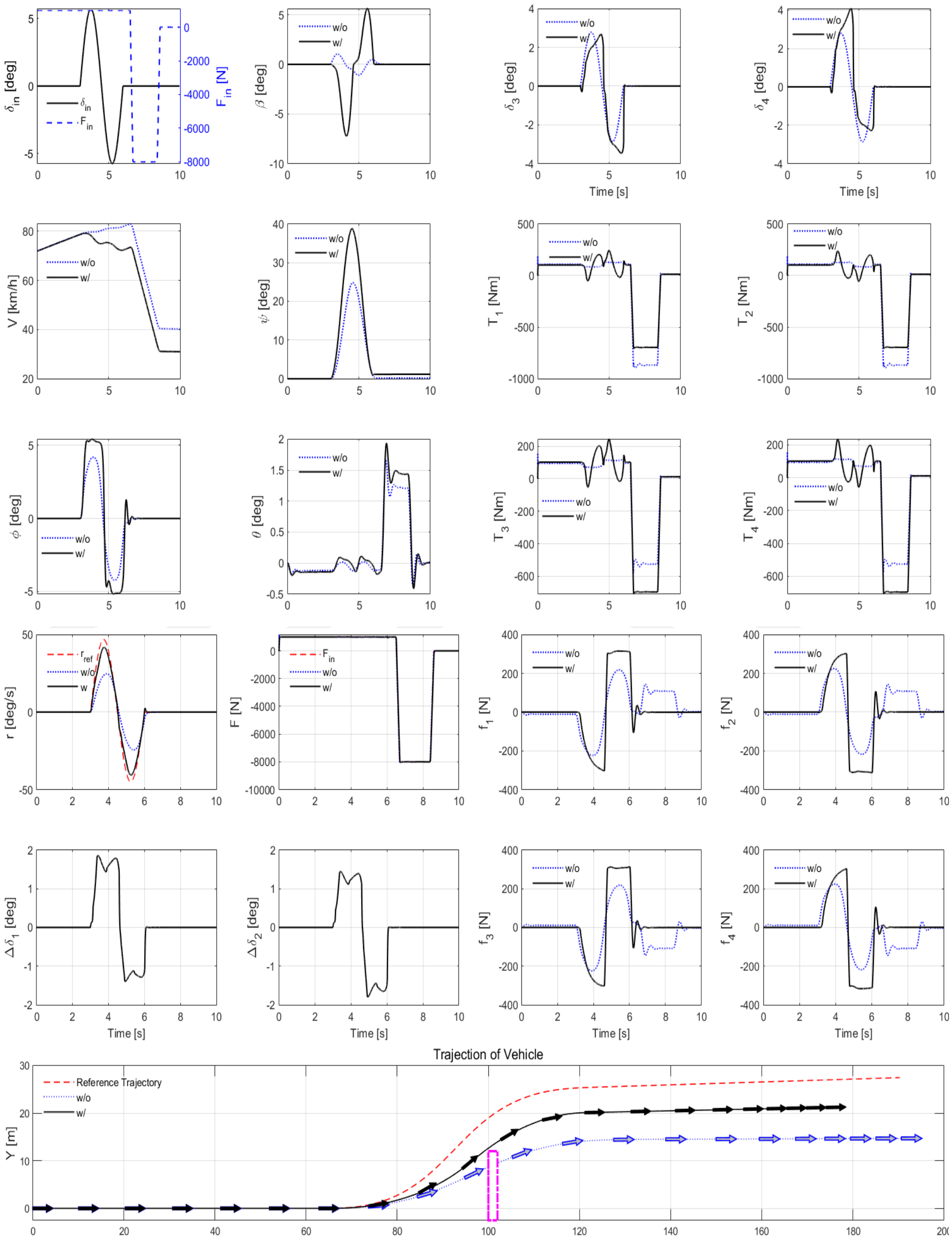

Figure 4.4: High Speed Performance

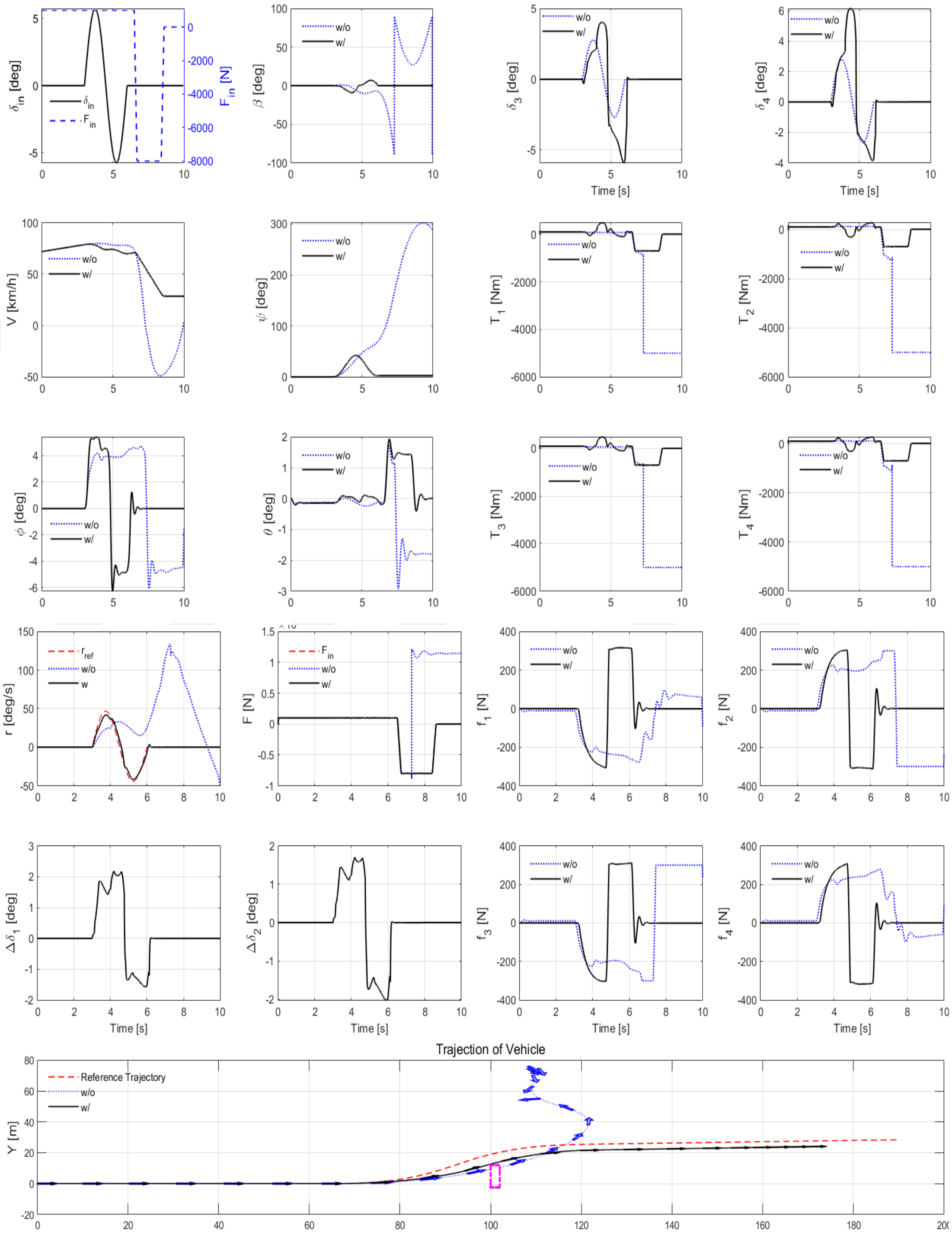

Figure 4.5: Object Avoidance Maneuver with Actuator Failure and Varying Road Conditions

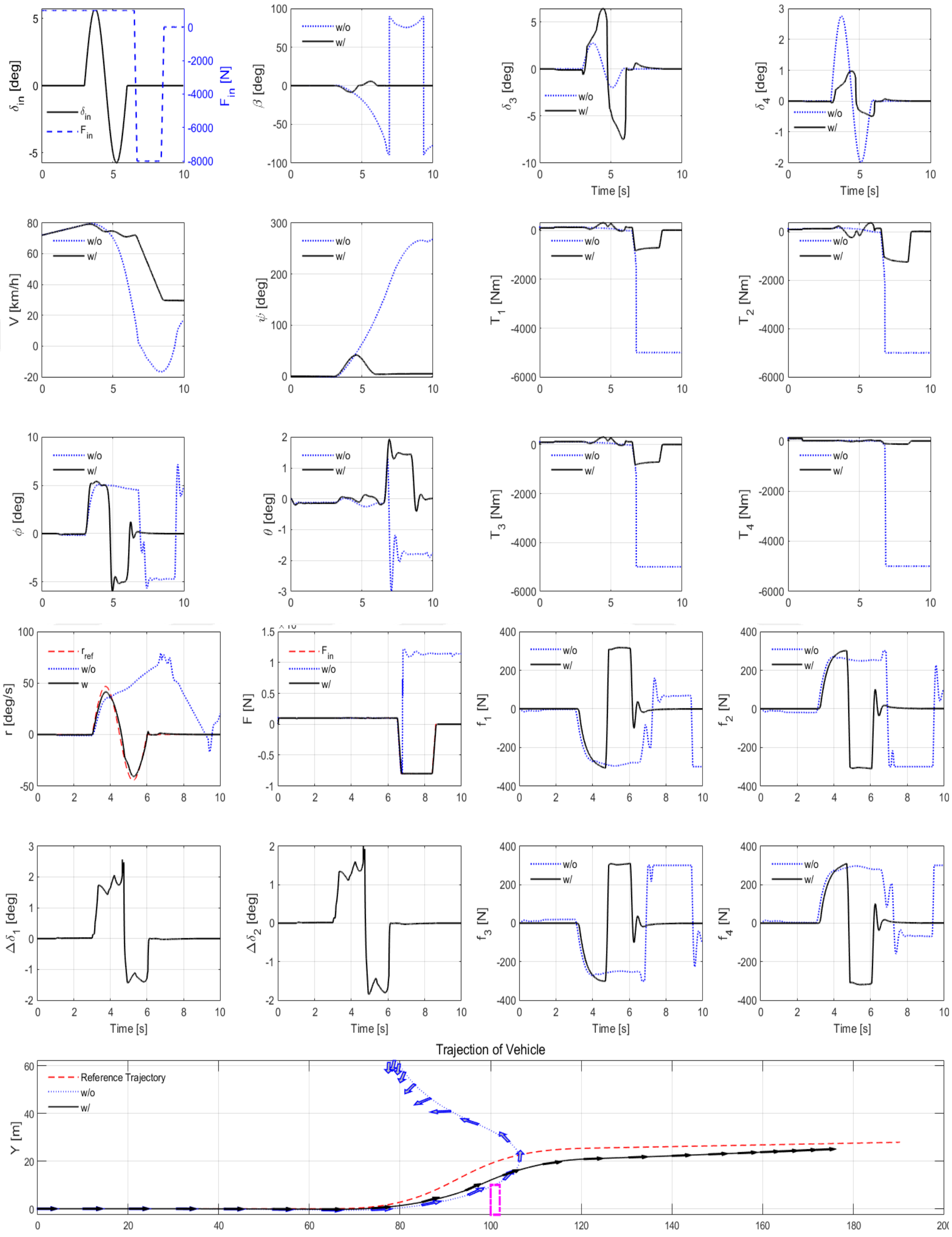

Figure 4.6: Object Avoidance Maneuver with Actuator Failure

Chapter 5

Conclusion and Future Work

Having an valid vehicle model is extremely important for controller development. Usually vehicle dynamics are studied in 3 different fields which are longitudinal, lateral and vertical. However, these dynamics affects each other. Therefore, it is beneficial to have a vehicle model that integrates all dynamics of the system. Similarly, since in automobiles each dynamic is associated with the each other, it is better to approach the control problem of the vehicle as a single system rather than developing different controllers for each subsystems.

In this study, initially, control oriented two non-linear and two linear vehicle models are developed and validated by using commercial 1-D simulation program Amesim. Results show that developed models shows similar performance with the 14 Dof iCar model at the Amesim. Moreover, linearized version of the models provides good approximation for the specified linerization parameters and creates ease for developing controllers.

Secondly, an adaptive control allocation system based on the 3 degrees of freedom vehicle model for longitudinal, yaw, roll and pitch control of ground vehicles is proposed. The controller is validated by using a 3 degrees of freedom vehicle model. Simulation results show that the proposed controller provides comparable performance with the baseline system in ideal conditions without any failure. However, it is shown that, unlike the baseline controller, the proposed approach can stabilize the vehicle in the case of certain failures.

Finally, adaptive control allocation algorithm is modified to incorporate the non-linearities due to trigonometric functions in the system. Modified adaptive control allocation algorithm is designed and validated by using the 14 degrees of freedom vehicle model. Designed controller utilizes the steering, motor and brake actuators to follow desired yaw and force reference while keeping the vehicle stable. Simulation results show that the proposed controller provides comparable performance with the baseline system in low velocities without any failure. However, when the velocity is higher baseline system cannot follow the reference yaw while proposed system can successfully follow the references. Moreover, it is shown that, then there is an fault or effectiveness loss in the vehicle, proposed system can tolerate the fault while baseline system oversteers and spins.

In the future work proposed overall adaptive allocation scheme will be modified to include the remaining non-linearities of the vehicle model such as tire dynamics. Moreover, currently allocation algorithm does not seek for any optimal solution. Adding an optimality criteria would improve the overall performance of the system. Lastly, in the future machine learning can be combined with the adaptive control allocation algorithm to find the optimal controller parameters.

Bibliography

[1] U. Kiencke and L. Nielsen, *Automotive control systems: For engine, driveline, and vehicle: Second edition*. 2005.

[2] A. G. Ulsoy, H. Peng, and M. Çakmakci, *Automotive Control Systems*. Cambridge University Press, 2012.

[3] R. N. Jazar, *Vehicle dynamics: theory and application*. New York: Springer, 2 ed., 2008.

[4] M. Abe, "Fundamentals of Vehicle Dynamics," *Vehicle Handling Dynamics*, pp. 45–107, 2015.

[5] M. Software, "Adams car web page," 2018.

[6] M. Simulation, "Carsim web page," 2018.

[7] Siemens, "Amesim web page," 2018.

[8] K. Berntorp, "Derivation of a Six Degrees-of- Freedom Ground-Vehicle Model for Automotive Applications," no. February, 2013.

[9] S. T. Hirtle, "Eight Degree of Freedom Vehicle Model With Pitch, Yaw, Tire Control and Sensor Inputs," vol. 53, no. 9, pp. 1689–1699, 2015.

[10] J. D. Setiawan, M. Safarudin, and A. Singh, "Modeling, simulation and validation of 14 DOF full vehicle model," *International Conference on Instrumentation, Communication, Information Technology, and Biomedical Engineering 2009, ICICI-BME 2009*, 2009.

[11] G. Genta and L. Morello, *The Automotive Chassis: Volume 2: System Design*. Mechanical Engineering Series, Springer Netherlands, 2008.

[12] R. Darus and Y. M. Sam, "Modeling and control active suspension system for a full car model," *5th International Colloquium on Signal Processing Its Applications*, vol. 4, no. 7, pp. 13–18, 2009.

[13] S. Ikenaga, F. L. Lewis, J. Campos, and L. Davis, "Active suspension control of ground vehicle based on a full-vehicle model," in *Proceedings of the American Control Conference*, 2000.

[14] T. Chung and K. Yi Kyongsu, "Design and evaluation of side slip angle-based vehicle stability control scheme on a virtual test track," *IEEE Transactions on Control Systems Technology*, vol. 14, no. 2, pp. 224–234, 2006.

[15] R. Rajamani and D. N. Piyabongkarn, "New paradigms for the integration of yaw stability and rollover prevention functions in vehicle stability control," *IEEE Transactions on Intelligent Transportation Systems*, vol. 14, no. 1, pp. 249–261, 2013.

[16] J. Yoon, W. Cho, B. Koo, and K. Yi, "Unified chassis control for rollover prevention and lateral stability," *IEEE Transactions on Vehicular Technology*, 2009.

[17] M. S. Basrah, E. Siampis, E. Velenis, and D. Cao, "Wheel slip control with torque blending using linear and nonlinear model predictive control," *Vehicle System Dynamics*, vol. 3114, no. May, 2017.

[18] P. Dix, B. Ashrafi, S. Drakunov, and U. Özguner, "ABS Control Using Optimum Search via Sliding Modes," *IEEE Transactions on Control Systems Technology*, vol. 3, no. 1, pp. 79–85, 1995.

[19] Tor A. Johansen, Idar Petersen, Jens Kalkkuhl and J. Lüdemann, "Gain-Scheduled Wheel Slip Control in Automotive Brake Systems," *IEEE Transactions on Control Systems Technology*, vol. 11, no. 6, pp. 799–811, 2003.

[20] J. H. Park and C. Y. Kim, "Wheel Slip Control in Traction Control System for Vehicle Stability," *Vehicle System Dynamic*, 1999.

[21] K. Nam, H. Fujimoto, and Y. Hori, "Lateral stability control of in-wheel-motor-driven electric vehicles based on sideslip angle estimation using lateral tire force sensors," *IEEE Transactions on Vehicular Technology*, 2012.

[22] H. I. Dokuyucu and M. Cakmakci, "Concurrent Design of Energy Management and Vehicle Traction Supervisory Control Algorithms for Parallel Hybrid Electric Vehicles," *IEEE Transactions on Vehicular Technology*, vol. 65, pp. 555–565, feb 2016.

[23] M. Ataei, A. Khajepour, and S. Jeon, "A Novel Reconfigurable Integrated Vehicle Stability Control with Omni Actuation Systems," *IEEE Transactions on Vehicular Technology*, vol. 67, no. 4, pp. 2945–2957, 2018.

[24] M. Mirzaei and H. Mirzaeinejad, "Fuzzy Scheduled Optimal Control of Integrated Vehicle Braking and Steering Systems," *IEEE/ASME Transactions on Mechatronics*, vol. 22, no. 5, pp. 2369–2379, 2017.

[25] S. Fergani, O. Sename, and L. Dugard, "An LPV/H integrated Vehicle Dynamic Controller," *IEEE Transactions on Vehicular Technology*, vol. 65, no. c, pp. 1–1, 2015.

[26] J. Ni, J. Hu, and C. Xiang, "Envelope Control for Four-Wheel Independently Actuated Autonomous Ground Vehicle Through AFS/DYC Integrated Control," *IEEE Transactions on Vehicular Technology*, vol. 66, no. 11, pp. 9712–9726, 2017.

[27] G. Yin, N. Chen, and P. Li, "Improving handling stability performance of four-wheel steering vehicle via μ-synthesis robust control," *IEEE Transactions on Vehicular Technology*, vol. 56, no. 5 I, pp. 2432–2439, 2007.

[28] H. E. B. Russell and J. C. Gerdes, "Design of Variable Vehicle Handling Characteristics Using Four-Wheel Steer-by-Wire," *IEEE Transactions on Control Systems Technology*, vol. 24, pp. 1529–1540, sep 2016.

[29] E. Ono, Y. Hattori, Y. Muragishi, and K. Koibuchi, "Vehicle dynamics integrated control for four-wheel-distributed steering and four-wheel-distributed traction/braking systems," *Vehicle System Dynamics*, vol. 44, no. 2, pp. 139–151, 2006.

[30] A. Tavasoli, M. Naraghi, and H. Shakeri, "Optimized coordination of brakes and active steering for a 4WS passenger car," *ISA Transactions*, vol. 51, pp. 573–583, sep 2012.

[31] R. Wang, H. Zhang, and J. Wang, "Linear parameter-varying controller design for four-wheel independently actuated electric ground vehicles with active steering systems," *IEEE Transactions on Control Systems Technology*, vol. 22, no. 4, pp. 1281–1296, 2014.

[32] Y. Wang, G. Liu, D. Zhang, H. Zhou, H. Ye, and X. Chen, "Combined Fault-Tolerant Control with Optimal Control Allocation for Four-Wheel Independently Driven Electric Vehicles," in *2016 IEEE Vehicle Power and Propulsion Conference (VPPC)*, pp. 1–5, IEEE, oct 2016.

[33] M. W. Oppenheimer, D. B. Doman, and M. A. Bolender, "Control allocation for over-actuated systems," in *2006 14th Mediterranean Conference on Control and Automation*, pp. 1–6, June 2006.

[34] *Control Allocation*, pp. 89–106. London: Springer London, 2009.

[35] T. A. Johansen and T. I. Fossen, "Control allocation - A survey," *Automatica*, vol. 49, no. 5, pp. 1087–1103, 2013.

[36] O. Härkegård, *Backstepping and Control Allocation with Applications to Flight Control*. No. 820, 2003.

[37] J. Tjonnas and T. A. Johansen, "Stabilization of Automotive Vehicles Using Active Steering and Adaptive Brake Control Allocation," *IEEE Transactions on Control Systems Technology*, vol. 18, pp. 545–558, may 2010.

[38] J. Tjønnås and T. A. Johansen, "Adaptive control allocation," *Automatica*, vol. 44, pp. 2754–2765, nov 2008.

[39] C. Canudas De Wit and P. Tsiotras, "Dynamic tire friction models for vehicle traction control," *Proceedings of the 38th IEEE Conference on Decision and Control (Cat. No.99CH36304)*, vol. 4, no. December, pp. 3746–3751, 1999.

[40] K. J. Åström and C. Canudas-de wit, "Revisting the LuGre Friction Model," *IEEE Control Systems Magazine*, no. December, pp. 101–114, 2008.

[41] C. Canudas-de Wit, P. Tsiotras, E. Velenis, M. Basset, and G. Gissinger, "Dynamic Friction Models for Longitudinal Road/Tire Interaction: Experimental Results," *IASTED Conference on Modelling, Identification and Control, Innsbruck*, pp. 3–8, 2002.

[42] E. Tönük and Y. S. Ünlüsoy, "Prediction of automobile tire cornering force characteristics by finite element modeling and analysis," *Computers and Structures*, vol. 79, no. 13, pp. 1219–1232, 2001.

[43] H. B. Pacejka and E. Bakker, "The magic formula tire model," *Vehicle System Dynamics*, vol. 21, no. 1, pp. 1–18, 1992.

[44] H. B. Pacejka, *Tire and Vehicle Dynamics*. 2006.

[45] G. Genta and L. Morello, *The Automotive Chassis: Volume 1: Components Design*. Mechanical Engineering Series, Springer Netherlands, 2008.

[46] J. Deur, V. Ivanovic, M. Hancock, and F. Assadian, "Modeling and Analysis of Active Differential Dynamics," *Journal of Dynamic Systems, Measurement, and Control*, vol. 132, no. 6, p. 061501, 2010.

[47] G. Genta and L. Morello, *The automotive chassis: Components design. Vol. 1*, vol. 1. Springer Netherlands, 1 ed., 2009.

[48] R. Rajamani, *Vehicle Dynamics and Control*. 2006.

[49] S. S. Tohidi, Y. Yildiz, and I. Kolmanovsky, "Fault tolerant control for over-actuated systems: An adaptive correction approach," *Proceedings of the American Control Conference*, vol. 2016-July, pp. 2530–2535, 2016.

[50] S. S. Tohidi, Y. Yildiz, and I. Kolmanovsky, "Adaptive Control Allocation for Over-Actuated Systems with Actuator Saturation," *IFAC-PapersOnLine*, vol. 50, no. 1, pp. 5492–5497, 2017.

[51] E. Lavretsky and T. E. Gibson, "Projection Operator in Adaptive Systems," 2011.

[52] Y. Yildiz, I. V. Kolmanovsky, and D. Acosta, "A control allocation system for automatic detection and compensation of phase shift due to actuator rate

limiting," *Proceedings of the 2011 American Control Conference*, pp. 444–449, 2011.

[53] R. Marino, S. Scalzi, and F. Cinili, "Nonlinear PI front and rear steering control in four wheel steering vehicles," *User Modeling and User-Adapted Interaction*, vol. 45, no. 12, pp. 1149–1168, 2007.

Appendix A

Matrices for Linear Models and Controllers

$$
\mathbf{B_{u2}}(t) = \begin{bmatrix}
0 & 0 & 0 & 0 & 0 & 0 & 0 & 0 & 0 & 0 & 0 & 0 \\
0 & 0 & 0 & 0 & 0 & 0 & 0 & 0 & 0 & 0 & 0 & 0 \\
0 & 0 & 0 & 0 & 0 & 0 & 0 & 0 & 0 & 0 & 0 & 0 \\
0 & 0 & 0 & 0 & 1/I_w & 0 & 0 & 0 & 0 & 0 & 0 & 0 \\
0 & 0 & 0 & 0 & 0 & 0 & 0 & 0 & 0 & 0 & 0 & 0 \\
0 & 0 & 0 & 0 & 0 & 1/I_w & 0 & 0 & 0 & 0 & 0 & 0 \\
0 & 0 & 0 & 0 & 0 & 0 & 0 & 0 & 0 & 0 & 0 & 0 \\
0 & 0 & 0 & 0 & 0 & 0 & 1/I_w & 0 & 0 & 0 & 0 & 0 \\
0 & 0 & 0 & 0 & 0 & 0 & 0 & 0 & 0 & 0 & 0 & 0 \\
0 & 0 & 0 & 0 & 0 & 0 & 0 & 1/I_w & 0 & 0 & 0 & 0 \\
0 & 0 & 0 & 0 & 0 & 0 & 0 & 0 & 0 & 0 & 0 & 0 \\
0 & 0 & 0 & 0 & 0 & 0 & 0 & 0 & -1 & 0 & 0 & 0 \\
0 & 0 & 0 & 0 & 0 & 0 & 0 & 0 & 0 & 0 & 0 & 0 \\
0 & 0 & 0 & 0 & 0 & 0 & 0 & 0 & 0 & -1 & 0 & 0 \\
0 & 0 & 0 & 0 & 0 & 0 & 0 & 0 & 0 & 0 & 0 & 0 \\
0 & 0 & 0 & 0 & 0 & 0 & 0 & 0 & 0 & 0 & -1 & 0 \\
0 & 0 & 0 & 0 & 0 & 0 & 0 & 0 & 0 & 0 & 0 & 0 \\
0 & 0 & 0 & 0 & 0 & 0 & 0 & 0 & 0 & 0 & 0 & -1
\end{bmatrix} \tag{A.3}
$$

$$
\mathbf{B_u}(t) = \begin{bmatrix}
0 & 0 & 0 & 0 & 0 & 0 & 0 & 0 & 0 & 0 & 0 & 0 \\
\frac{cos(\delta_1)}{R} & \frac{cos(\delta_2)}{R} & \frac{cos(\delta_3)}{R} & \frac{cos(\delta_4)}{2} & 0 & 0 & 0 & 0 & 0 & 0 & 0 & 0 \\
0 & 0 & 0 & 0 & 0 & 0 & 0 & 0 & 0 & 0 & 0 & 0 \\
\frac{N_1 C_{af} cos(\delta_1)}{m} & \frac{N_2 C_{af} cos(\delta_2)}{m} & \frac{N_3 C_{ar} cos(\delta_3)}{m} & \frac{N_4 C_{ar} cos(\delta_4)}{m} & 0 & 0 & 0 & 0 & 0 & 0 & 0 & 0 \\
0 & 0 & 0 & 0 & 0 & 0 & 0 & 0 & 0 & 0 & 0 & 0 \\
\frac{-N_1 C_{af} hcos(\delta_1)}{I_r} & \frac{-N_2 C_{af} hcos(\delta_2)}{I_r} & \frac{-N_3 C_{ar} hcos(\delta_3)}{I_r} & \frac{-N_4 C_{ar} hcos(\delta_4)}{I_r} & 0 & 0 & 0 & 0 & -\frac{w}{2} & \frac{w}{2} & -\frac{w}{2} & \frac{w}{2} \\
0 & 0 & 0 & 0 & 0 & 0 & 0 & 0 & 0 & 0 & 0 & 0 \\
0 & 0 & 0 & 0 & 0 & 0 & 0 & 0 & -a & -a & b & b \\
0 & 0 & 0 & 0 & 0 & 0 & 0 & 0 & 0 & 0 & 0 & 0 \\
\frac{aN_1 C_{af} cos(\delta_1)}{I_z} & \frac{aN_2 C_{af} cos(\delta_2)}{I_z} & \frac{-bN_3 C_{ar} cos(\delta_3)}{I_z} & \frac{-bN_4 C_{ar} cos(\delta_4)}{I_z} & \frac{-wcos(\delta_1)}{2R} & \frac{wcos(\delta_2)}{2R} & \frac{-wcos(\delta_3)}{2R} & \frac{wcos(\delta_4)}{2R} & 0 & 0 & 0 & 0 \\
0 & 0 & 0 & 0 & 0 & 0 & 0 & 0 & 0 & 0 & 0 & 0 \\
0 & 0 & 0 & 0 & 0 & 0 & 0 & 0 & 0 & 0 & 0 & 0 \\
0 & 0 & 0 & 0 & 0 & 0 & 0 & 0 & 0 & 0 & 0 & 0 \\
0 & 0 & 0 & 0 & 1/I_w & 0 & 0 & 0 & 0 & 0 & 0 & 0 \\
0 & 0 & 0 & 0 & 0 & 0 & 0 & 0 & 0 & 0 & 0 & 0 \\
0 & 0 & 0 & 0 & 0 & 1/I_w & 0 & 0 & 0 & 0 & 0 & 0 \\
0 & 0 & 0 & 0 & 0 & 0 & 0 & 0 & 0 & 0 & 0 & 0 \\
0 & 0 & 0 & 0 & 0 & 0 & 1/I_w & 0 & 0 & 0 & 0 & 0 \\
0 & 0 & 0 & 0 & 0 & 0 & 0 & 0 & 0 & 0 & 0 & 0 \\
0 & 0 & 0 & 0 & 0 & 0 & 0 & 1/I_w & 0 & 0 & 0 & 0 \\
0 & 0 & 0 & 0 & 0 & 0 & 0 & 0 & 0 & 0 & 0 & 0 \\
0 & 0 & 0 & 0 & 0 & 0 & 0 & 0 & -1 & 0 & 0 & 0 \\
0 & 0 & 0 & 0 & 0 & 0 & 0 & 0 & 0 & 0 & 0 & 0 \\
0 & 0 & 0 & 0 & 0 & 0 & 0 & 0 & 0 & -1 & 0 & 0 \\
0 & 0 & 0 & 0 & 0 & 0 & 0 & 0 & 0 & 0 & 0 & 0 \\
0 & 0 & 0 & 0 & 0 & 0 & 0 & 0 & 0 & 0 & -1 & 0 \\
0 & 0 & 0 & 0 & 0 & 0 & 0 & 0 & 0 & 0 & 0 & 0 \\
0 & 0 & 0 & 0 & 0 & 0 & 0 & 0 & 0 & 0 & 0 & -1
\end{bmatrix} \tag{A.1}
$$

$$\mathbf{B_{u1}}(t) = \begin{bmatrix} 0 & 0 & 0 & 0 & 0 & 0 & 0 & 0 & 0 & 0 & 0 & 0 \\ 0 & 0 & 0 & 0 & \frac{cos(\delta_1)}{m\ R} & \frac{cos(\delta_2)}{m\ R} & \frac{cos(\delta_3)}{m\ R} & \frac{cos(\delta_4)}{m\ R} & 0 & 0 & 0 & 0 \\ 0 & 0 & 0 & 0 & 0 & 0 & 0 & 0 & 0 & 0 & 0 & 0 \\ \frac{N_1 C_{af} cos(\delta_1)}{m} & \frac{N_2 C_{af} cos(\delta_2)}{m} & \frac{N_3 C_{ar} cos(\delta_3)}{m} & \frac{N_4 C_{ar} cos(\delta_4)}{m} & 0 & 0 & 0 & 0 & 0 & 0 & 0 & 0 \\ 0 & 0 & 0 & 0 & 0 & 0 & 0 & 0 & 0 & 0 & 0 & 0 \\ \frac{-N_1 C_{af} h cos(\delta_1)}{I_x} & \frac{-N_2 C_{af} h cos(\delta_2)}{I_x} & \frac{-N_3 C_{ar} h cos(\delta_3)}{I_x} & \frac{-N_4 C_{ar} h cos(\delta_4)}{I_x} & 0 & 0 & 0 & 0 & -\frac{w}{2I_x} & \frac{w}{2I_x} & -\frac{w}{2I_x} & \frac{w}{2I_x} \\ 0 & 0 & 0 & 0 & 0 & 0 & 0 & 0 & 0 & 0 & 0 & 0 \\ 0 & 0 & 0 & 0 & 0 & 0 & 0 & 0 & -a/I_y & -a/I_y & b/I_y & b/I_y \\ 0 & 0 & 0 & 0 & 0 & 0 & 0 & 0 & 0 & 0 & 0 & 0 \\ \frac{a N_1 C_{af} cos(\delta_1)}{I_z} & \frac{a N_2 C_{af} cos(\delta_2)}{I_z} & \frac{-b N_3 C_{ar} cos(\delta_3)}{I_z} & \frac{-b N_4 C_{ar} cos(\delta_4)}{I_z} & \frac{-w cos(\delta_1)}{2I_z\ R} & \frac{w cos(\delta_2)}{2I_z\ R} & \frac{-w cos(\delta_3)}{2I_z\ R} & \frac{w cos(\delta_4)}{2I_z\ R} & 0 & 0 & 0 & 0 \end{bmatrix} \quad (A.2)$$

$$
\mathbf{B}(t) = \begin{bmatrix}
0 & 0 & 0 & 0 & cos(\delta_1) & cos(\delta_2) & cos(\delta_3) & cos(\delta_4) & 0 & 0 & 0 & 0 \\
C_\alpha a N_1(t) cos(\delta_1) & C_\alpha a N_2(t) cos(\delta_2) & -C_\alpha b N_3(t) cos(\delta_3) & -C_\alpha b N_4(t) cos(\delta_4) & -\frac{w cos(\delta_1)}{2} & \frac{w cos(\delta_2)}{2} & -\frac{w cos(\delta_3)}{2} & \frac{w cos(\delta_4)}{2} & 0 & 0 & 0 & 0 \\
C_\alpha N_1(t) cos(\delta_1) & C_\alpha N_2(t) cos(\delta_2) & C_\alpha N_3(t) cos(\delta_3) & C_\alpha N_4(t) cos(\delta_4) & 0 & 0 & 0 & 0 & 0 & 0 & 0 & 0 \\
0 & 0 & 0 & 0 & 0 & 0 & 0 & 0 & -a & -a & b & b \\
0 & 0 & 0 & 0 & 0 & 0 & 0 & 0 & \frac{w}{2} & -\frac{w}{2} & \frac{w}{2} & -\frac{w}{2}
\end{bmatrix} \tag{A.4}
$$

$$
\mathbf{B_l} = \begin{bmatrix} 0 & 0 & 0 & 0 & 1 & 1 & 1 & 1 & 0 & 0 & 0 & 0 \\ C_\alpha a m_q & C_\alpha a m_q & -C_\alpha b m_q & -C_\alpha b m_q & -\frac{w}{2} & \frac{w}{2} & -\frac{w}{2} & \frac{w}{2} & 0 & 0 & 0 & 0 \\ C_\alpha m_q & C_\alpha m_q & C_\alpha m_q & C_\alpha m_q & 0 & 0 & 0 & 0 & 0 & 0 & 0 & 0 \\ 0 & 0 & 0 & 0 & 0 & 0 & 0 & 0 & -a & -a & b & b \\ 0 & 0 & 0 & 0 & 0 & 0 & 0 & 0 & \frac{w}{2} & -\frac{w}{2} & \frac{w}{2} & -\frac{w}{2} \end{bmatrix} \tag{A.5}
$$

$$
\mathbf{B_v}(t) = \begin{bmatrix} 0 & 0 & 0 & 0 & 0 \\ \frac{w}{2m \; R} & 0 & 0 & 0 & 0 \\ 0 & 0 & 0 & 0 & 0 \\ 0 & 0 & 1/m & 0 & 0 \\ 0 & 0 & 0 & 0 & 0 \\ 0 & 0 & h/I_x & 0 & 1/I_x \\ 0 & 0 & 0 & 0 & 0 \\ 0 & 0 & 0 & 0 & 0 \\ 0 & 0 & 0 & 0 & 0 \\ 0 & 1/I_z & 0 & 0 & 0 \end{bmatrix} \tag{A.7}
$$

$$
\mathbf{B_n}(t) = \begin{bmatrix}
\frac{N_1}{m_q}cos(\delta_1) & 0 & 0 & 0 & 0 & 0 & 0 & 0 & 0 & 0 & 0 & 0 \\
0 & \frac{N_2}{m_q}cos(\delta_2) & 0 & 0 & 0 & 0 & 0 & 0 & 0 & 0 & 0 & 0 \\
0 & 0 & \frac{N_3}{m_q}cos(\delta_3) & 0 & 0 & 0 & 0 & 0 & 0 & 0 & 0 & 0 \\
0 & 0 & 0 & \frac{N_4}{m_q}cos(\delta_4) & 0 & 0 & 0 & 0 & 0 & 0 & 0 & 0 \\
0 & 0 & 0 & 0 & cos(\delta_1) & 0 & 0 & 0 & 0 & 0 & 0 & 0 \\
0 & 0 & 0 & 0 & 0 & cos(\delta_2) & 0 & 0 & 0 & 0 & 0 & 0 \\
0 & 0 & 0 & 0 & 0 & 0 & cos(\delta_3) & 0 & 0 & 0 & 0 & 0 \\
0 & 0 & 0 & 0 & 0 & 0 & 0 & cos(\delta_4) & 0 & 0 & 0 & 0 \\
0 & 0 & 0 & 0 & 0 & 0 & 0 & 0 & 1 & 0 & 0 & 0 \\
0 & 0 & 0 & 0 & 0 & 0 & 0 & 0 & 0 & 1 & 0 & 0 \\
0 & 0 & 0 & 0 & 0 & 0 & 0 & 0 & 0 & 0 & 1 & 0 \\
0 & 0 & 0 & 0 & 0 & 0 & 0 & 0 & 0 & 0 & 0 & 1
\end{bmatrix} \tag{A.6}
$$

$$X = \begin{bmatrix} X \\ V_x \\ Y \\ V_y \\ \phi \\ \dot{\phi} \\ \theta \\ \dot{\theta} \\ \psi \\ \dot{\psi} \\ Z \\ V_z \\ \theta_{wfl} \\ \omega_{wfl} \\ \theta_{wfr} \\ \omega_{wfr} \\ \theta_{wrl} \\ \omega_{wrl} \\ \theta_{wrr} \\ \omega_{wrr} \\ Z_{wfl} \\ \dot{Z}_{wfl} \\ Z_{wfr} \\ \dot{Z}_{wfr} \\ Z_{wrl} \\ \dot{Z}_{wrl} \\ Z_{wrr} \\ \dot{Z}_{wrr} \end{bmatrix} \tag{A.8}$$

$$\mathbf{D} = \begin{bmatrix} 0 \\ \frac{V_0^2 \rho C_d A}{2m} \\ 0 \\ 0 \\ 0 \\ 0 \\ 0 \\ 0 \\ 0 \\ 0 \\ 0 \\ 0 \\ 0 \\ \frac{N_1 C_r}{I_w} \\ 0 \\ \frac{N_2 C_r}{I_w} \\ 0 \\ \frac{N_3 C_r}{I_w} \\ 0 \\ \frac{N_4 C_r}{I_w} \\ \frac{k_{sf} z_{r1}}{m_u} \\ \frac{k_{sf} z_{r2}}{m_u} \\ \frac{k_{sr} z_{r3}}{m_u} \\ \frac{k_{sr} z_{r4}}{m_u} \end{bmatrix} \tag{A.9}$$

Appendix B

Sensitivity Studies

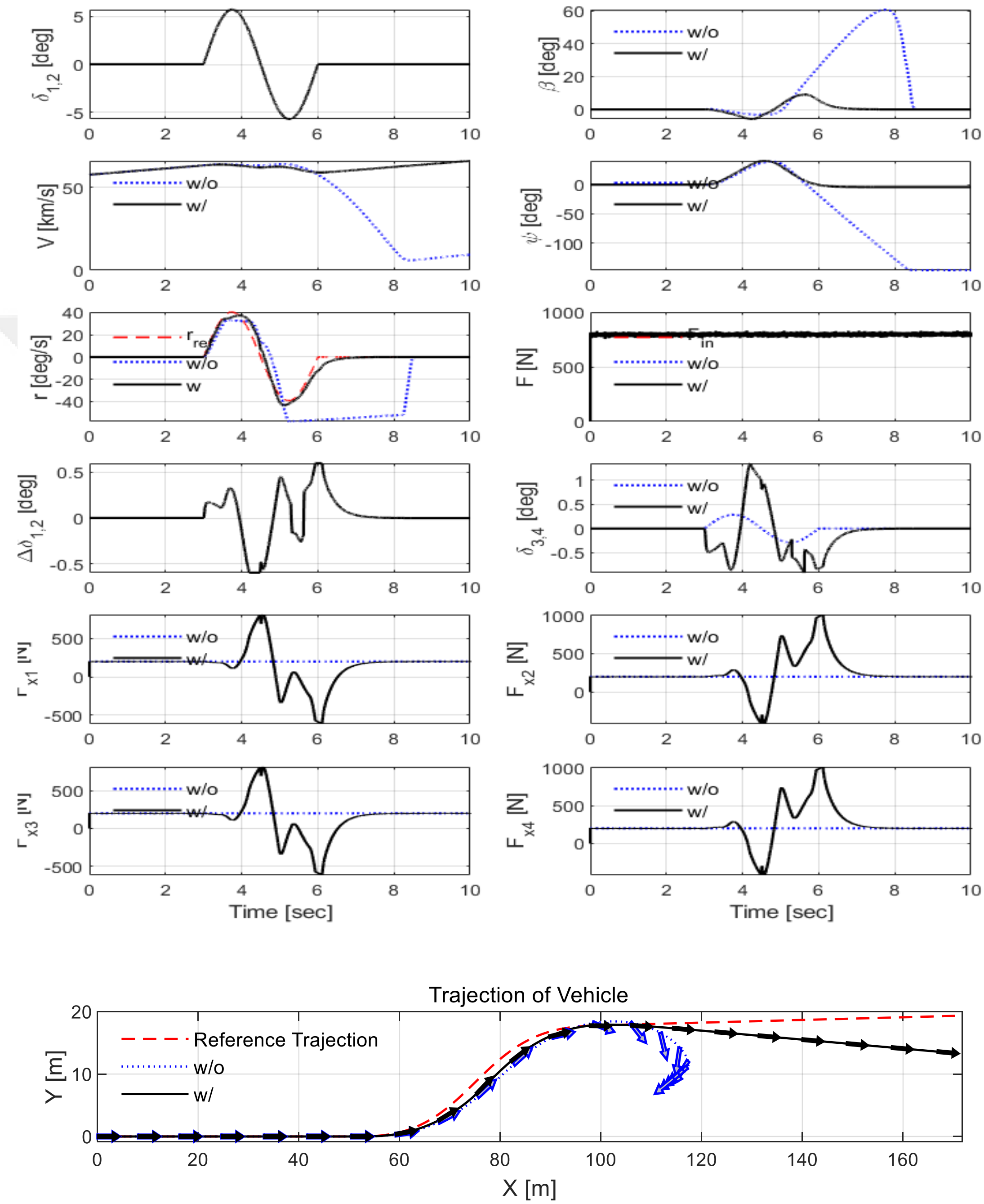

Figure B.1: Sensitivity to Parameter Estimation Noise

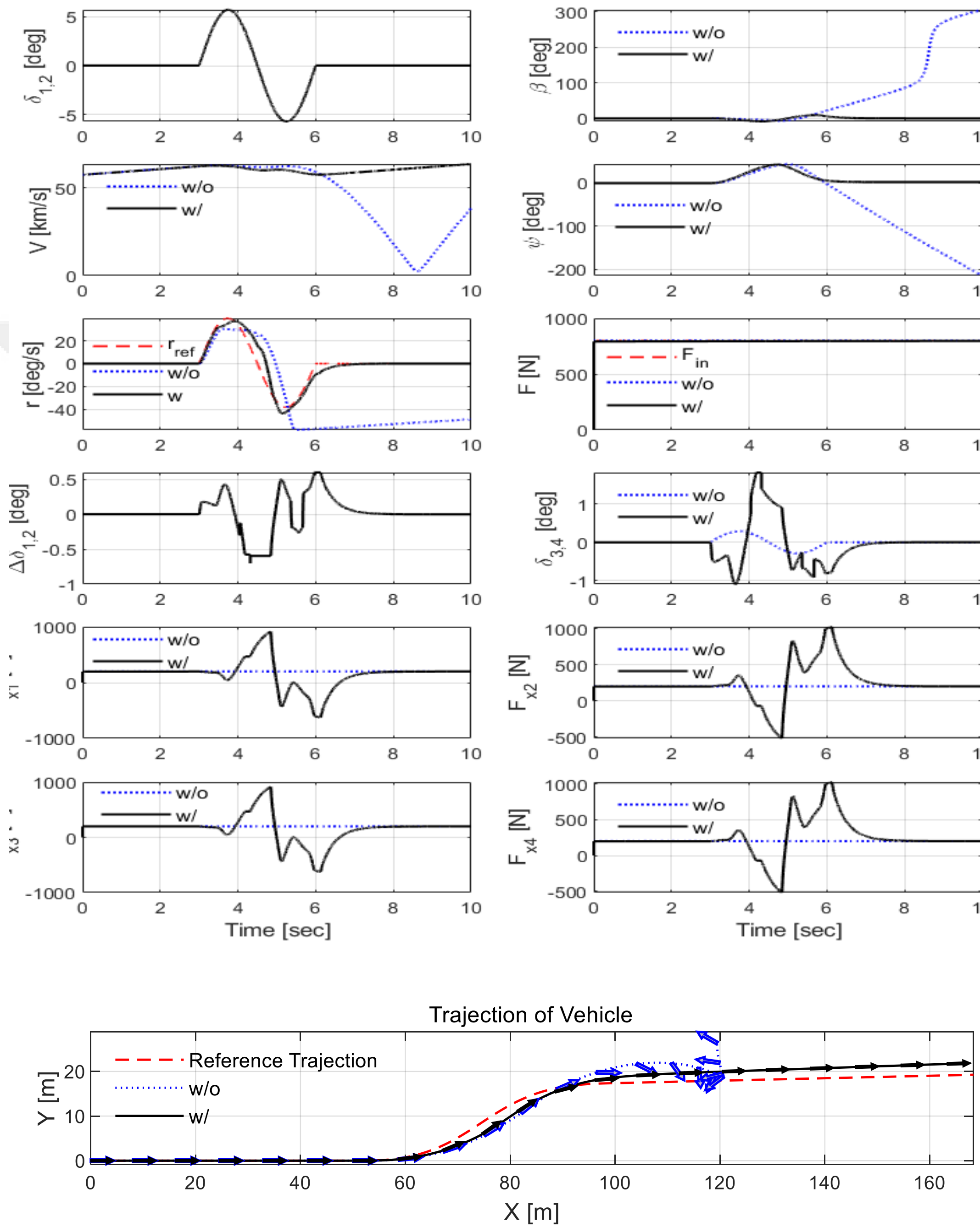

Figure B.2: Sensitivity to Different Vehicle Mass

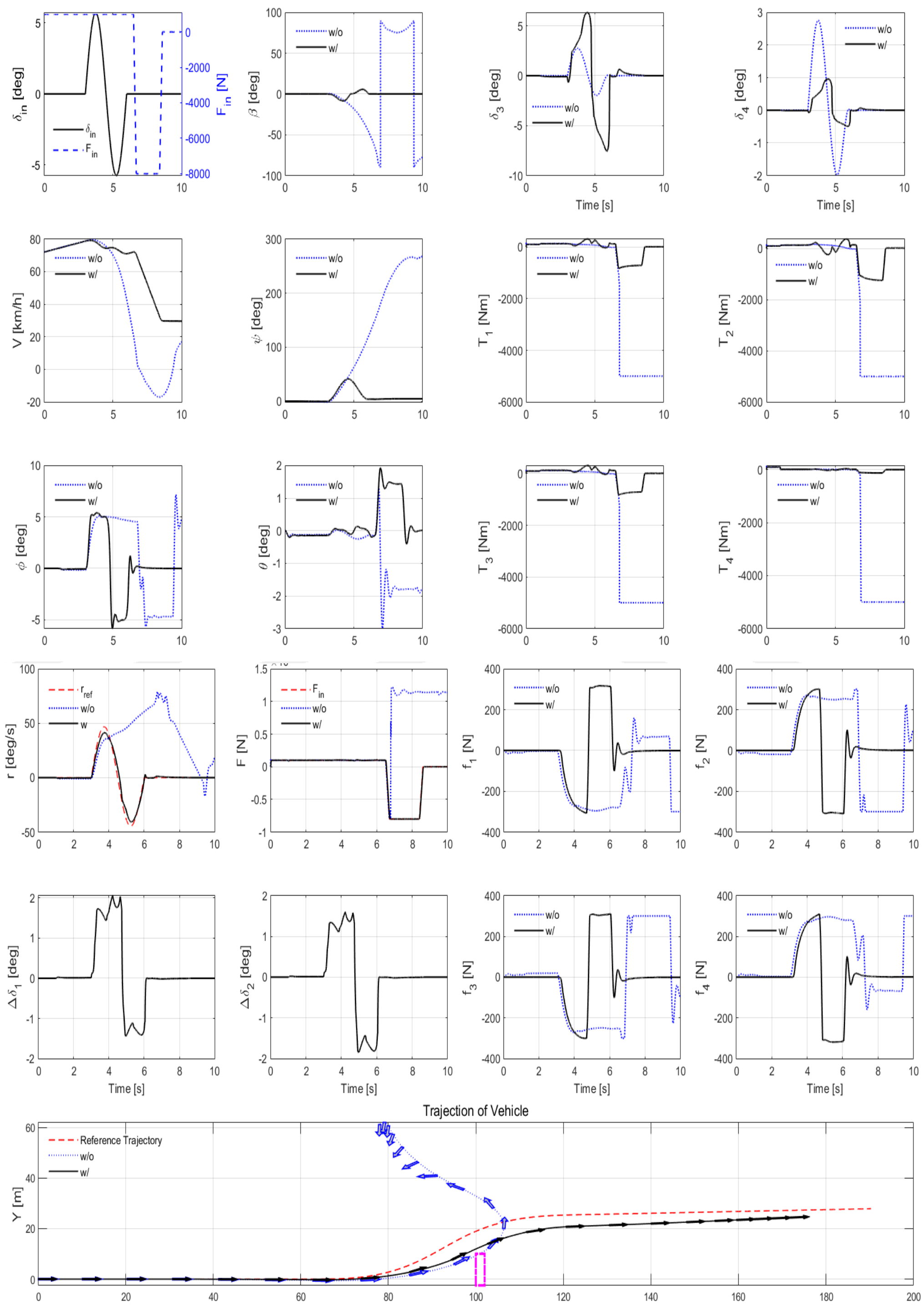

Figure B.3: Sensitivity to Parameter Estimation Noise

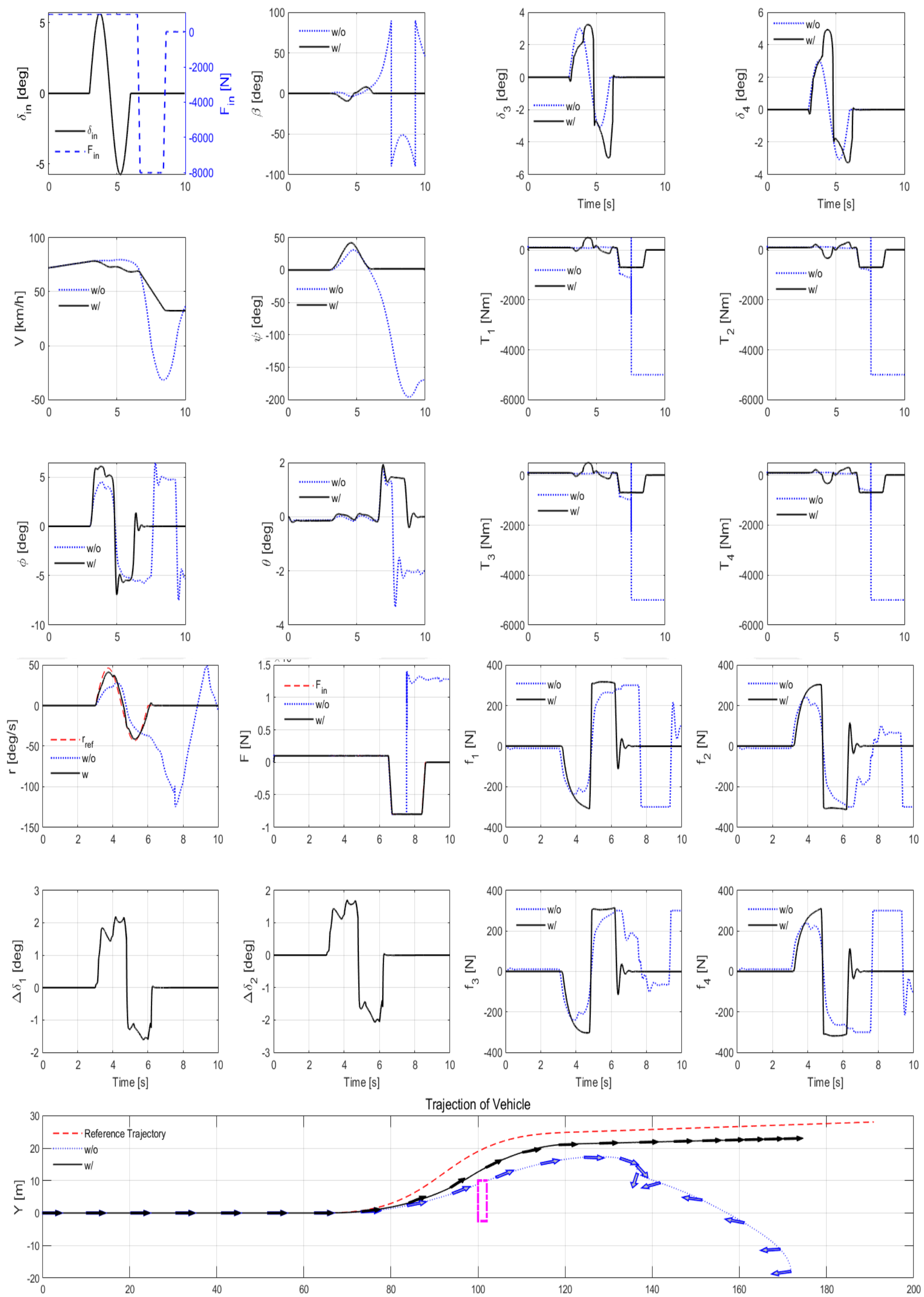

Figure B.4: Sensitivity to Different Vehicle Mass

Appendix C

Matlab Codes

C.1 Initialization for Proposed Vehicle Models

```
clc, clear, close all;
%% vehicle constants
Cd=0.3;     %drag coefficient
Nt=4.2;%4.2;       %gear ratio of transmission
Nf=1;%2.47;       %gear ratio of final drive shaft
u=0.8;      %efficiency of transmission
R=0.33;     %wheel radius (pirelli p215/65/r15)
w=1.6;
Area=2.2;
density_air=1.292;     %density of air
rho=density_air;
Q_x=0;             %slope of the road in rad
Q_y=0;             %slope of the road in rad
m=1300;           %mass of car
g=9.81;             %gravity
l=2.5;
a=1.054;
b=l-a;
fi_f=atan((w/2)/a);
fi_r=atan((w/2)/b);
```

```
l_cross_front=sqrt((w/2)^2+a^2);
l_cross_rear=sqrt((w/2)^2+b^2);
friction_coeff=0.95;
h=0.375;              %vehicle height
Cfront=1100.*1.5;
Crear=1100.*1.6;
Iz=1300; %yaw rotation axis
I_p=1000;
I_r=250;
Iw=2.7;
r=-1; %differential ratio
k_sf=21000; % front sprung mass spring coeff
c_sf=1500; % front sprung mass damping coeff
k_sr=21000; % rear sprung mass spring coeff
c_sr=1500; % rear sprung mass damping coeff
k_u=200000;
k_uf=200000;%unsprung mass spring coeff
k_ur=200000;%unsprung mass spring coeff
mus=30;
musf=30;%unsprung mass
musr=30;%unsprung mass
%% Linearization Parameters

N_f=m*g*b/(2*l)+musf*g;
N_r=m*g*a/(2*l)+musr*g;
qm=m*g/4+musf*g;
C_l=29.6; %linearized longutidunal friction (valid until 0.03 ...
    longitudinal slip)  [null]
C_af=45000/N_f; %linearized lateral friction (valid until 4.5 ...
    degree slip) [1/[rad]]
C_ar=37590/N_r; %linearized lateral friction (valid until 4.5 ...
    degree slip) [1/[rad]]
F=250;
F_b=1000;
T=F*R;
T_b=F_b*R;
C_long=10.41;
Cr=0.01; %[null] rolling resistance coefficient

%% initial conditions
```

```
v0=22; %vehicle longitudinal IC
v_t=v0/R;
v_cog0=28;
side_slip0=0;
yaw_0=0;
v_x0=v_cog0*cos(side_slip0);
v_y0=v_cog0*sin(side_slip0);
K_us=(m*b/(l*C_af*N_f))-(m*a/(l*C_ar*N_r));

%% State Space
A=[0 1 0 0 0 0 0 0 0 0 0 0 0 0 0 0 0 0 0 0 0 0 0 0 0 0 0 0 ; ...
   0 (((-2*N_r*C_l-2*N_f*C_l)/v0)-v0*rho*Cd*Area)/m 0 0 0 0 0 ...
       0 0 0 0 0 0 N_f*C_l*R/(m*v0) 0 N_f*C_l*R/(m*v0) 0 ...
       N_r*C_l*R/(m*v0) 0 N_r*C_l*R/(m*v0) 0 0 0 0 0 0 0 0 ; ...
   0 0 0 1 0 0 0 0 0 0 0 0 0 0 0 0 0 0 0 0 0 0 0 0 0 0 0 0 ; ...
   0 0 0 (-2*N_r*C_ar-2*N_f*C_af)/(v0*m) 0 0 0 0 0 0 0 ...
       (2*N_r*l_cross_rear*cos(fi_r)*C_ar - ...
       2*N_f*l_cross_front*cos(fi_f)*C_af)/(v0*m)-v0 0 0 0 0 0 ...
       0 0 0 0 0 0 0 0 0 0 0 ; ...
   0 0 0 0 0 1 0 0 0 0 0 0 0 0 0 0 0 0 0 0 0 0 0 0 0 0 0 0 ; ...
   0 0 0 0 (-2*k_sf-2*k_sr)/m (-2*c_sf-2*c_sr)/m 0 0 ...
       (2*a*k_sf-2*b*k_sr)/m (2*a*c_sf-2*b*c_sr)/m 0 0 0 0 0 0 ...
       0 0 0 0 k_sf/m c_sf/m k_sf/m c_sf/m k_sr/m c_sr/m ...
       k_sr/m c_sr/m ; ...
   0 0 0 0 0 0 0 1 0 0 0 0 0 0 0 0 0 0 0 0 0 0 0 0 0 0 0 0 ; ...
   0 0 0 (2*N_r*C_ar + 2*N_f*C_af)*h/(v0*I_r) 0 0 (-k_sf*w^2 ...
       - k_sr*w^2)/(2*I_r) (-c_sf*w^2 - c_sr*w^2)/(2*I_r) 0 0 ...
       0 -(2*N_r*l_cross_rear*cos(fi_r)*C_ar - ...
       2*N_f*l_cross_front*cos(fi_f)*C_af)*h/(v0*I_r) 0 0 0 0 ...
       0 0 0 0 w*k_sf/(2*I_r) w*c_sf/(2*I_r) -w*k_sf/(2*I_r) ...
       -w*c_sf/(2*I_r) w*k_sr/(2*I_r) w*c_sr/(2*I_r) ...
       -w*k_sr/(2*I_r) -w*c_sr/(2*I_r) ; ...
   0 0 0 0 0 0 0 0 0 1 0 0 0 0 0 0 0 0 0 0 0 0 0 0 0 0 0 0 ; ...
```

```
    0 -(((-2*N_r*C_l-2*N_f*C_l)/v0)-v0*rho*Cd*Area)*h/(I_p) 0 ...
        0 (2*a*k_sf-2*b*k_sr)/I_p (2*a*c_sf-2*b*c_sr)/I_p 0 0 ...
        (-2*a^2*k_sf-2*b^2*k_sr)/I_p ...
        (-2*a^2*c_sf-2*b^2*c_sr)/I_p 0 0 0 ...
        -h*N_f*C_l*R/(I_p*v0) 0 -h*N_f*C_l*R/(I_p*v0) 0 ...
        -h*N_r*C_l*R/(I_p*v0) 0 -h*N_r*C_l*R/(I_p*v0) ...
        -a*k_sf/I_p -a*c_sf/I_p -a*k_sf/I_p -a*c_sf/I_p ...
        b*k_sr/I_p b*c_sr/I_p b*k_sr/I_p b*c_sr/I_p ; ...
    0 0 0 0 0 0 0 0 0 0 0 1 0 0 0 0 0 0 0 0 0 0 0 0 0 0 0 0 ; ...
    0 0 0 (-2*a*N_f*C_af + b*N_r*C_ar)/(v0*Iz) 0 0 0 0 0 0 0 ...
        (-2*a*N_f*C_af*l_cross_front*cos(fi_f) - ...
        2*C_ar*b*N_r*l_cross_rear*cos(fi_r))/(v0*Iz) 0 ...
        -w*N_f*C_l*R/(2*v0*Iz) 0 w*N_f*C_l*R/(2*v0*Iz) 0 ...
        -w*N_r*C_l*R/(2*v0*Iz) 0 w*N_r*C_l*R/(2*v0*Iz) 0 0 0 0 ...
        0 0 0 0 ; ...
    0 0 0 0 0 0 0 0 0 0 0 0 0 1 0 0 0 0 0 0 0 0 0 0 0 0 0 0 ; ...
    0 N_f*R*C_l/(v0*Iw) 0 0 0 0 0 0 0 0 0 0 0 ...
        -N_f*R*C_l*R/(v0*Iw) 0 0 0 0 0 0 0 0 0 0 0 0 0 0 ; ...
    0 0 0 0 0 0 0 0 0 0 0 0 0 0 0 1 0 0 0 0 0 0 0 0 0 0 0 0 ; ...
    0 N_f*R*C_l/(v0*Iw) 0 0 0 0 0 0 0 0 0 0 0 0 0 ...
        -N_f*R*C_l*R/(v0*Iw) 0 0 0 0 0 0 0 0 0 0 0 ; ...
    0 0 0 0 0 0 0 0 0 0 0 0 0 0 0 0 0 1 0 0 0 0 0 0 0 0 0 0 ; ...
    0 N_r*R*C_l/(v0*Iw) 0 0 0 0 0 0 0 0 0 0 0 0 0 0 0 ...
        -N_r*R*C_l*R/(v0*Iw) 0 0 0 0 0 0 0 0 0 0 ; ...
    0 0 0 0 0 0 0 0 0 0 0 0 0 0 0 0 0 0 0 1 0 0 0 0 0 0 0 0 ; ...
    0 N_r*R*C_l/(v0*Iw) 0 0 0 0 0 0 0 0 0 0 0 0 0 0 0 0 0 ...
        -N_r*R*C_l*R/(v0*Iw) 0 0 0 0 0 0 0 0 ; ...
    0 0 0 0 0 0 0 0 0 0 0 0 0 0 0 0 0 0 0 0 0 1 0 0 0 0 0 0 ; ...
    0 0 0 0 k_sf/musf c_sf/musf 0.5*w*k_sf/musf ...
        0.5*w*c_sf/musf -a*k_sf/musf -a*c_sf/musf 0 0 0 0 0 0 0 ...
        0 0 0 (-k_sf-k_uf)/musf -c_sf/musf 0 0 0 0 0 0 ; ...
    0 0 0 0 0 0 0 0 0 0 0 0 0 0 0 0 0 0 0 0 0 0 0 1 0 0 0 0 ; ...
    0 0 0 0 k_sf/musf c_sf/musf -0.5*w*k_sf/musf ...
        -0.5*w*c_sf/musf -a*k_sf/musf -a*c_sf/musf 0 0 0 0 0 0 ...
        0 0 0 0 0 0 (-k_sf-k_uf)/musf -c_sf/musf 0 0 0 0 ; ...
    0 0 0 0 0 0 0 0 0 0 0 0 0 0 0 0 0 0 0 0 0 0 0 0 0 1 0 0 ; ...
    0 0 0 0 k_sr/musr c_sr/musr 0.5*w*k_sr/musr ...
        0.5*w*c_sr/musr b*k_sr/musr b*c_sr/musr 0 0 0 0 0 0 0 0 ...
        0 0 0 0 0 0 (-k_sr-k_ur)/musr -c_sr/musr 0 0 ; ...
    0 0 0 0 0 0 0 0 0 0 0 0 0 0 0 0 0 0 0 0 0 0 0 0 0 0 0 1 ; ...
```

```
    0 0 0 0 k_sr/musr c_sr/musr -0.5*w*k_sr/musr ...
        -0.5*w*c_sr/musr b*k_sr/musr b*c_sr/musr 0 0 0 0 0 0 0 ...
        0 0 0 0 0 0 0 0 0 (-k_sr-k_ur)/musr -c_sr/musr ];

B=[0 0 0 0 0 0 0 0 0 0 0 0 0 0 0 0 0 ; ...
    0 0 0 0 0 0 0 0 0 0 0 0 0 0 0 0 ...
        (+(v0)^2/(2*m)*rho*Cd*Area) ; ...
    0 0 0 0 0 0 0 0 0 0 0 0 0 0 0 0 0 ; ...
    N_f*C_af/m N_f*C_af/m N_r*C_ar/m N_r*C_ar/m 0 0 0 0 0 0 0 ...
        0 0 0 0 0 0 ; ...
    0 0 0 0 0 0 0 0 0 0 0 0 0 0 0 0 0 ; ...
    0 0 0 0 0 0 0 0 -a -a b b 0 0 0 0 0 ; ...
    0 0 0 0 0 0 0 0 0 0 0 0 0 0 0 0 0 ; ...
    -N_f*C_af*h/I_r -N_f*C_af*h/I_r -N_r*C_ar*h/I_r ...
        -N_r*C_ar*h/I_r 0 0 0 0 w/2 -w/2 w/2 -w/2 0 0 0 0 0 ; ...
    0 0 0 0 0 0 0 0 0 0 0 0 0 0 0 0 0 ; ...
    0 0 0 0 0 0 0 0 0 0 0 0 0 0 0 0 0 ; ...
    0 0 0 0 0 0 0 0 0 0 0 0 0 0 0 0 0 ; ...
    a*N_f*C_af/Iz a*N_f*C_af/Iz -b*N_r*C_ar/Iz -b*N_r*C_ar/Iz ...
        0 0 0 0 0 0 0 0 0 0 0 0 0 ; ...
    0 0 0 0 0 0 0 0 0 0 0 0 0 0 0 0 0 ; ...
    0 0 0 0 1/Iw 0 0 0 0 0 0 0 0 0 0 0 -N_f*Cr/Iw ; ...
    0 0 0 0 0 0 0 0 0 0 0 0 0 0 0 0 0 ; ...
    0 0 0 0 0 1/Iw 0 0 0 0 0 0 0 0 0 0 -N_f*Cr/Iw ; ...
    0 0 0 0 0 0 0 0 0 0 0 0 0 0 0 0 0 ; ...
    0 0 0 0 0 0 1/Iw 0 0 0 0 0 0 0 0 0 -N_r*Cr/Iw ; ...
    0 0 0 0 0 0 0 0 0 0 0 0 0 0 0 0 0 ; ...
    0 0 0 0 0 0 0 1/Iw 0 0 0 0 0 0 0 0 -N_r*Cr/Iw ; ...
    0 0 0 0 0 0 0 0 0 0 0 0 0 0 0 0 0 ; ...
    0 0 0 0 0 0 0 0 -1 0 0 0 k_uf/musf 0 0 0 0 ; ...
    0 0 0 0 0 0 0 0 0 0 0 0 0 0 0 0 0 ; ...
    0 0 0 0 0 0 0 0 0 0 -1 0 0 k_uf/musf 0 0 0 ; ...
    0 0 0 0 0 0 0 0 0 0 0 0 0 0 0 0 0 ; ...
    0 0 0 0 0 0 0 0 0 0 0 0 -1 0 k_ur/musr 0 0 ; ...
    0 0 0 0 0 0 0 0 0 0 0 0 0 0 0 0 0 ; ...
    0 0 0 0 0 0 0 0 0 0 0 0 0 0 -1 k_ur/musr 0 ];

C=[0 1 0 0 0 0 0 0 0 0 0 0 0 0 0 0 0 0 0 0 0 0 0 0 0 0 0 0 ; ...
    0 0 0 1 0 0 0 0 0 0 0 0 0 0 0 0 0 0 0 0 0 0 0 0 0 0 0 0 ; ...
    0 0 0 0 1 0 0 0 0 0 0 0 0 0 0 0 0 0 0 0 0 0 0 0 0 0 0 0 ; ...
```

```
    0 0 0 0 0 0 1 0 0 0 0 0 0 0 0 0 0 0 0 0 0 0 0 0 0 0 0 0 ; ...
    0 0 0 0 0 0 0 0 1 0 0 0 0 0 0 0 0 0 0 0 0 0 0 0 0 0 0 0 ; ...
    0 0 0 0 0 0 0 0 0 0 1 0 0 0 0 0 0 0 0 0 0 0 0 0 0 0 0 0 ; ...
    0 0 0 0 0 0 0 0 0 0 0 1 0 0 0 0 0 0 0 0 0 0 0 0 0 0 0 0 ; ...
    0 0 0 0 0 0 0 0 0 0 0 0 0 1 0 0 0 0 0 0 0 0 0 0 0 0 0 0 ; ...
    0 0 0 0 0 0 0 0 0 0 0 0 0 0 0 1 0 0 0 0 0 0 0 0 0 0 0 0 ; ...
    0 0 0 0 0 0 0 0 0 0 0 0 0 0 0 0 0 1 0 0 0 0 0 0 0 0 0 0 ; ...
    0 0 0 0 0 0 0 0 0 0 0 0 0 0 0 0 0 0 0 1 0 0 0 0 0 0 0 0 ; ...
    0 0 0 0 0 0 0 0 0 0 0 0 0 0 0 0 0 0 0 0 1 0 0 0 0 0 0 0 ; ...
    0 0 0 0 0 0 0 0 0 0 0 0 0 0 0 0 0 0 0 0 0 0 1 0 0 0 0 0 ; ...
    0 0 0 0 0 0 0 0 0 0 0 0 0 0 0 0 0 0 0 0 0 0 0 0 1 0 0 0 ; ...
    0 0 0 0 0 0 0 0 0 0 0 0 0 0 0 0 0 0 0 0 0 0 0 0 0 0 1 0 ];

D=zeros(15,17);

ICs=[0 v0 0 0 0 0 0 0 0 0 0 0 0 v0/R 0 v0/R 0 v0/R 0 v0/R 0 0 ...
    0 0 0 0 0 0]';
```

C.2 3 Degrees of Freedom Vehicle Controller Initialization

```
clc,clear;
%% vehicle constants

w=1.6;
m=1300;           %mass of car
g=9.81;             %gravity
l=2.5;
a=1.14;
b=l-a;
fi_f=atan((w/2)/a);
fi_r=atan((w/2)/b);
lf=sqrt((w/2)^2+a^2); %cross distance between com and front wheel
lr=sqrt((w/2)^2+b^2); %cross distance between com and rear wheel
friction_coeff=0.95;
```

```
h=0.375;                %vehicle height
Cfront=1100.*1.5;
Crear=1100.*1.6;
I_z=1300; %yaw rotation axis
I_p=1000;
I_r=250;
Iw=2.7;
N_f=m*g*b/(2*l);
N_r=m*g*a/(2*l);
density_air=1.292;      %density of air
A=2.2; % frontal area
Cd=0.3;      %drag coefficient
Q=0;
C_l=29.6; %linearized longutidunal friction (valid until 0.03 ...
    longitudinal slip)  [null]
C_alpha=0.23*360/(2*pi); %linearized lateral friction (valid ...
    until 3.4 degree slip) [1/[rad]]
T=200;
v0=16;
K_us=(m*b/(l*C_alpha*N_f))-(m*a/(l*C_alpha*N_r));
K_side_d=1e-5;
K_side_p=2.5;
side_threshold=(10-7*(v0^2/40^2))*2*pi/360;
%% Controller Parameters

Am=-1e7*eye(3);
LAMB=eye(6);
LAMB_fail=[1 0 0 0 0 0; 0 1 0 0 0 0; 0 0 1 0 0 0; 0 0 0 1 0 ...
    0; 0 0 0 0 1 0; 0 0 0 0 0 0.1];
L=eye(3);
P=eye(3);
v_rsteer=1.2e-05;
v_fsteer=(v_rsteer/6);
v_Fy_r=3.5e-06;
v_Fy_f=v_Fy_r/6;
v_tractionF=0.5;
v_tractionM=0.2;
v_other=1e-15;
E_rsteer=1.2e-06;
E_fsteer=E_rsteer/6;
```

```
E_Fy_r=3.5e-07;
E_Fy_f=E_Fy_r/6;
E_tractionF=0.05;
E_tractionM=0.02;
E_other=1e-20;
C_trac=[1;1;1;1;1;1];
C_trac0=[1;1;1;1;1;0.1];
gamma_force=1;
gamma_moment=1;
gamma_fsteer=1e-8;
gamma_rsteer=1e-7;
gamma_Fy_f=1e-9;
gamma_Fy_r=1e-9;
gamma_other=0;
theta_tracF0=[1/4 1/4 1/4 1/4];
theta_tracM0=0;
theta_fsteer0=2e-6;
theta_rsteer0=-3.1e-6;
theta_other0=[0 0 0 0 0 0];
theta_Fy_f0=0;
theta_Fy_r0=0;
format long
B=[2*C_alpha*a*N_f -2*C_alpha*b*N_r -w/2 w/2 -w/2 w/2; 0 0 1 ...
    1 1 1; 2*C_alpha*N_f 2*C_alpha*N_r 0 0 0 0];
Bu=[ 0 0 1/m 1/m 1/m 1/m ;...
     2*N_f*C_alpha/(m*v0) 2*N_r*C_alpha/(m*v0) 0 0 0 0 ;...
     2*a*N_f*C_alpha/I_z -2*b*N_r*C_alpha/I_z -w/(2*I_z) ...
         w/(2*I_z) -w/(2*I_z) w/(2*I_z)];
```

C.3 14 Degrees of Freedom Vehicle Controller Initialization

```
clc, clear, close all;
%% vehicle constants
Cd=0.3;     %drag coefficient
```

```
Nt=4.2;%4.2;       %gear ratio of transmission
Nf=1;%2.47;        %gear ratio of final drive shaft
u=0.8;      %efficiency of transmission
R=0.33;     %wheel radius (pirelli p215/65/r15)
w=1.6;
A=2.2;
density_air=1.292;     %density of air
Q_x=0;             %slope of the road in rad
Q_y=0;             %slope of the road in rad
m=1300;            %mass of car
g=9.81;              %gravity
l=2.5;
a=1.125;
b=l-a;
fi_f=atan((w/2)/a);
fi_r=atan((w/2)/b);
l_cross_front=sqrt((w/2)^2+a^2);
l_cross_rear=sqrt((w/2)^2+b^2);
friction_coeff=0.95;
h=0.375;               %vehicle height
Cfront=1100.*1.5;
Crear=1100.*1.6;
Iz=1300; %yaw rotation axis
I_p=1000;
I_r=250;
Iw=2.7;
r=-1; %differential ratio
k_sf=21000; % front sprung mass spring coeff
c_sf=1000; % front sprung mass damping coeff
k_sr=21000; % rear sprung mass spring coeff
c_sr=1500; % rear sprung mass damping coeff
k_u=200000;%unsprung mass spring coeff
mus=30;%unsprung mass

%% Linearization Parameters

N_f=m*g*b/(2*l)+mus*g;
N_r=m*g*a/(2*l)+mus*g;
qm=m*g/4+mus*g;
```

```
C_l=29.6; %linearized longutidunal friction (valid until 0.03 ...
    longitudinal slip)  [null]
C_af=45000/N_f; %linearized lateral friction (valid until 4.5 ...
    degree slip) [1/[rad]]
C_ar=37590/N_r; %linearized lateral friction (valid until 4.5 ...
    degree slip) [1/[rad]]
T=250;
T_b=2000;
C_long=10.41;

%% initial conditions
v0=17; %vehicle longitudinal IC
v_t=v0/R;
v_cog0=28;
side_slip0=0;
yaw_0=0;
v_x0=v_cog0*cos(side_slip0);
v_y0=v_cog0*sin(side_slip0);
K_us=(m*b/(l*C_af*N_f))-(m*a/(l*C_ar*N_r));
K_side_d=1e-5;
K_side_p=2.5;

%% Controller Parameters
K_torque=Iw*10;
Ki_torque=10;
K_f=2/R;
Ki_f=10;
Am=-1e7*eye(5);
B_notmodify=eye(12);
B_notmodify(12,12)=1;
B_notmodify(11,11)=1;
B_notmodify(10,10)=1;
B_notmodify(9,9)=1;
LAMB=eye(12);
LAMB_fail=LAMB;
LAMB_fail(4,4)=0.7;
L=eye(5);
P=eye(5);
%%
v_rsteer=1.2e-05;
```

```
v_fsteer=(v_rsteer/6);
v_Fy_r=1.9e-05;
v_Fy_f=v_Fy_r/6;
v_tractionF=0.5;
v_tractionM=0.1;
v_roll=0.5;
v_pitch=0.5;
v_other=1e-18;
%%
E_rsteer=1e-06;
E_fsteer=E_rsteer/5;
E_Fy_r=1e-06;
E_Fy_f=E_Fy_r/6;
E_tractionF=0.05;
E_tractionM=0.02;
E_roll=0.1;
E_pitch=0.1;
E_other=1e-19;
%%
C_trac=[1;1;1;1;1;1;1;1;1;1;1;1];
C_trac0=[1;1;1;0.1;1;1;1;0.1;1;1;1;1];
gamma_force=0.1;
gamma_moment=0.1;
gamma_fsteer=1e-9;
gamma_rsteer=1e-9;
gamma_Fy_f=1e-9;
gamma_Fy_r=1e-9;
gamma_roll=10;
gamma_pitch=10;
gamma_other=0;
theta_tracF0=[1/4 1/4 1/4 1/4];
theta_tracM0=0;
theta_fsteer0=2e-6;
theta_rsteer0=-3.1e-6;
theta_other0=[0 0 0 0 0 0];
theta_Fy_f0=0;
theta_Fy_r0=0;
N_fmin=3500;
N_rmin=2800;
format long
```

```
B=[C_af*a*qm C_af*a*qm -C_ar*b*qm -C_ar*b*qm -w/(2*R) w/(2*R) ...
    -w/(2*R) w/(2*R) 0 0 0 0;...
     0 0 0 0 1 1 1 1 0 0 0 0;...
     C_af*qm C_af*qm C_ar*qm C_ar*qm 0 0 0 0 0 0 0 0;...
     0 0 0 0 0 0 0 0 -a -a b b;...
     0 0 0 0 0 0 0 0 0.5*w -0.5*w 0.5*w -0.5*w];
Bu=[ 0 0 1/m 1/m 1/m 1/m ;...
     2*N_f*C_af/(m*v0) 2*N_r*C_ar/(m*v0) 0 0 0 0 ;...
     2*a*N_f*C_af/Iz -2*b*N_r*C_ar/Iz -w/(2*Iz) w/(2*Iz) ...
        -w/(2*Iz) w/(2*Iz)];
B_modify=[2*N_f 2*N_r 1 1 1 1; 1 1 1 1 1 1; 2*N_f 2*N_r 1 1 1 1];
```

C.4 Magic Formula for Longitudinal Friction

```
clc; clear; close all;
normal_force=3800;
%normal_force=3160;
linslip=-0.1:0.01:0.1;
linf=45500*linslip;
steering_angle=0;
normal_force=normal_force/1000;
b0=1.569;
b1=-25.58;
b2=1225;
b3=-4.908;
b4=397.6;
b5=-0.02669;
b6=0.00356;
b7=-0.009426;
b8=0.6581;
b9=0; b10=0; b11=0; b12=0;
%coefficient calculations
C=b0;
u_p=(b1*normal_force)+b2;
D=u_p*normal_force;
BCD=(b3*(normal_force^2)+(b4*normal_force))*exp(-b5*normal_force);
```

```
B=BCD/(C*D);
E=b6*(normal_force^2)+b7*normal_force+b8;
Sh=(b9*normal_force)+b10;
Sv=b11*normal_force+b12;
%lateral coupling
bm0=1.257;
bm1=0.6596;
bm2=0.2246;
bm3=0.1585;
%coupling coefficient calculations
CD=bm0;
AD=bm1;
slip=-0.5:0.01:0.5;
for i=1:length(slip)
BD=bm2*cosd(atand(bm3*slip(i)));
%Fx
fi=(1-E)*(slip(i)+Sh)+(E/B)*atand(B*(slip(i)+Sh));
Fx0=D*sind(C*atand(B*fi))+Sv;
Fx(i)=Fx0*(cosd(CD*atand(BD*(steering_angle - ...
    AD))))/(cosd(CD*atand(-BD*AD)));
end
figure (1)
hold on
plot(slip,Fx,'--k',"LineWidth",2);
plot(linslip,linf,'b',"LineWidth",2);
hold off
box on
grid on
xlabel('Slip (%)');
ylabel('Traction Force [N]')
legend({'Nonlinear Longutidunal Friction','Linear ...
    Longutidunal Friction'},'FontSize',10);
legend('boxoff');
```

C.5 Magic Formula for Lateral Friction

```
clc; clear; close all;
camber=0;
%Fz0=3800;
%Fz=3800;
linslip=-0.07:0.01:0.07;
linf=45000*linslip;
Fz0=3160;
Fz=3160;
df=(Fz-Fz0)/Fz0;
%constants for lateral
pcy1 = 1.3507; %Shape factor Cfy for lateral forces
pdy1 = 1.0489; %Lateral friction Muy
pdy2 = -0.18033; %Variation of friction Muy with load
pdy3 = -2.8821; %Variation of friction Muy with squared camber
pey1 = -0.0074722; %Lateral curvature Efy at Fznom
pey2 =  -0.0063208; %Variation of curvature Efy with load
pey3 = -9.9935; %Zero order camber dependency of curvature Efy
pey4 = -760.14; %Variation of curvature Efy with camber
pky1 =  -21.92; %Maximum value of stiffness Kfy/Fznom
pky2 = 2.0012; %Load at which Kfy reaches maximum value
pky3 =  -0.024778; %Variation of Kfy/Fznom with camber
% pky4=2;
% pky5=0;
phy1 = 0.0026747; %Horizontal shift Shy at Fznom
phy2 =  8.9094e-005; %Variation of shift Shy with load
phy3 =  0.031415; %Variation of shift Shy with camber
pvy1 = 0.037318; %Vertical shift in Svy/Fz at Fznom
pvy2 = -0.010049; %Variation of shift Svy/Fz with load
pvy3 = -0.32931; %Variation of shift Svy/Fz with camber
pvy4 = -0.69553; %Variation of shift Svy/Fz with camber and load
% rby1 = 7.1433; %Slope factor for combined Fy reduction
% rby2 = 9.1916; %Variation of slope Fy reduction with alpha
% rby3 = -0.027856; %Shift term for alpha in slope Fy reduction
% rcy1 = 1.0719; %Shape factor for combined Fy reduction
% rey1 = -0.27572; %Curvature factor of combined Fy
% rey2 = 0.32802; %Curvature factor of combined Fy with load
% rhy1 = 5.7448e-006; %Shift factor for combined Fy reduction
% rhy2 = -3.1368e-005; %Shift factor for combined Fy ...
    reduction with load
```

```matlab
% rvy1 = -0.027825; %Kappa induced side force Svyk/Muy*Fz at ...
    Fznom
% rvy2 = 0.053604; %Variation of Svyk/Muy*Fz with load
% rvy3 = -0.27568; %Variation of Svyk/Muy*Fz with camber
% rvy4 = 12.12; %Variation of Svyk/Muy*Fz with alpha
% rvy5 = 1.9; %Variation of Svyk/Muy*Fz with kappa
% rvy6 = -10.704; %Variation of Svyk/Muy*Fz with atan(kappa)
% pty1 = 2.1439; %Peak value of relaxation length SigAlp0/R0
% pty2 = 1.9829; %Value of Fz/Fznom where SigAlp0 is extreme
%coefficient calculation
C=pcy1;
mu_y=(pdy1+pdy2*df)*(1-pdy3*camber^2);
D=mu_y*Fz;
Kya=pky1*Fz0*sin(2*atan(Fz/(pky2*Fz0))*(1-pky3*abs(camber)));
B=Kya/(C*D);
Shy0=(phy1+phy2*df);
Shyy=phy3*camber;
%Shy=Shy0+Shyy;
Shy=0;
%Svy=Fz*((pvy1+pvy2*df)+(pvy3+pvy4*df)*camber);
Svy=0;
slip=-(-pi/6:0.001:pi/6);
for i=1:length(slip);
slip_y=slip(i)+Shy;
E=(pey1+pey2*df)*(1-(pey3+pey4*camber)*sign(slip_y))*camber;
lateral_force(i)=(D*sin(C*atan(B*slip_y-E*(B*slip_y - ...
    atan(B*slip_y))))+Svy);
end
slip=-slip;
figure (1)
hold on
plot(slip,lateral_force,'--k',"LineWidth",2)
plot(linslip,linf,'b',"LineWidth",2)
hold off
xlabel('Slip [rad]');
ylabel('Lateral Force [N]')
legend({'Nonlinear Lateral Friction','Linear Lateral ...
    Friction'},'FontSize',10);
legend('boxoff');
box on
```

```
grid on
```

Appendix D

Simulink Models

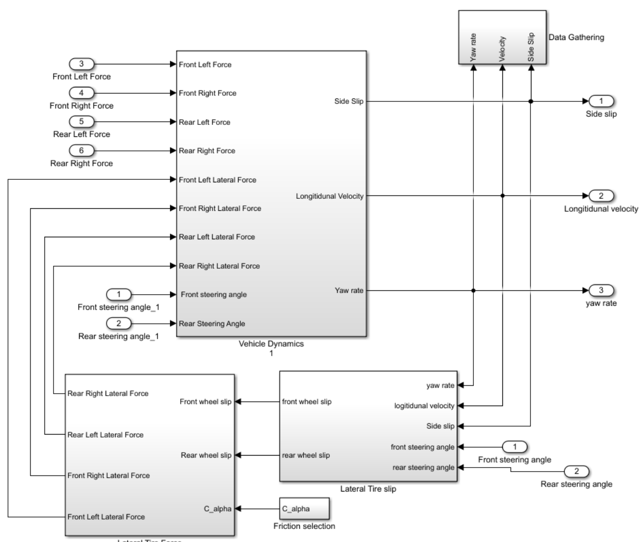

Figure D.1: 3 Degrees of Freedom Vehicle Model

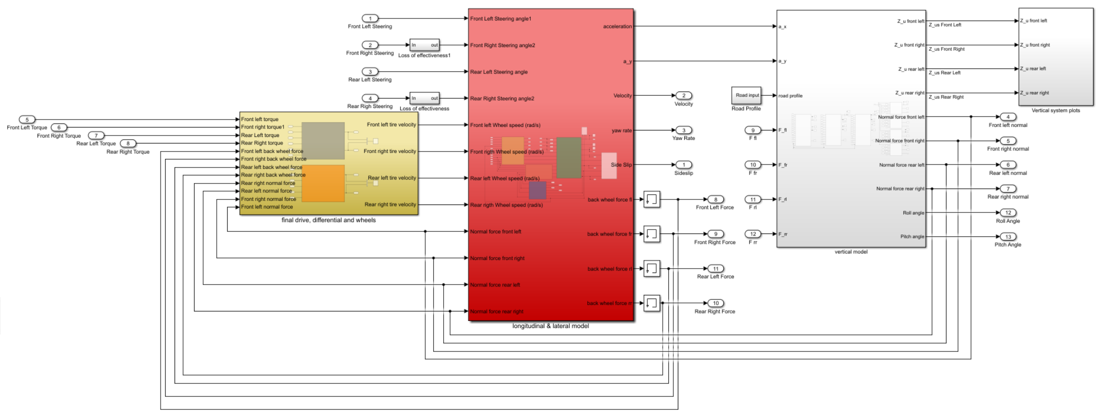

Figure D.2: 14 Degrees of Freedom Vehicle Model

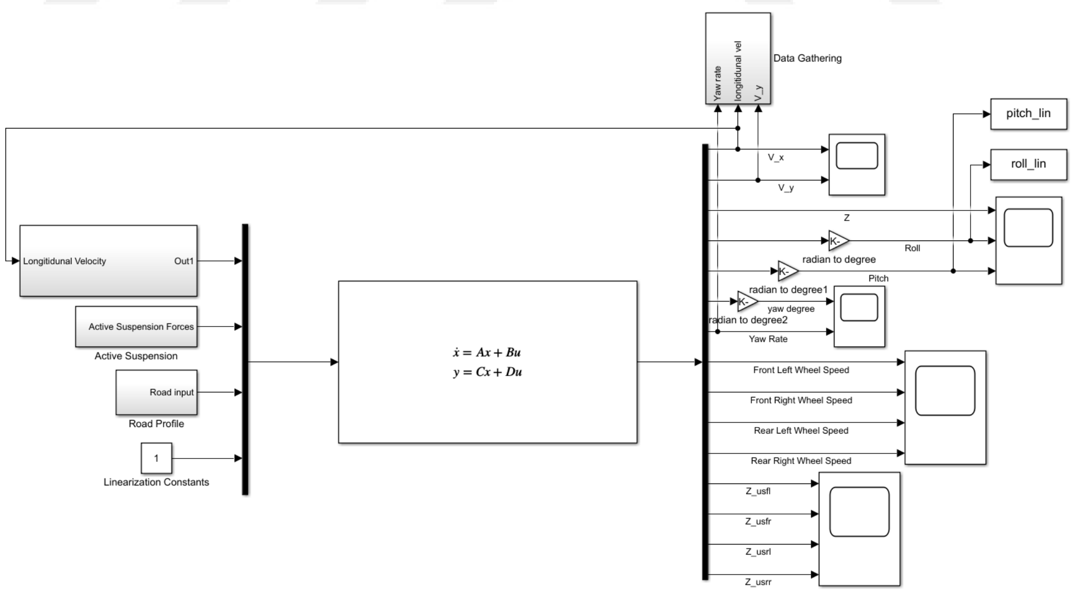

Figure D.3: Linearized 14 Degrees of Freedom Vehicle Model

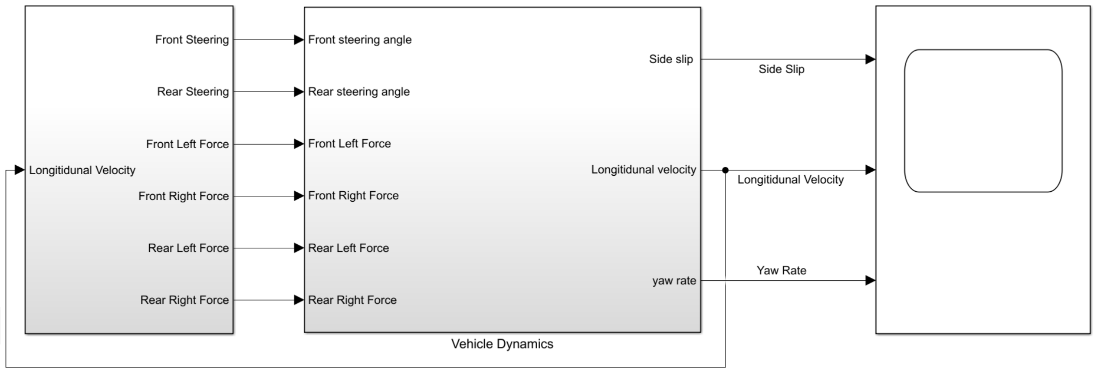

Figure D.4: Baseline Vehicle Model for Allocation System with 3 Degrees of Freedom

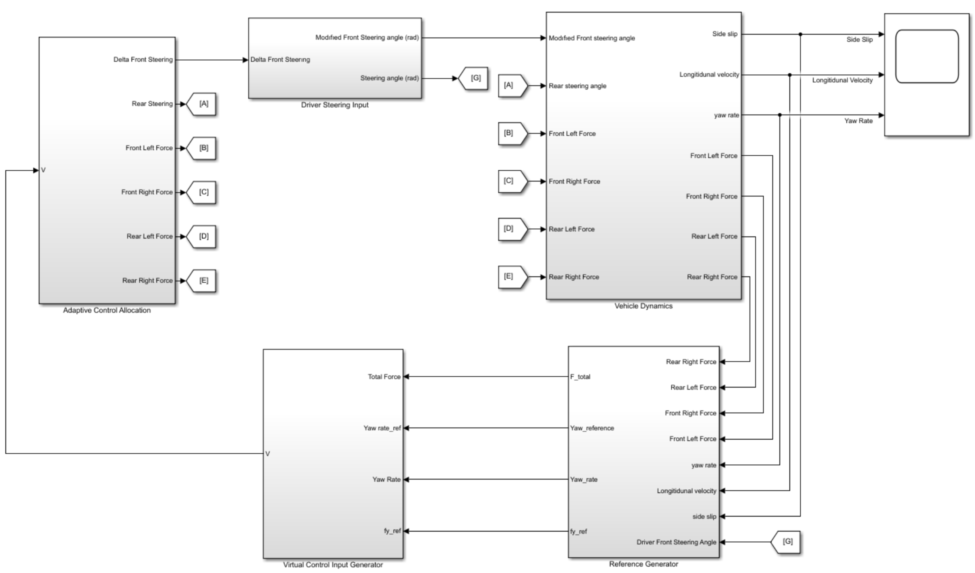

Figure D.5: Overall Adaptive Control Allocation Scheme with 3 Degrees of Freedom

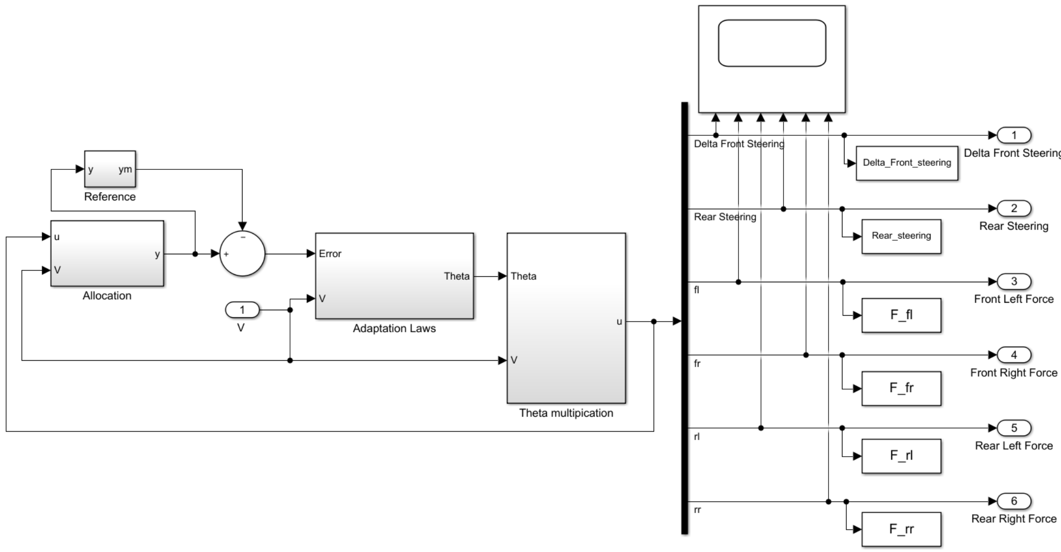

Figure D.6: Adaptive Control Allocation with 3 Degrees of Freedom

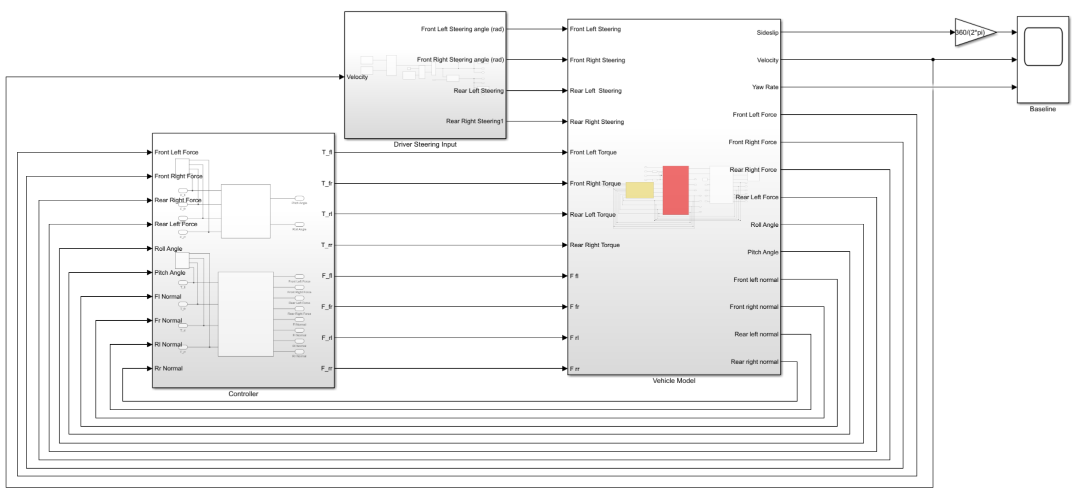

Figure D.7: Baseline Vehicle Model for Allocation System with 14 Degrees of Freedom

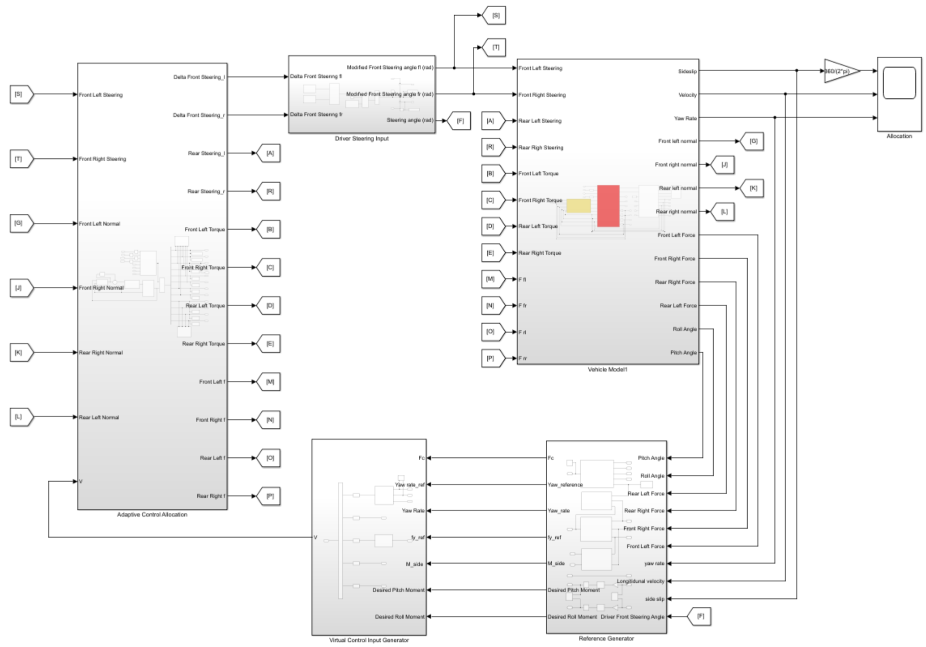

Figure D.8: Overall Adaptive Control Allocation Scheme with 14 Degrees of Freedom

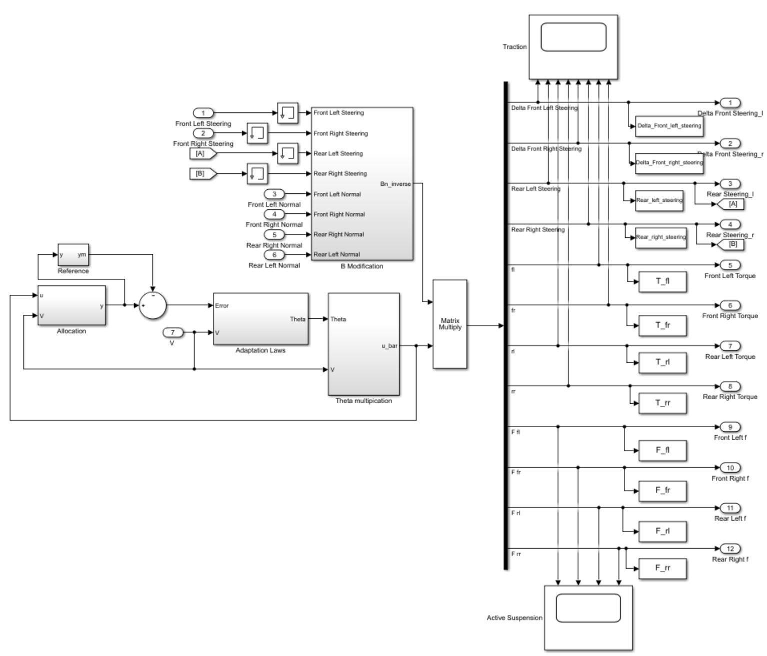

Figure D.9: Adaptive Control Allocation with 14 Degrees of Freedom